Field Measurements of Intermediate External Diaphragms on a Trapezoidal Steel Box Girder Bridge

by

Benjamin Ari Cheplak, B.S.C.E.

Thesis
Presented to the Faculty of the Graduate School of
The University of Texas at Austin
in Partial Fulfillment
of the Requirements
for the Degree of

Master of Science in Engineering

The University of Texas at Austin
May 2001

Field Measurements of Intermediate External Diaphragms on a Trapezoidal Steel Box Girder Bridge

Approved by
Supervisory Committee:

Karl H. Frank

Joseph A. Yura

ACKNOWLEDGEMENTS

I would like to extend my deepest appreciation to Dr. Karl Frank for his guidance over the last two years. His wisdom and understanding were essential for the success of this research. Additional insight from Dr. Joseph Yura and Dr. Eric Williamson was also extremely valuable.

I would also like to thank the Texas Department of Transportation and the College of Engineering at the University of Texas at Austin for their financial support of this research. Further thanks go to Bill West and the rest of the J.D. Abrams crew for their patience and help during the instrumentation and testing.

Special thanks go to Brian Chen for his countless hours of hard work. He has been a mentor and a great friend. Also, I would like to thank Reagan Herman, Cem Topkaya, Matthew Memberg, Michael Hagenberger, Patrick Wagener, and Taichiro Okazaki for their donation of time and labor.

Finally, I wish to thank my family, Vicki, and my closest friends: Dave & Melissa Figurski, and Joey & Alisa Dowd. All of their support and encouragement over the last two years will always be remembered.

April 23, 2001

ABSTRACT

Field Measurements of Intermediate External Diaphragms on a Trapezoidal Steel Box Girder Bridge

Benjamin Ari Cheplak, M.S.E.
The University of Texas at Austin, 2001
Supervisor: Karl H. Frank

Trapezoidal steel box girders are being used more frequently for curved bridges due to their high torsional rigidity and aesthetic appeal. A typical system uses two U-shaped girders with a cast-in-place concrete deck. The deck acts compositely with the U-shaped steel girder, which adds significant stiffness to the bridge as it completes the closed section. A critical design stage occurs during the deck pour since the curved girders are non-composite and may have excessive relative distortions. External diaphragms are commonly installed between the girders to control these distortions.

Using intermediate external diaphragms will increase time and costs through design, fabrication, and construction; therefore, it would be very beneficial to minimize their use on box girder bridges. Forces in three external diaphragms and several top lateral-bracing members were measured during the construction of a three-span trapezoidal steel box girder bridge built in Austin, Texas. The stresses in the bridge were monitored during three main loadings. The measured forces in these members were compared to analysis using a finite element model.

TABLE OF CONTENTS

LIST OF TABLES

LIST OF FIGURES

NOTATION

Sign Convention

+	Tensile Force / Stress
-	Compressive Force / Stress

Material & Section Properties

E	Modulus of Elasticity
A	Cross sectional Area of Member
f'_c	28-day Concrete Strength

Forces & Strains

P	Axial Force
T1,T2	Torsional External Reactions on U-Girder from External Diaphragm
H	Horizontal External Reaction on U-Girder from External Diaphragm
ε	Strain at gage location
$\varepsilon_{centroid}$	Strain at centroid of member

Circuitry

V	Voltage
V_o	Output Voltage
V_{exc}	Full Bridge Excitation Voltage
I	Current
R	Resistance

Other

β	Slope of Linear Trendline in Plot of Crane Load VS Member Axial Force

CHAPTER 1
Introduction

1.1 BACKGROUND

Trapezoidal steel box girders are often used for curved bridges due to their high torsional rigidity and aesthetic appeal. A conventional twin box girder system is designed with a cast-in-place concrete deck. The deck acts compositely with the steel U-shaped girders through the use of shear studs on the top flanges of the girders. This adds significant stiffness to the bridge as it completes two closed box girders. Figure 1.1 shows the cross section of a trapezoidal box girder system.

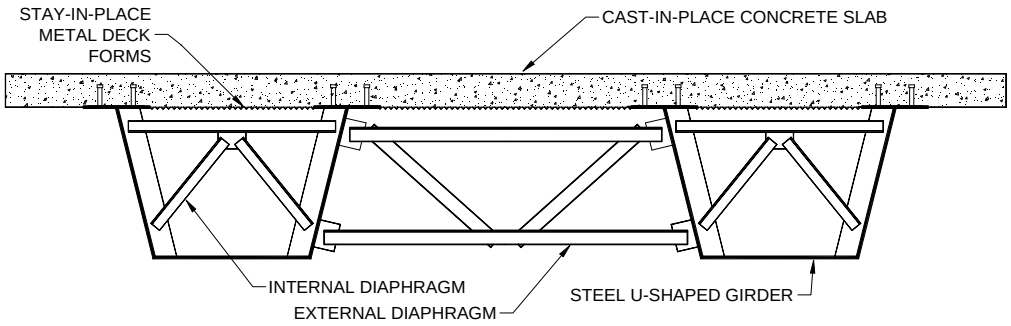

Figure 1.1 Cross section of Trapezoidal Box Girder System

For stability during construction, the top flanges of each girder require bracing. Also, to limit twisting distortions between one box girder and the other during construction, external cross frames or diaphragms are often temporarily installed between the girders at intermediate points along the span. The forces in the top lateral bracing and external diaphragms were investigated during this study.

1.2 BRIDGE UNDER STUDY

Trapezoidal steel box girders were used for the addition of overpasses at the intersection of IH 35 and US 290 in Austin, TX. The overpasses were erected over heavy traffic and required sharp curves with long spans. Each overpass uses concrete U-beams for the straight on-ramps and steel box girders for the curved portions. The Texas Department of Transportation (TxDOT) designed the girders and the contractor, J. D. Abrams, Inc., was responsible for the construction of the interchange. Trinity Industries, Inc. fabricated the steel girders in Houston, TX.

The overpass chosen for this study was Direct Connect Z, which provides a direct route going east on RM 2222 (towards US 290) to south on IH35 as shown in Figure 1.2. This overpass allowed the easiest access for instrumentation and testing. Also, it was the first overpass at the interchange to be erected and future instrumentation of the other bridges could benefit from monitoring Z-connect.

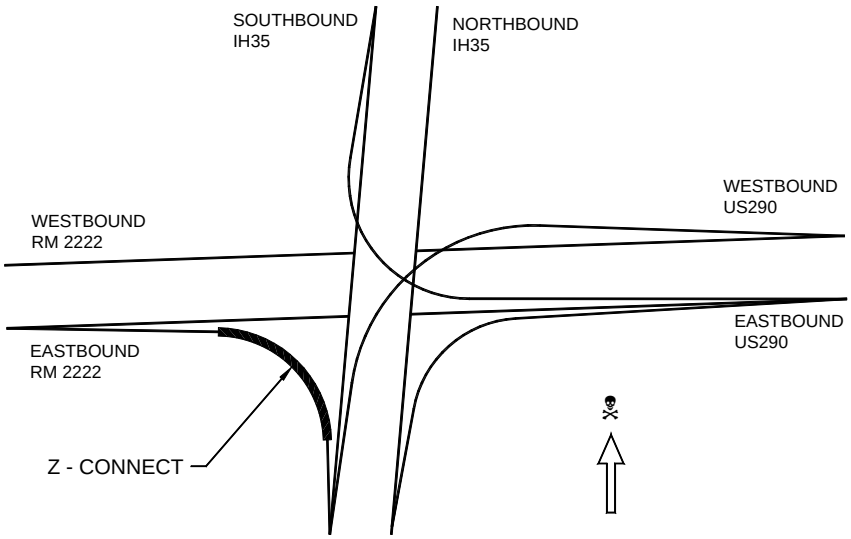

Figure 1.2 Site Location

1.2.1 Z-Connect Dimensions

The steel portion of Z-connect consists of one three-span bridge followed by a two-span bridge. The three-span bridge was under investigation and is shown below in Figure 1.3. The top laterals, internal diaphragms, and external diaphragms can be seen in Figure 1.4. The symmetrical bridge has two side spans of about 150 ft in length and a middle span of 190 ft. The radius of the centerline of the bridge is 450 ft.

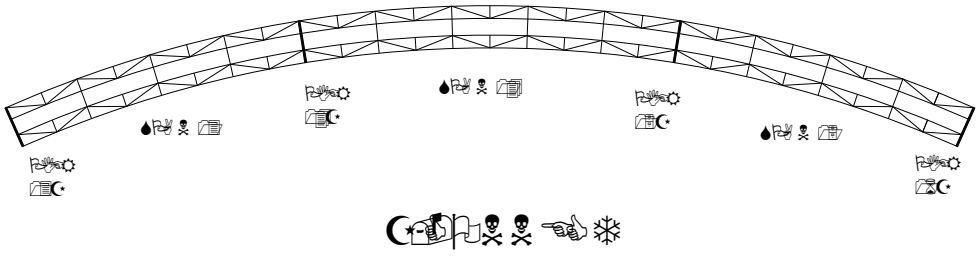

Figure 1.3 Plan View of Bridge Under Study

Figure 1.4 Picture of Z-Connect During Construction

Figure 1.5 shows the dimensions of the girder cross section. The top and bottom flanges vary in thickness along the length of the bridge (APPENDIX A). Internal diaphragms (Figure 1.6), which prevent warping of the trapezoidal cross section of the girder due to torsion, are spaced approximately every 20 feet. Solid plates with stiffeners are used as internal diaphragms at the end piers. Plates with access holes and stiffeners are located at the intermediate piers (Figure 1.7).

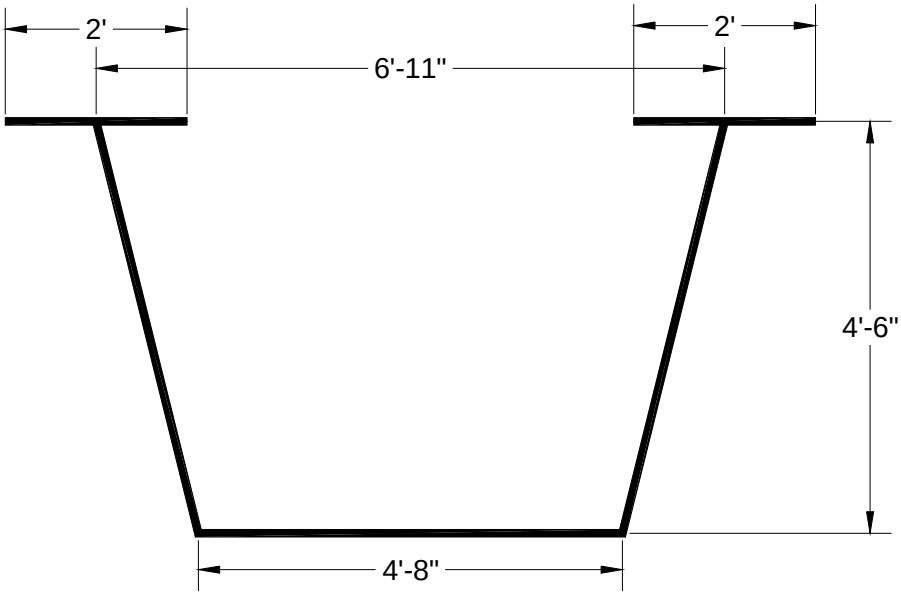

Figure 1.5 Girder Cross Section

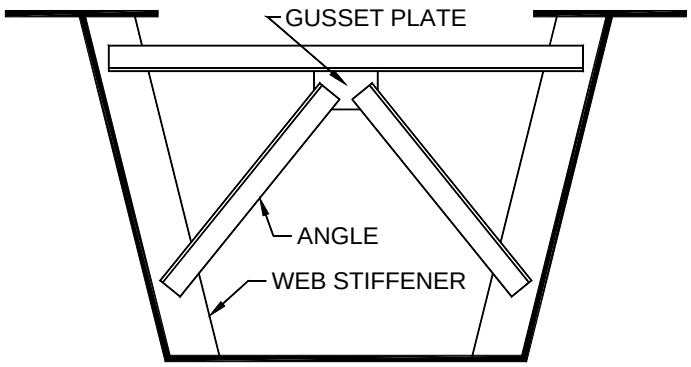

Figure 1.6 Intermediate Internal Diaphragm

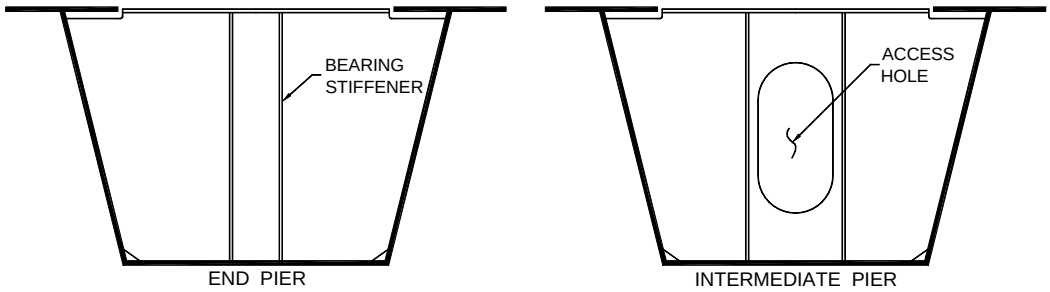

Figure 1.7 End and Pier Diaphragms

A top lateral truss fastened to the top flanges of each girder was used to increase the torsional stiffness of the steel section during construction. This truss system forms a "quasi-closed" box section. The top laterals (Figure 1.4) are WT7x21.5 sections and are designed to resist torsion. These members also have stresses due to bending although these stresses are not considered in design (Fan and Helwig, 1999).

1.2.2 Erection Procedure

Each girder was delivered to the site in 90-110 ft sections. The beam sections for each girder were erected according to their piece number shown in Figure 1.8. Field splices were bolted as the girders were supported by a combination of shore towers and cranes. Pier diaphragms and intermediate

external diaphragms were installed after the inner and outer girders were in place. The intermediate external diaphragms were attached at every other internal diaphragm location (approximately 40 feet) to control distortions between the two girders during the concrete pour. All external diaphragms between piers were removed after the concrete deck hardened for aesthetic reasons and fatigue concerns.

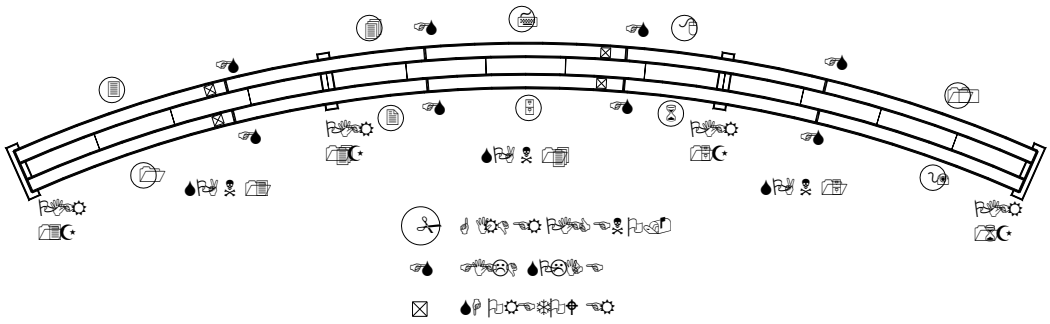

Figure 1.8 Bridge Assembly Sequence

1.3 EXTERNAL DIAPHRAGM DESIGN

In typical I-girder construction, intermediate cross frames or diaphragms are necessary to control lateral flange bending stresses and to provide stability for the girders. These diaphragms act as primary load-carrying elements due to the interaction of bending and torsion in the girders. Preliminary design equations can be used to estimate the necessary diaphragm spacing using parameters such as span length, girder radius of curvature, and girder flange width (Davidson et al., 1996).

For U-girder design, a combination of internal diaphragms and lateral bracing can be used to control the warping stresses and the stability of the girders (Chen, 1999). These members form the girder into a quasi-closed section. A closed cross section can have over a thousand times greater torsional stiffness

than a similar open section, such as an I-girder (Basler and Kollbrunner, 1969). Therefore, intermediate external diaphragms are not as essential as major load-carrying elements on box girders as they are in I-girders. The primary function of these members is to control distortions between the box girders during construction. Trapezoidal box girders have been successfully built with external diaphragms only at the piers (Fan, 1999)

Currently, the AASHTO (American Association of State Highway and Transportation Officials) *Guide Specifications for Horizontally Curved Highway Bridges* (1993) does not require the use of external diaphragms between box girders. There are no provisions for the design of external diaphragms. However, internal diaphragms are specified according to Section 2.28:

> *Intermediate diaphragms or cross frames within each box girder shall be required to limit the normal stresses and the transverse bending stresses due to distortion… The longitudinal spacing and stiffness of such diaphragms, if required, shall be determined using a rational analysis.*

External diaphragms are discussed in the commentary section 10.2.3 of the NCRHP (National Cooperative Highway Research Program) *Recommended Specifications for Steel Curved-Girder Bridges* (1998), which states:

> *External bracing at other than support points is usually not necessary. If analysis shows that the boxes will rotate excessively when the deck is placed, temporary external bracing may be desirable.*

As an additional aid in the design of the external diaphragms, TxDOT engineers referred to section 10 of the Colorado Department of Transportation *Bridge Design Manual*. It recommends the following for box girders:

> *When the radius of curvature, R, is less than 1000 feet, temporary external diaphragms shall be provided at every internal cross frame…. These temporary frames serve to unify the overall action of the steel box girders during deck pouring while also providing additional restraint for temperature effects.*

The diaphragms were designed using angle members since they were the most economical shape. The angle size was determined by satisfying kL/r requirements in AASHTO Guide Specifications.

Finite-element analysis tools capable of modeling the details of the complex geometry and loading of curved girders are available. However, this type of analysis is complicated and is usually costly and time consuming. In addition, further testing and work with finite-element analysis is needed to determine its reliability in predicting the behavior of curved bridges.

1.4 SCOPE

The work presented was part of research project 1896, "Field Monitoring of Steel Trapezoidal Box Girders". The research was funded by TxDOT and mainly focused on the field monitoring of the external diaphragms that connect the two box girders and the top flange lateral bracing system. Forces in the top lateral bracing system were measured and results from these members were used to establish the distribution of forces between the two girders.

The field testing research was conducted in conjunction with analytical work using a finite element model (herein referred to as FEM). The analytical model is described in detail in section 1.5. Forces were measured in the external diaphragms and were compared with the analytical model throughout different loadings during construction. The aim of the research was to provide a better understanding of the function of the diaphragms and determine their necessity. It

is important to minimize the number of external diaphragms due to their added cost for design, fabrication, installation and removal.

For this study, stresses in the external diaphragms and top laterals were monitored through three main loadings. The first was a full-scale load test using a crane to lift the girders before the concrete deck was placed. The test setup and results will be discussed in Chapter 3. Chapter 4 will focus on the second loading, the concrete deck placement. The third loading was a live load test performed with trucks on the composite girder bridge (Chapter 5).

1.5 ANALYSIS USING FINITE ELEMENT MODEL

1.5.1 Finite Element Model Description

The Z-Connect was analyzed by a commercially available finite element code called ABAQUS. A three dimensional model[1] was prepared using the dimensions given in the design drawings. The structural components were modeled with shell, beam, and brick elements. Eight node quadratic shell elements with reduced integration (S8R5) were used to model the top and bottom flanges, webs and pier diaphragms. Four shell elements were used in webs and bottom flanges, whereas two shell elements were used for each top flange. Three dimensional 2-node linear beam elements (B31) were used to model internal diaphragms, external diaphragms, and top lateral bracing members. Three-dimensional 20-node quadratic bricks (C3D20) were used to model the concrete deck. No deformation was allowed between flange and deck.

Eight shell elements were employed between each internal brace locations. One and twenty brick elements were used along the thickness and width of the

[1]Analysis and description of model provided by Cem Topkaya, PhD candidate (2001), The University of Texas at Austin

deck, respectively. All analyses were linear. Figure 1.9 shows a portion of the composite bridge model.

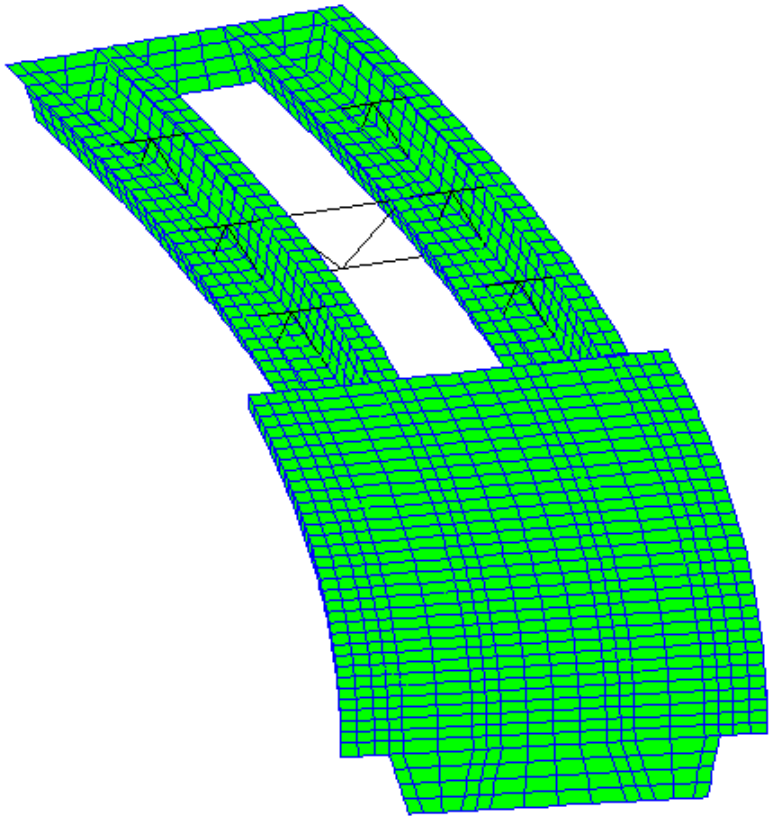

Figure 1.9 Section of Finite Element Model

1.5.2 FEM Studies Prior to Construction

Originally the bridge was designed to have 23 diaphragms installed every 20 feet, but further analysis with the FEM showed that the number could be reduced to 10 diaphragms at 40 feet (Figure 1.10). There was very little difference in the relative displacements between the girders when using 23 external diaphragms compared to 10 diaphragms. A system using only four external diaphragms was also investigated; relative displacements between the

girders significantly increased using this system compared to the 23-diaphragm system. Based upon the analysis results, TxDOT agreed to only install every other diaphragm that was originally designed (10 diaphragms). This reduction saved construction time on Z-connect since fewer diaphragms were installed and then removed. Analysis on other spans produced similar results to save construction time and fabrication costs. The FEM was also used to refine the lengths of each segment during concrete placement to minimize the top lateral forces.

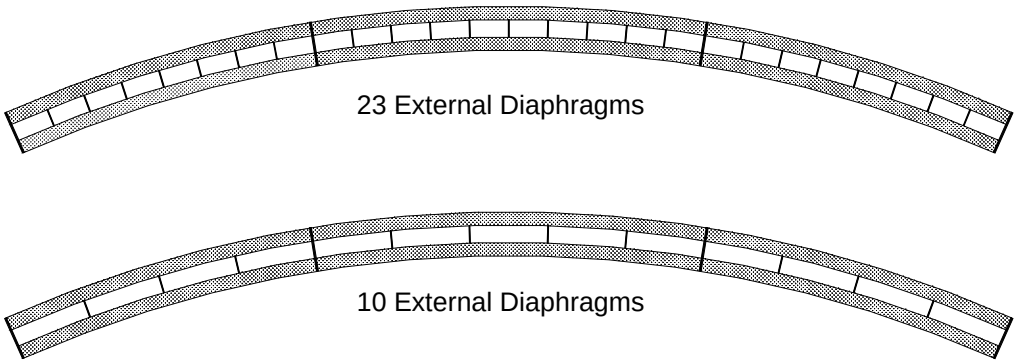

Figure 1.10 Reduction in External Diaphragms

The FEM was also used to predict the forces in the external diaphragms and top lateral bracing system due to different types of loading, including the field tests. The measured forces are compared to the predicted forces from the FEM.

Table of Contents

CHAPTER 2
Instrumentation

2.1 INTRODUCTION

This chapter presents the procedures of the field studies conducted during the construction of a curved steel box girder bridge. A description of the data acquisition system, calibration of the system, and results from lab tests will be discussed in this chapter. The reliability of the data that was collected from the field study will also be discussed.

2.2 DATA ACQUISITION SYSTEM

The majority of the field data was measured using a Campbell Scientific 21X Micrologger. Several AM416 Multiplexers were connected to the 21X in the field to increase the number of channels that could be read. A 12-volt deep-cycle marine battery that was charged by a solar panel powered the system. In series with the solar panel, a regulator was installed to insure that the battery was not overcharged. Since the system was not always easily accessible, a modem and a cell phone were connected to the datalogger. This setup allowed for data to be collected using cellular communication from a remote site. The modem was activated at specified times for short intervals to prevent excessive power drain. A schematic of the system is shown in Figure 2.1.

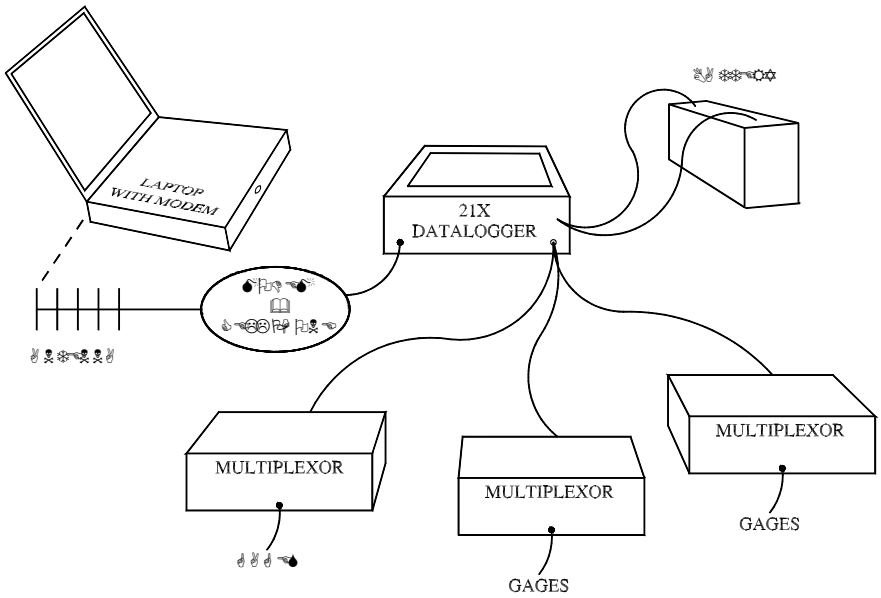

Figure 2.1 Overview of Data Acquisition System

A multiplexer can read up to 16 different channels sequentially. All of the measurements in the study were taken by strain gages that were temperature compensated for steel. After bonded to the steel, the gage's resistance changes in proportion to the strain in the member. The gage is wired in a full bridge configuration (Figure 2.2) with three precision resistors. If an excitation is applied to the full bridge, a change in gage resistance will change the voltage across the bridge. The 21X records an output voltage, V_o, divided by the bridge excitation, V_{exc}. The strain, ε, can then be calculated using the equation $\varepsilon = 4 \times V_o \div \left(GF \times V_{exc} \right)$, where GF is the gage factor.

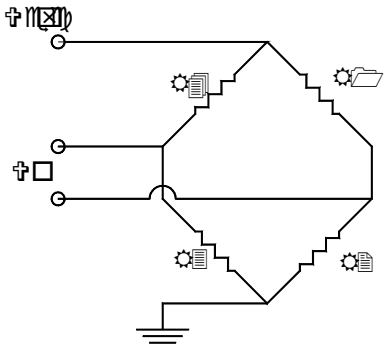

Figure 2.2 Full Bridge Configuration

Since the gages are temperature compensated, the strain in the steel due to temperature changes will produce little or no change in gage resistance and therefore no apparent strain. If the steel changes temperature and is not allowed to expand or contract accordingly, then an apparent strain will be read in the gage.

Since the gages would be exposed to the elements for a long period of time, wax and sealant were applied to the gage as weather protection. Also, mechanical protection such as plywood, steel angle, and steel plate surrounded the instrumentation to prevent damage during the erection of the bridge (Figure 2.3 and Figure 2.4).

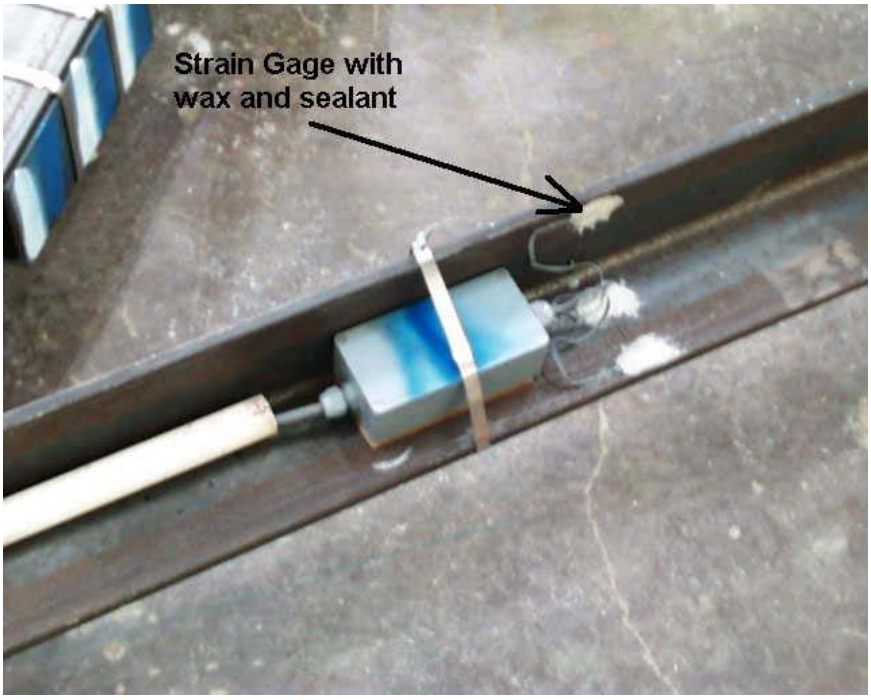

Figure 2.3 Installed Gages on Angle Member

Figure 2.4 Instrumentation Protection

2.3 LAB TEST ON ANGLE MEMBER

Using the common assumption in mechanics that plane sections remain plane, the axial force and biaxial bending moments in a member can be calculated with a minimum of three strain measurements at a cross section. Lab tests were performed on angle members to determine a reliable strain gage configuration. Eight strain gages were installed on a 5ft long L5x5x3/8 member as shown in Figure 2.5. This member is similar to the angles used on the external diaphragms (L5x5x1/2).

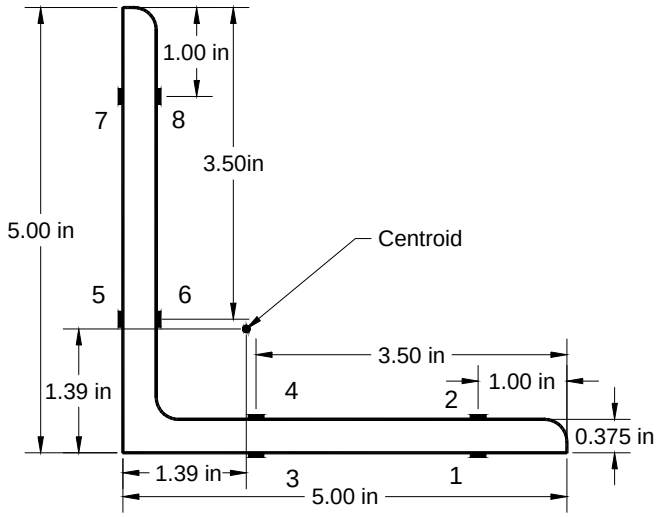

Figure 2.5 Strain Gage Configuration of Angle for Lab Test

Steel tabs were welded to the outside of one angle leg at both ends that could fit into the test machine grips. The angle was loaded eccentrically, simulating the angle connection on the external diaphragm. The gaged cross section was located at the mid length of the angle to prevent shear lag from the loaded tabs at the ends of the angle from affecting the strain readings. The strain measurements from the tests were used to calculate the axial force in the member. The measured axial force was then compared to the load cell from the testing machine.

Since it is assumed that plane sections remain plane, the strain at the centroid of the angle, $\varepsilon_{centroid}$, was calculated by forming a plane with the combination of three strain measurements. The formula used for this calculation was $\varepsilon_i = a \times x_i + b \times y_i + c$, where x_i and y_i are the Cartesian coordinates of any point i on the cross section measured from the heel of the angle. The constants a, b, and c can be solved for simultaneously with the coordinates of three gages and their corresponding strain readings. Once the constants are found, the strain at the centroid can be found using the previous equation and the coordinates of the centroid. The axial force, P, can then be calculated using the formula $P = \varepsilon_{centroid} \times E \times A$, where E is the modulus of elasticity (29000ksi for steel) and A is the cross sectional area of the member. An example of this calculation is shown in APPENDIX B.

A typical graph from the load test is shown below in Figure 2.6. If the angle remains linear-elastic, the measured load (y-axis) should always be equal to the applied load (x-axis) creating a line of slope 1.0. The plot in Figure 2.6 has a slope relatively close to 1.0, but the trendline is offset and crosses the y-axis above zero. The reason for this is uncertain, but it is probably due to the sensitivity of the testing machine at low loads. Figure 2.7 is a plot of the same data, except the zero reading for the force in the member is taken at an applied load of 5kips. Also, the x-axis is now the change in applied load, as opposed to the applied load. This data correlates much better than the previous plot and results in approximately 3% difference between the measured load in the angle and the applied load from the test machine.

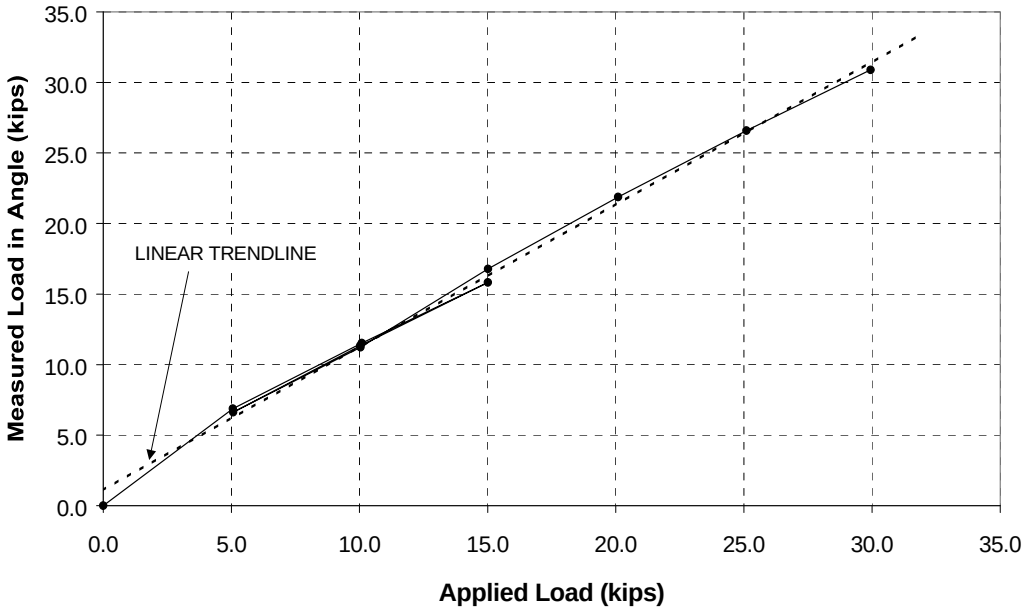

Figure 2.6 Axial Force Measurement of Angle in Lab Test

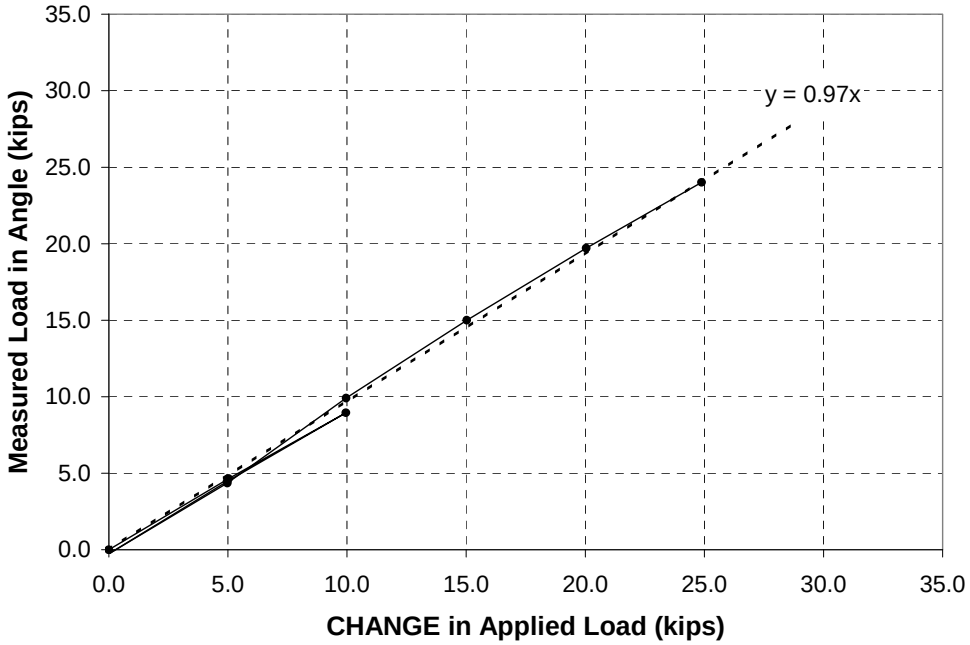

Figure 2.7 Axial Force Measurement of Angle in Lab Test - Adjusted

Using sets of three of the eight gages in different configurations, axial forces were calculated using the method described above. The slopes for each configuration were compared and are shown in Table 2.1. The axial force estimates varied very little between the different gage configurations, although some configurations were slightly more accurate than others. The tests showed that only three gages at a cross section were necessary to accurately predict the axial force on the angle in tension. The gage configuration that was eventually used on the diaphragms is shown in Figure 2.8. Arranging all of the gages on the inside of the legs of the angles made it easier to add mechanical protection to the gages.

Table 2.1 Lab Test Results on Angle Member

	GAGE CONFIGURATION							
	135	**137**	**157**	**357**	**246**	**248**	**268**	**468**
SLOPE	**1.002**	**0.990**	**0.995**	**0.984**	**1.007**	**0.987**	**0.999**	**0.981**

2.4 DIAPHRAGM INSTRUMENTATION

For this study, three external diaphragms on Z-connect were instrumented before they were installed on the bridge. The external diaphragms consist of angle members in a K truss configuration. All five members were instrumented with three strain gages at each cross section as shown in Figure 2.8. Figure 2.9 shows the locations of the instrumented diaphragms along the bridge. After each inner and outer girder was erected, the diaphragms were bolted and then welded to WT stubs that were bolted to the webs of the girders (Figure 2.10). Once the concrete deck hardened, the external diaphragms were removed by flame cutting the WT stubs (Figure 2.11).

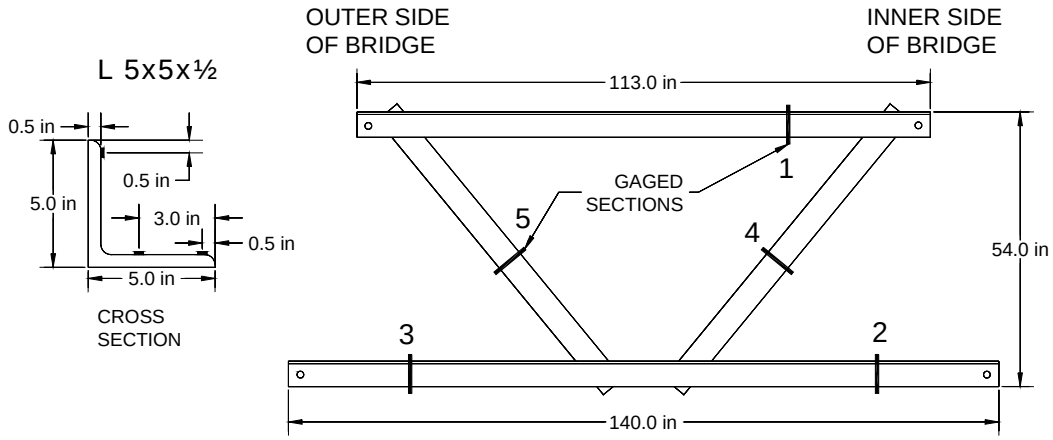

Figure 2.8 Instrumented External Diaphragm

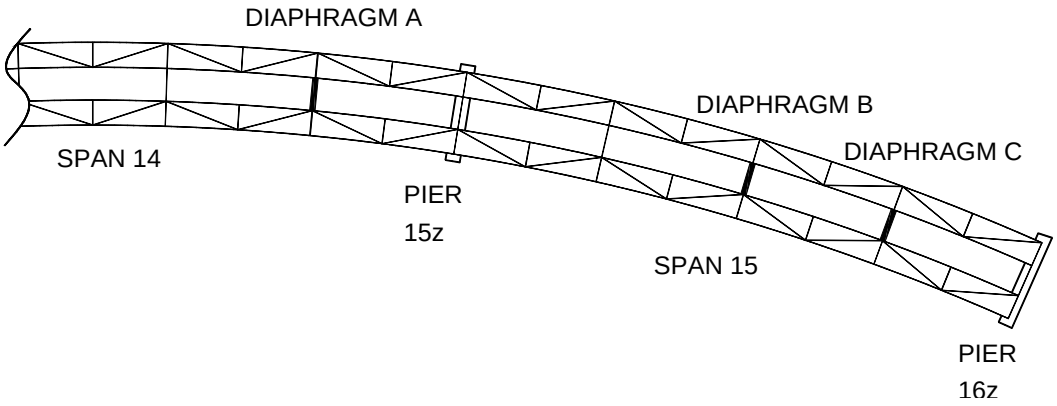

Figure 2.9 Instrumented External Diaphragm Locations

Figure 2.10 Installed External Diaphragms on Z-Connect

Figure 2.11 Flame Cut Removal of External Diaphragms

The instrumentation setup allowed for one multiplexer to be assigned per diaphragm. Since each multiplexer has 16 available channels and 15 channels were used as gages on the angle members, the last channel was used to read "dummy" gage. This gage was bonded to a steel plate that was placed inside a protective box. The plate would have zero change in stress since it was not attached to any other member. Since it is temperature compensated, the dummy gage should not have a change in resistance, even if the steel plate expands or contracts due to temperature variations. However, the dummy gage did have a slight change in strain measurement, although this change was small compared to strains in the bridge members. The dummy gage readings were subtracted from the other strain measurements since it was assumed that the same small error due to temperature was occurring in each gage.

The disadvantage of the strain gage layout was that there was no redundancy in each angle member. If one gage in a member did not function properly, the other two gages at the cross section were useless. Three strain measurements are needed at a cross section to find the strain at the centroid and the axial force.

2.5 DIAPHRAGM LAB TEST

Lab tests were performed on two external diaphragms that were used later for a different overpass. These diaphragms had slightly different dimensions from the diaphragms on Z-Connect, but the angle sizes were the same and the geometry was very similar. Figure 2.12 shows a picture of an identical diaphragm installed on K-Connect. In the lab, the diaphragm was bolted into a column and lifted at its end with an overhead crane equipped with a load cell. Each member had two cross sections instrumented for redundancy (the change in axial force in each

member should be constant along its length). The gaged sections and the load test setup are shown below in Figure 2.13 and

Figure 2.14, respectively. Unfortunately due to this setup, a perpendicular load on the diaphragm top chord resulted in a horizontal reaction on the overhead crane. This limited the amount of load that could be applied to the diaphragm since the crane would begin to roll when there was more than 2kips in the cable.

Figure 2.12 Installed External Diaphragm on K-Connect

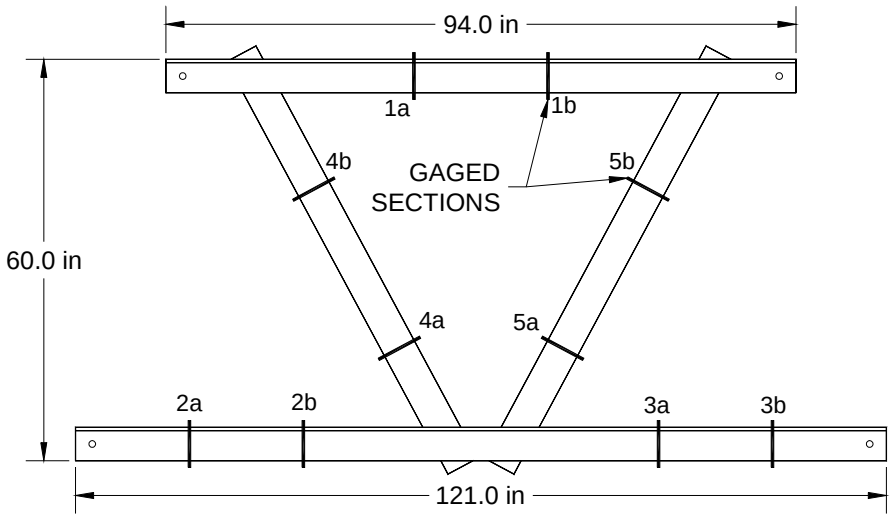

Figure 2.13 Instrumented Diaphragm for Lab Test

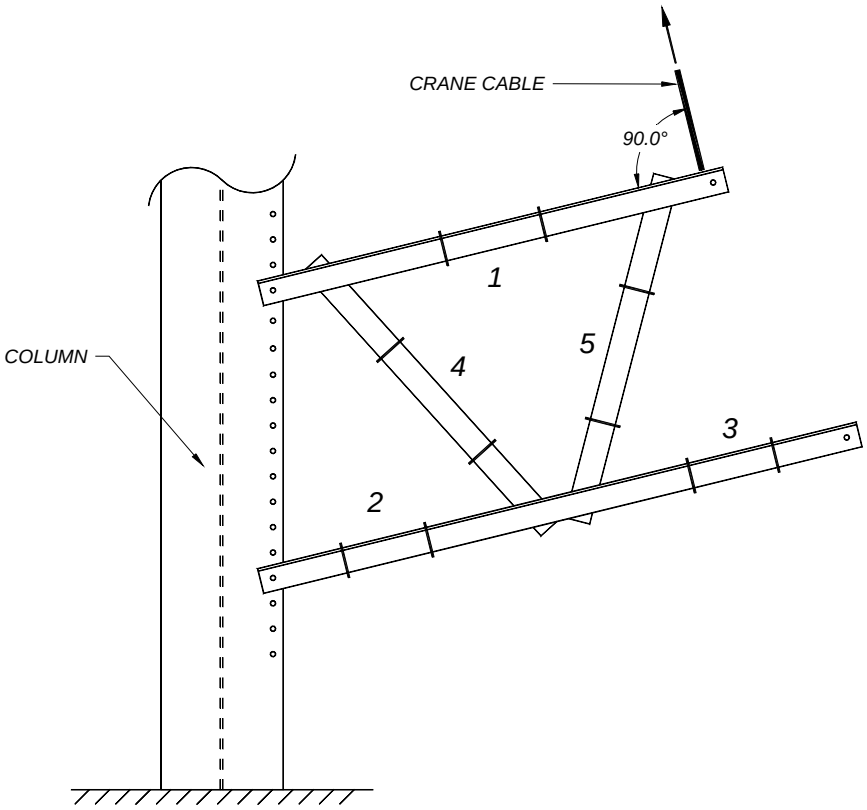

Figure 2.14 Diaphragm Lab Test Setup

2.5.1 Evaluation of the Test Data

Figure 2.15 shows the chord member results and Figure 2.16 shows the diagonal member results from the first lab test. The load increased in time at approximately 0.5kip increments. The maximum stresses during this test were very low however (less than 0.5ksi). The calculated force is very sensitive at this low stress and the two cross sections on the member are not always equal. In other words, a small error due to noise in the system makes a big difference at this level of stress. In member 1, the axial forces vary by as much as 0.8kips (0.2ksi). The axial forces in member 2 are equal at first, but then a small shift occurs midway through loading. This discrepancy shows the sensitivity of the analysis to noise in the system. For example, member 3 is a zero force member in this lab test, but axial forces up to 0.2kips were measured for this member. At this level of load, 0.2kips is a measure of the reliability of the axial force measurement from the strains in the member. The diagonals in this lab test show better correlation than the other two members. Also, it is apparent that the compression in one diagonal is almost equal to the tension in the other diagonal as expected.

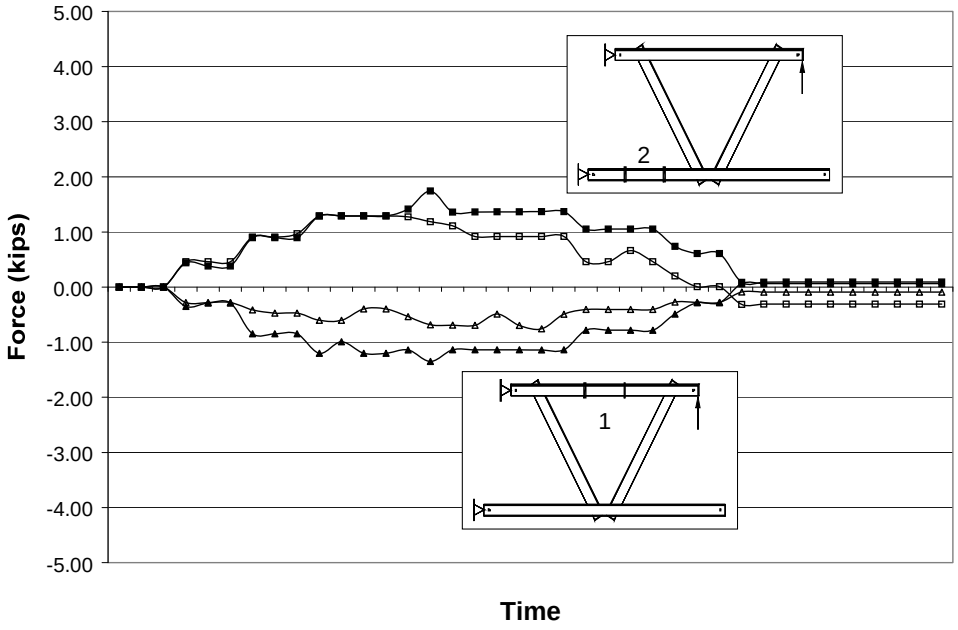

Figure 2.15 Diaphragm Lab Test 1 Results - Chords

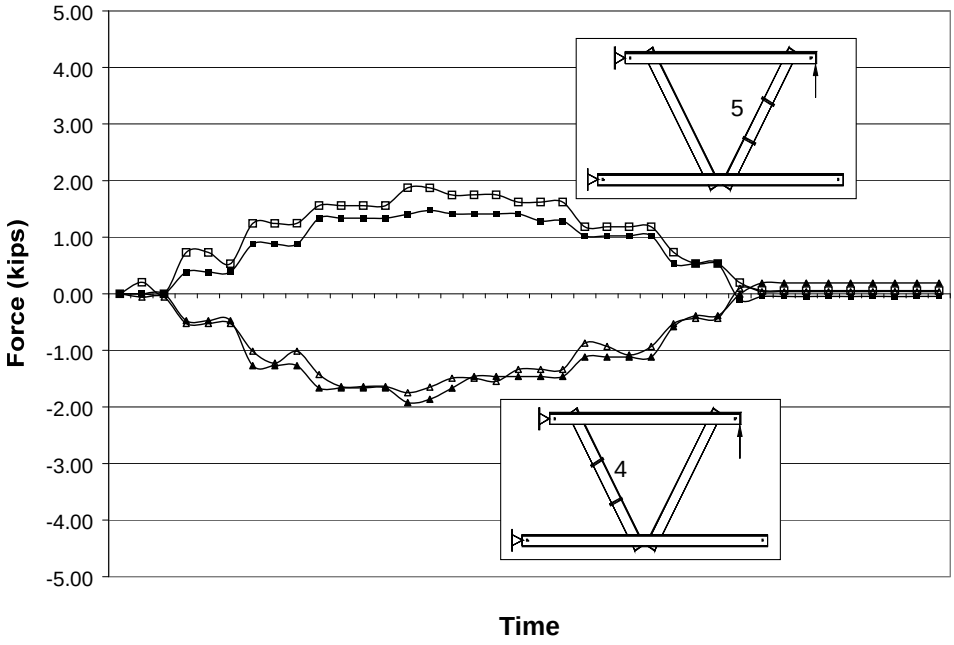

Figure 2.16 Diaphragm Lab Test 1 Results - Diagonals

From the test of the second diaphragm, the chord results (Figure 2.17) and the diagonal results (Figure 2.18), show less correlation between the two cross sections than in the first test. Member 2 shows good correlation between the cross sections, but the other members have a considerable difference. There are significant variations in forces especially in the diagonals during this test. The applied loads during test 2 are a little higher than in test 1, but the stresses in the members are still somewhat low (less than 1ksi).

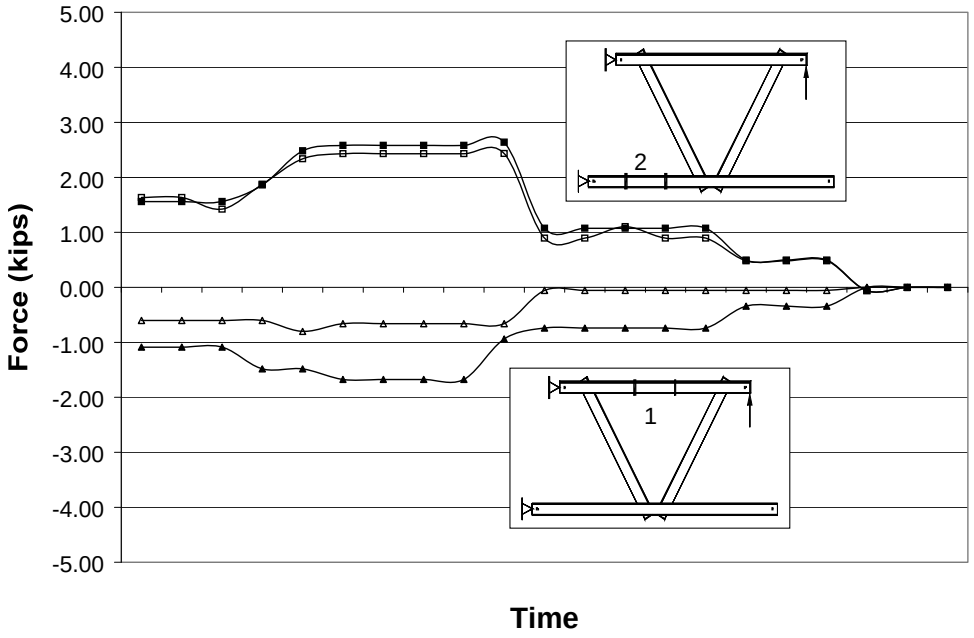

Figure 2.17 Diaphragm Lab Test 2 Results - Chords

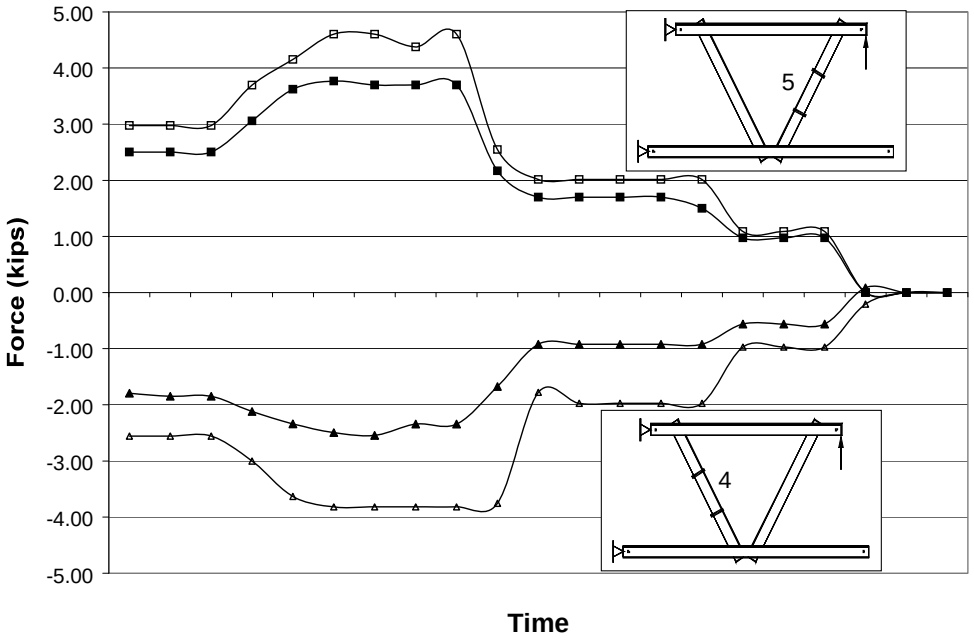

Figure 2.18 Diaphragm Lab Test 2 Results - Diagonals

Another reason why there may be some discrepancy in the measurements is because there is eccentric shear in the angles that produce some torsion and bending. This causes a large variation in stress along a cross section, so a very small error in the location of the gage can have a large effect on the axial force prediction. During the laboratory load test, for example, a member has a microstrain distribution as shown in Figure 2.19. If gage 1 has a location error of 1/16 in, the axial force calculation for the member changes by 10%.

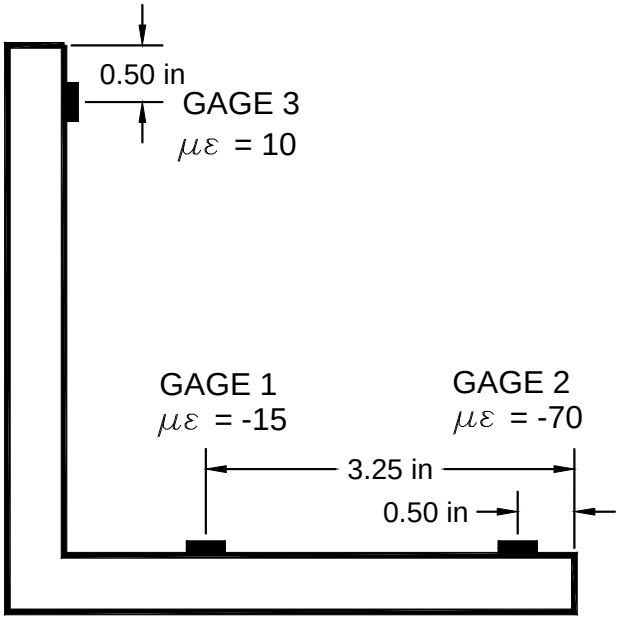

Figure 2.19 Microstrain Distribution Along Angle Cross section

2.5.2 SAP Model of External Diaphragm

To check the accuracy of the axial load measurements during the lab tests, SAP2000, a structural analysis program, was used to model the diaphragm. The diaphragm was modeled as frame elements with rigid connections since the angles were welded along one leg. The frame would need to be analyzed in 3D if out-of-plane bending moments were to be calculated, but the model was used to primarily to find the member axial forces, so a 2D analysis was used. The

connections to the column were modeled as pins (allowed end rotation) since only a single bolt was used for each angle. To some extent the axial forces changed if the column connections were modeled as pins or as fixed. There was considerable change in the axial forces, especially in the diagonals, if the ends of the angles were pinned or fixed. This probably contributes to the difference between the predicted and measured results.

Figure 2.20 shows the results from the SAP analysis for models with different connection stiffness. The connections to the columns were either modeled as pins or semi-fixed. The term "semi-fixed" in this analysis represents the column connection as a 5 in long angle member with the moment of inertia reduced by 90%. The ends of the reduced member were completely fixed. This is an approximation to take into account the small amount of fixity by the tightened bolt. The angle-to-angle connections were modeled as either pins, fixed, or semi-fixed, where "semi-fixed" indicates a 5 in long angle member with the moment of inertia equivalent to one leg of an angle ($I = 5.2\ in^4$).

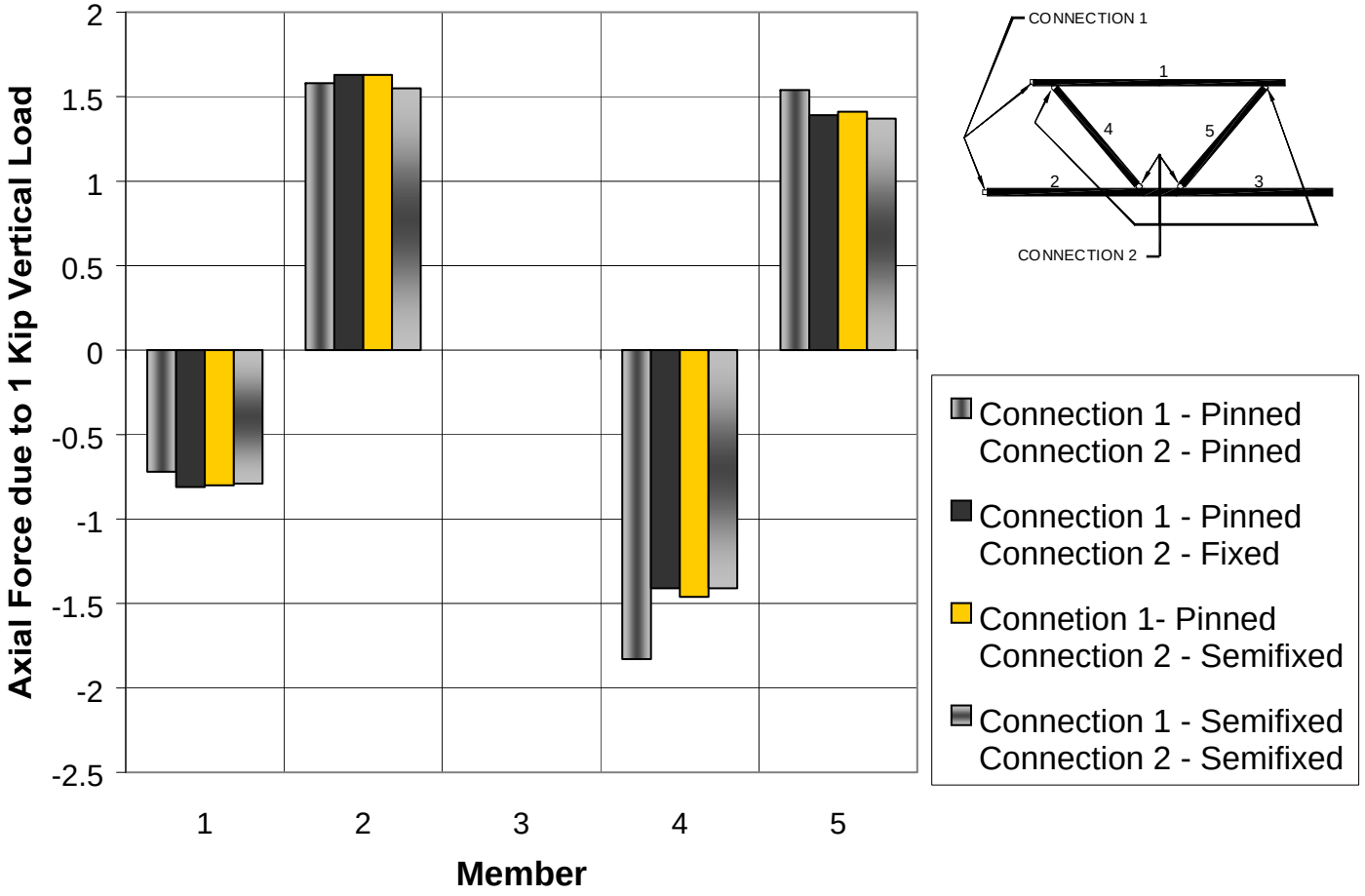

Figure 2.20 SAP Model Results for External Diaphragm

The SAP model forces and the measured axial forces are compared in Figure 2.21. The SAP results are from the model that includes semi-fixed connections at all ends of the angles. The displayed forces in the figure are due to the maximum applied loads on the diaphragms in the lab. The diagonals from test 1 correlate fairly well with the SAP predictions. In test 2, the diagonals do not match up as well and there is also more variation of measured force along the member.

The top chords of both diaphragms have one cross section that correlates well with the predicted forces. The other cross section on these members might have a bad gage, hence the large variation in force measurement. For the bottom chords of both diaphragms, there is little variation in the axial force measurements at both cross sections. However, the predicted forces underestimate the measured forces significantly. To maintain static equilibrium with these small bottom chord forces, a very large moment would be required at the single bolted ends of the angles (Figure 2.22). This is not very realistic and the measured forces are probably underestimating the true force in these members during the test.

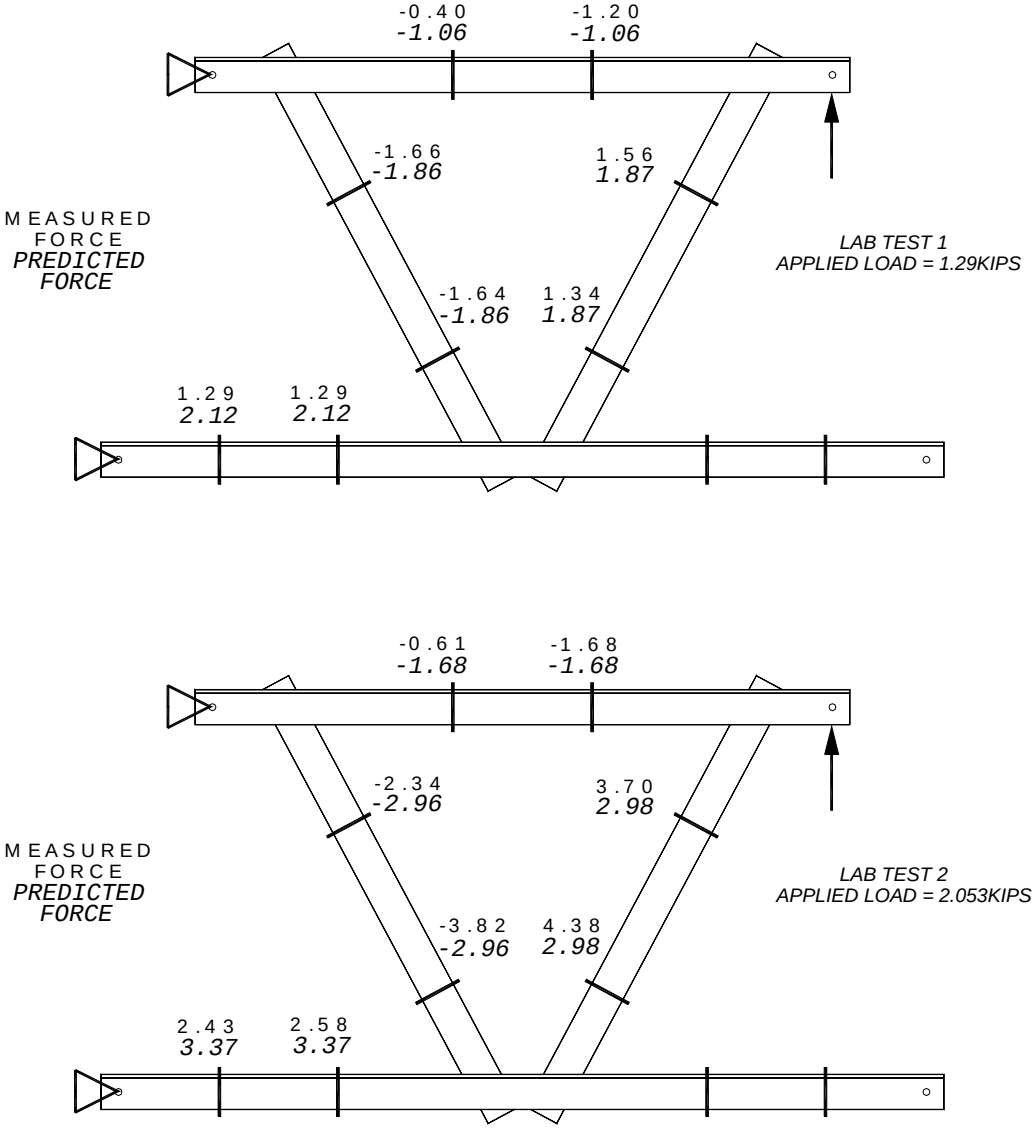

Figure 2.21 Diaphragm Lab Test – Measured VS Predicted Forces

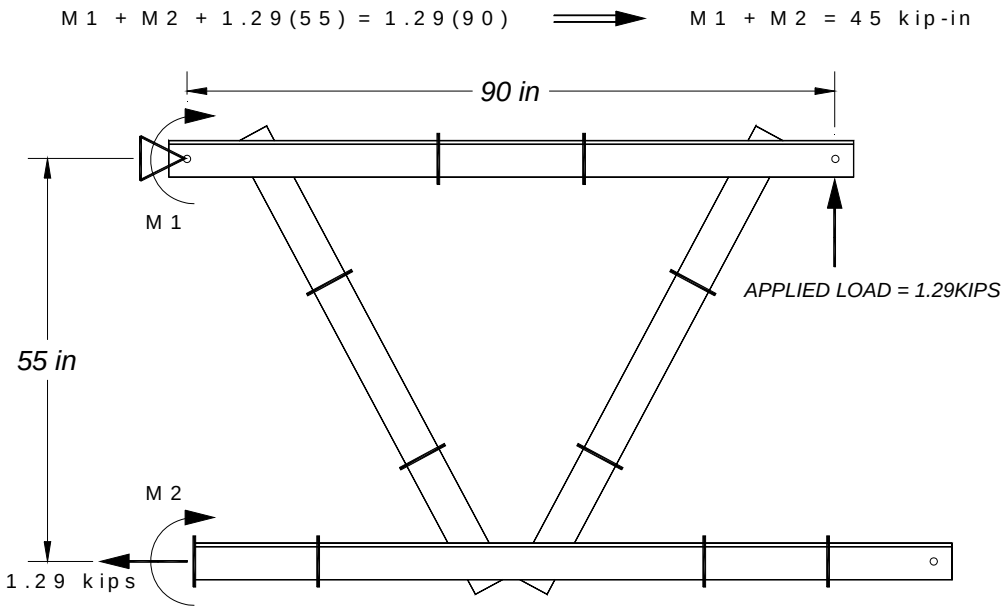

Figure 2.22 Equilibrium Calculation of External Diaphragm

2.6 SYSTEM CALIBRATION

Since the research project was constrained by the bridge construction schedule, the data acquisition system had to be quickly installed. The tight schedule did not allow for time to calibrate the system in the lab. Instead, the entire system was calibrated in the field once it was installed.

As mentioned earlier in chapter 1, a load test was performed on the girders before the concrete deck was poured. A crane lifted on the top flanges of the steel girders, creating an upward point load on the curved bridge. During this load test, a majority of the measurements taken by the data acquisition system had an error. The error was discovered shortly after the load test, but the system had to be calibrated first before correcting the problem.

The error occurred in the system because the current capacity of the 21X was exceeded. Some of the five multiplexers had to share the three available ports that were used for the full bridge excitation. Multiplexers A and B shared

one, multiplexers C and D shared another, and multiplexer E used the last port by itself. At multiplexers A, B and C, the excitation was applied to all 16 gages on the diaphragms simultaneously, while each channel had an individual signal. All of the full bridges on multiplexer A and B (32 total) were excited at the same time with 2V while one reading was taken. This parallel arrangement of gages resulted in very small total resistance. Since $I = V / R$, where I is the current, V is the voltage, and R is the total resistance, the current required for a certain voltage increases as the resistance decreases. The current capacity of the 21X was exceeded when too many gages were arranged in parallel, resulting in a smaller excitation voltage across the full bridge.

The system was calibrated by checking several channels on each multiplexer with a strain calibrator in place of the full bridge. Each full bridge needed to be replaced instead of only the gage since the completion resistors were not accessible. These calibrations were then used to back out the real strains from the load test data. The system was rewired by using a separate excitation for each member; therefore only 3 gages were excited at the same time. Lab tests discussed in the following section showed that this arrangement would solve the problem. The correction factors were only applied to the results for the crane load test.

2.7 LAB CALIBRATION TEST

Lab tests were also performed on a 21X by hooking up the calibrator in parallel with a variable resistor. This simulated the error in the field and verified the cause of error. The setup and results for the test are shown in Figure 2.23 and Figure 2.24.

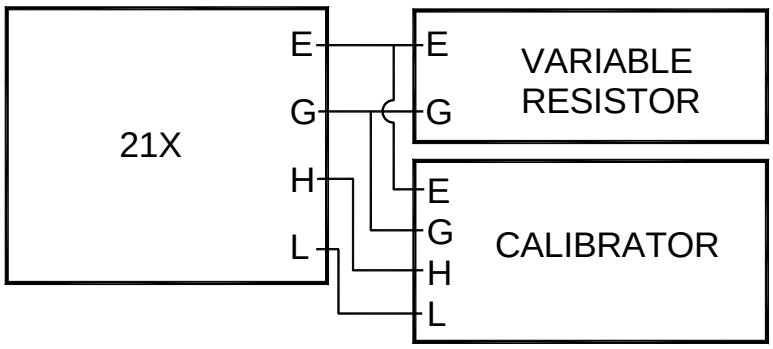

Figure 2.23 Lab Calibration Test Setup

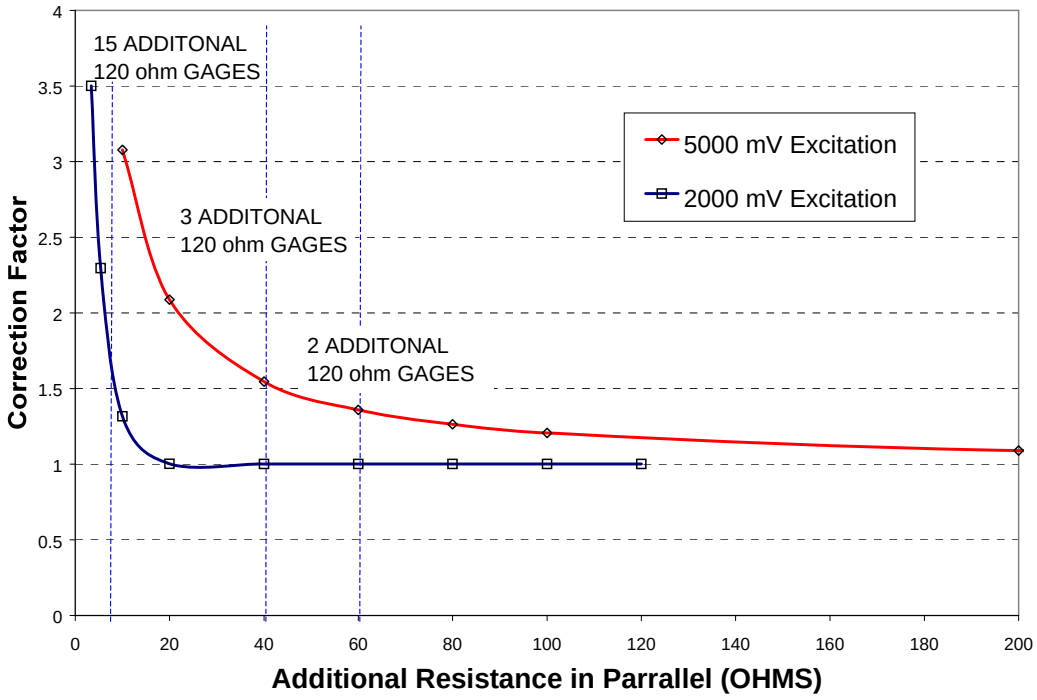

Figure 2.24 Calibration of 21X (120 ohm Gage)

The calibration factors from the lab test correlated very well with the error in the field using the 1550A Strain Indicator Calibrator. This verified that the simultaneous excitation was the source of error in the system. The lab test also showed that applying the correction factors to the field measurements would yield

the true strain results. The correction factor varied depending on how many gages were functional at the time of the crane load test. Also, there was no error (Correction Factor = 1) if more than 20ohms of resistance were in parallel when using a 2000mV excitation.

2.8 TOP LATERAL INSTRUMENTATION

After the girders were erected, strain gages were attached to four top laterals near pier 16z. The first two laterals on the inner girder and the first two laterals on the outer girder were gaged. Each lateral was instrumented at two cross sections with three gages (Figure 2.25). Since the axial force in the laterals should be constant throughout the length of the member, the two gaged cross sections added redundancy to the measurements.

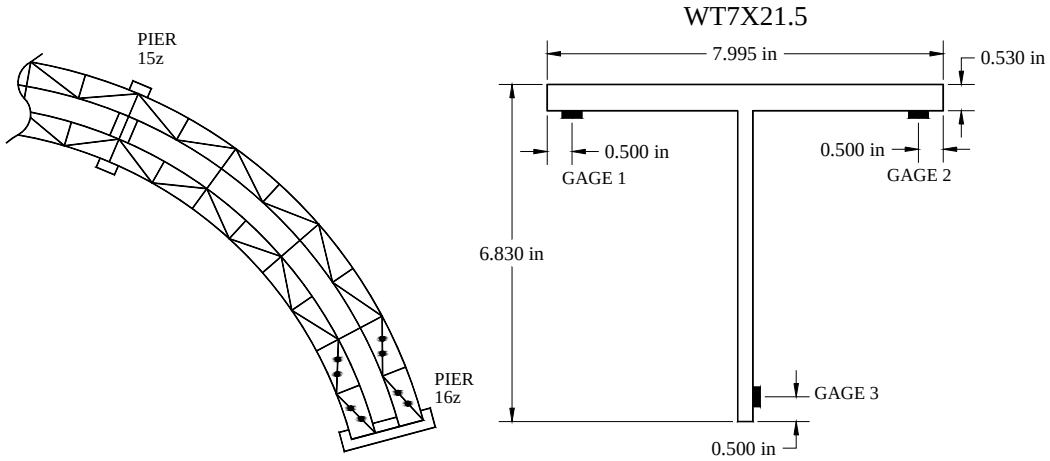

Figure 2.25 Instrumented 16z Top Laterals

Multiplexer D controlled the outer top lateral gages while multiplexer E was used for the inner top laterals. Unlike the diaphragm multiplexers, the excitation was not commoned for the individual gages for the top laterals. However, since the excitation port on multiplexers C and D was shared, the excitation sent to the outer top laterals was reduced from the resistance of the

diaphragm gages. No correction was needed for the inner top laterals since only one gage was excited at a time.

An identical gage configuration for top laterals was used on the opposite side of the bridge. These four laterals (Figure 2.26) were instrumented after the crane load test, but before the concrete pour. The readings for these laterals were taken on a separate 21X system. No correction factors were needed for these laterals.

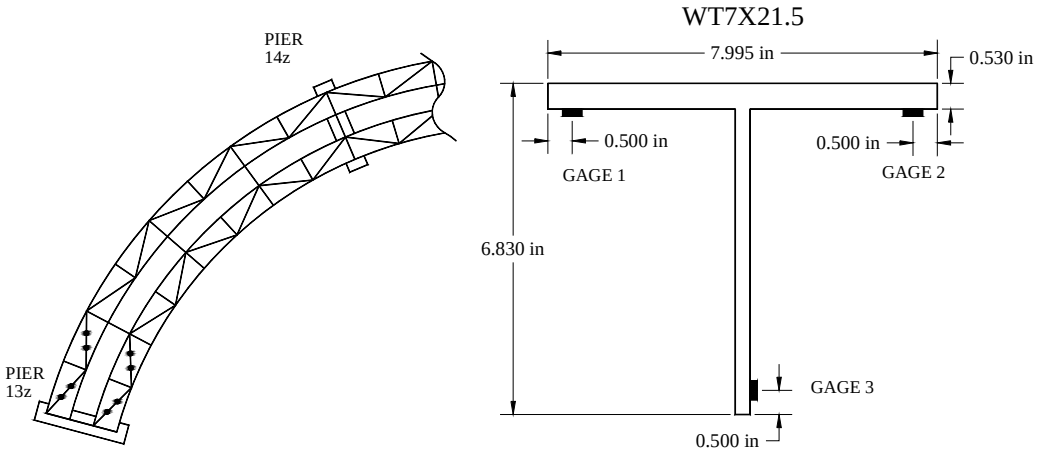

Figure 2.26 Instrumented 13z Top Laterals

2.9 SUMMARY

Several lab tests were performed to determine the reliability that could be expected in the field data for the external diaphragms. The diaphragms studied for this bridge had only one cross section instrumented per member, leaving no redundancy. In an ideal truss, the sum of axial forces at a joint can be used to check equilibrium. This could be used as a check of the measured forces, but in the welded diaphragms, equilibrium cannot be reached unless the shears at the cut sections are included in the summation of forces.

The tensile test of a single angle in a test machine showed good correlation between measured and applied loads. However, the tests on the diaphragms did not show nearly the same precision. This is due to several factors, including much lower member stresses and more bending in the angles. For both diaphragm tests, only one out of four members (Figure 2.21) in compression show good correlation between its two cross sections. In general, the tension members show better correlation between cross sections although they do not correlate well with the SAP model. It was found that the axial forces in the SAP model varied, depending on the fixity of each angle at the ends.

The diaphragm data is even less reliable during the crane load test since there were errors due to current loss. Although the data can be corrected with calibration factors, there are small uncertainties in the calibration factors. The measured data in Chapter 3 has been corrected as outlined in Section 2.7. On the average, the diaphragm data has a confidence level of about 15-20% for the crane load test and of about 15% for the remainder of the field studies. The reliability of this system is not very good and probably could have been improved by fabricating and instrumenting diaphragms that are made of concentrically loaded pipes (Zureick et al., 2000).

CHAPTER 3
Crane Load Test

3.1 DESCRIPTION AND PURPOSE

On March 7, 2000, a full-scale load test on the trapezoidal box girder bridge was performed. TxDOT and Abrams agreed to perform the test by lifting up on a portion of one girder using a crane equipped with a load cell. The test was a significant part of the research for two reasons. It provided a check of the reliability of the data acquisition system before the critical concrete deck pour. Also, the test provided a chance to evaluate the correlation between the finite element model and field measurements with a known point load. In contrast, the concrete pour is an imprecise, variably distributed load.

There was no type of decking attached to the steel girders at the time of the load test. The crane lifted up on the outer flange of the outer girder near pier 16z as shown in Figure 3.1. The bridge was loaded and unloaded twice at approximately 5 kip increments up to 20 kips. Figure 3.2 shows the crane attachment used to lift the girder.

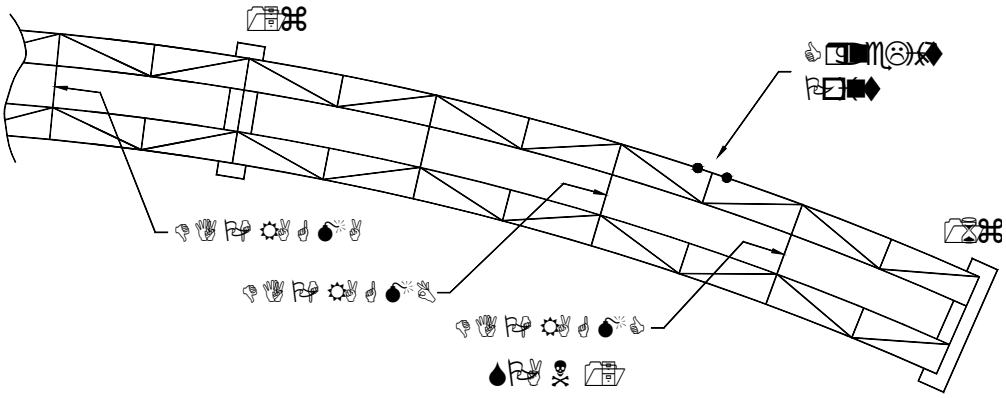

Figure 3.1 Crane Lift Points

Figure 3.2 Crane Attachment

3.2 TOP LATERAL CRANE LOAD TEST RESULTS

Since the crane lifted only on a single girder, the forces had to be distributed through the external diaphragms from the outer girder to the inner. By examining the forces in the top lateral truss system in both girders, the distribution of load between the girders can be demonstrated. Since two cross sections on each lateral were instrumented (Chapter 2), there was redundancy in the axial force measurements. Figure 3.3 shows a typical graph of the axial forces of two top laterals with time during the crane load test. The forces at both cross sections on a lateral are nearly identical and the plots are on top of each other. This gives considerable confidence in the top lateral measurements.

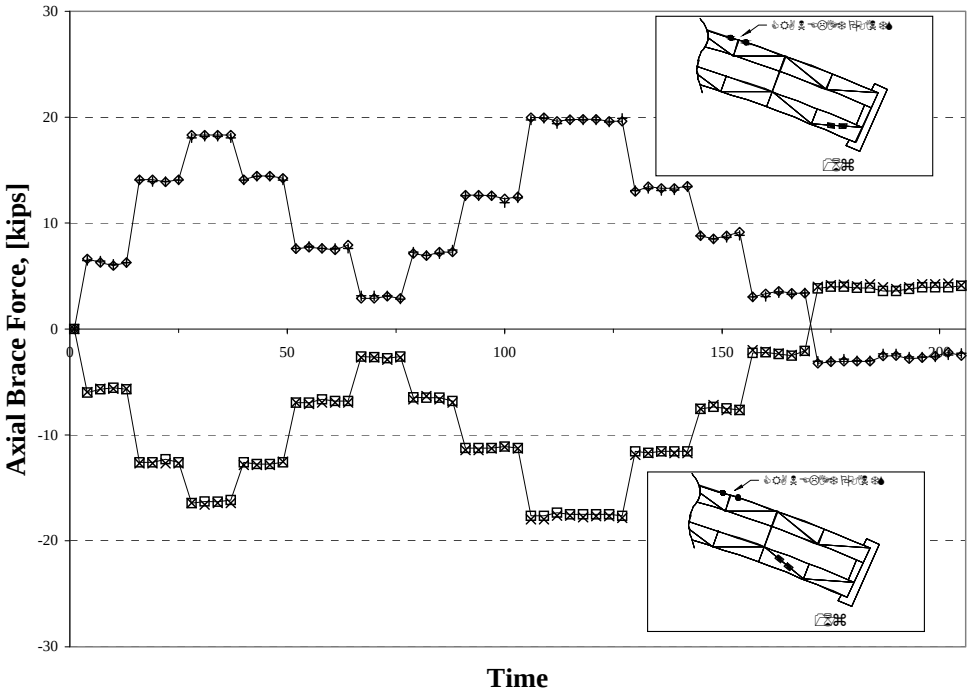

Figure 3.3 Inner Girder Top Laterals – Crane Test Force VS Time

The force measurements stay nearly constant as the crane is held at the same load. However, the forces in the laterals do not go back to zero once the

crane releases the girder. The reason for this is unknown although a similar feature occurs in the outer girder laterals. This may be due to twists in the girders from temperature effects since the entire crane test took approximately one hour. A force change of 5kips can occur within that time since the load test occurred between 10am-11am, a period in the day in which the girder has a high temperature gradient. It was typical that the top laterals would change roughly 10kips in axial force from morning to night due to normal temperature changes.

Figure 3.4 through Figure 3.7 show plots of the applied crane load VS the measured axial force for each lateral. The graphs show data as the bridge is loaded and unloaded twice. Ideally, these plots should be linear. The plotted points are the average of the two cross sections for each lateral. A linear trendline is also shown on the graphs as a bold line. This trendline does not pass through the origin of the plot due to the data during unloading. The important aspect of the trendline is the slope since it represents change in force of the lateral with the applied load. This slope was used for further comparisons to the FEM. The correlation coefficient (the proportion of the variance in y attributable to the variance in x) for each trendline was calculated. If the data were perfectly linear, then this value would be equal to 1.0. The lowest coefficient was 0.98, which shows that the trendlines represent the data very well.

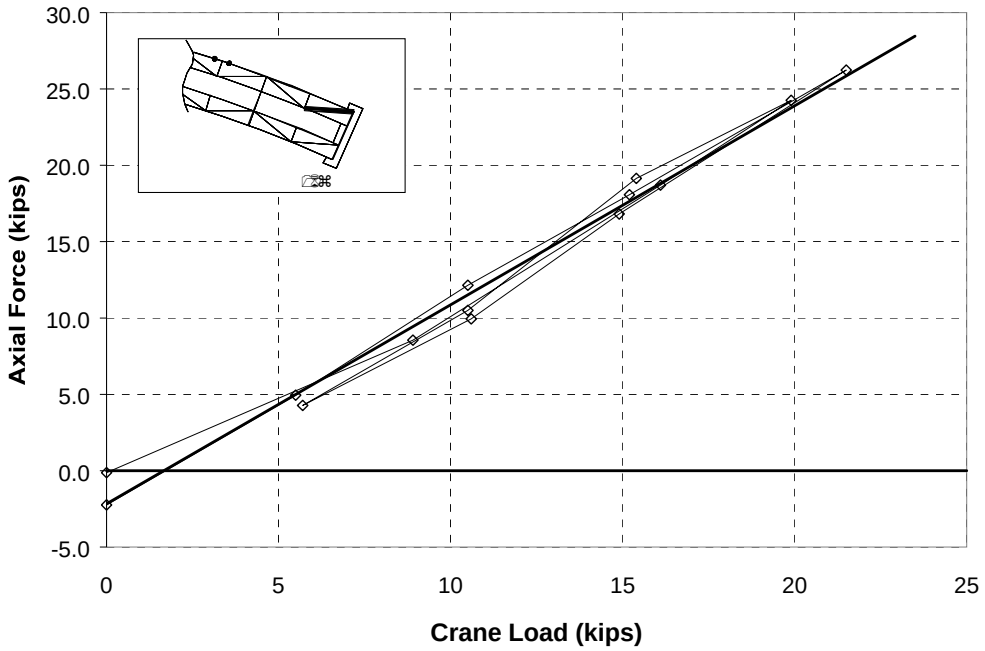

Figure 3.4 Outer 1st Lateral Force VS Crane Load

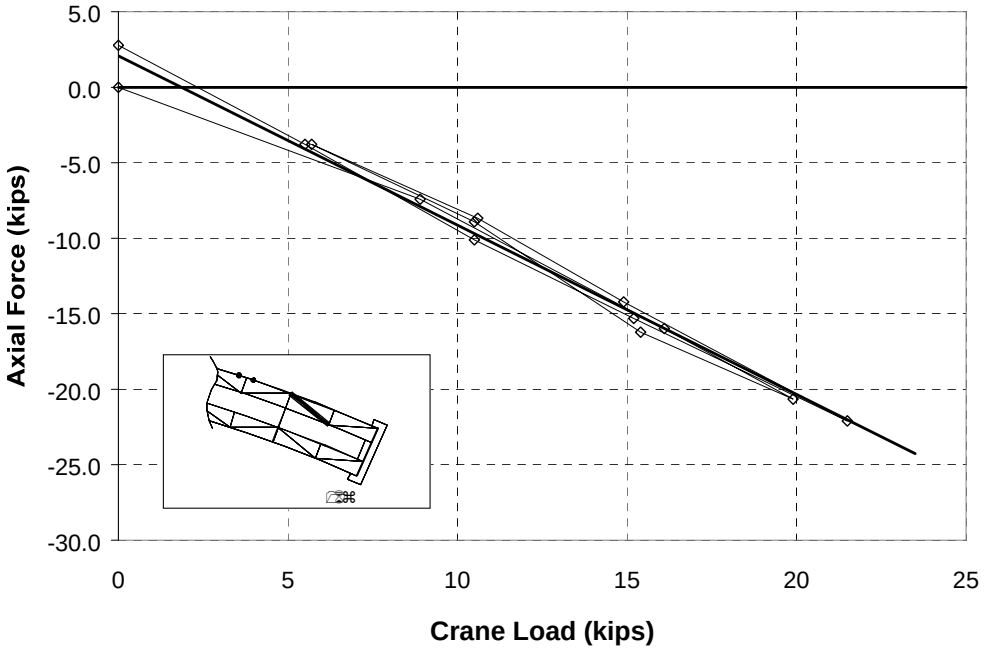

Figure 3.5 Outer 2nd Lateral Force VS Crane Load

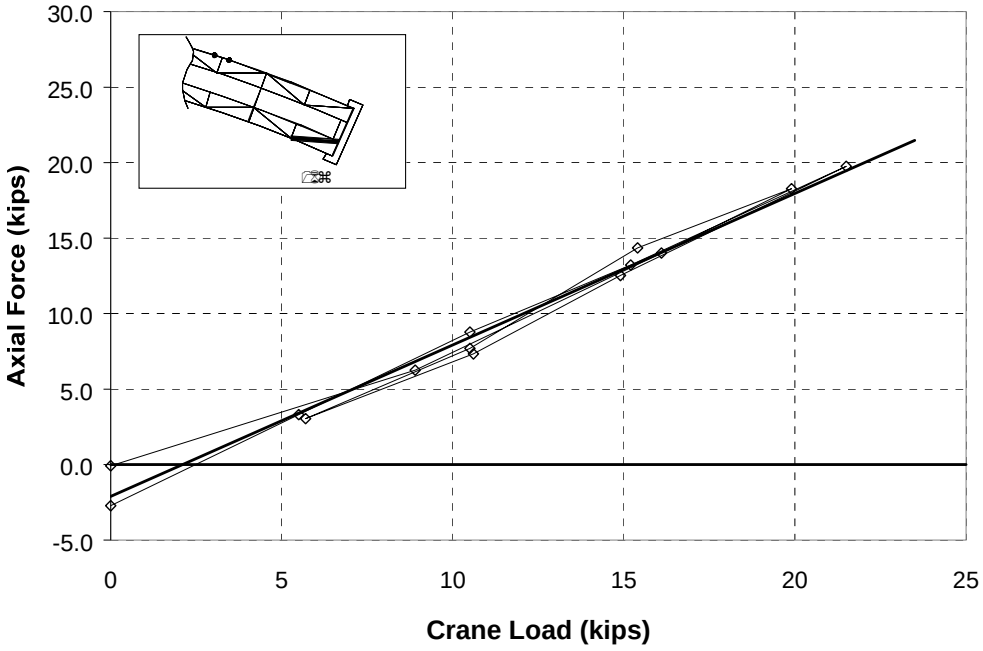

Figure 3.6 Inner 1st Lateral Force VS Crane Load

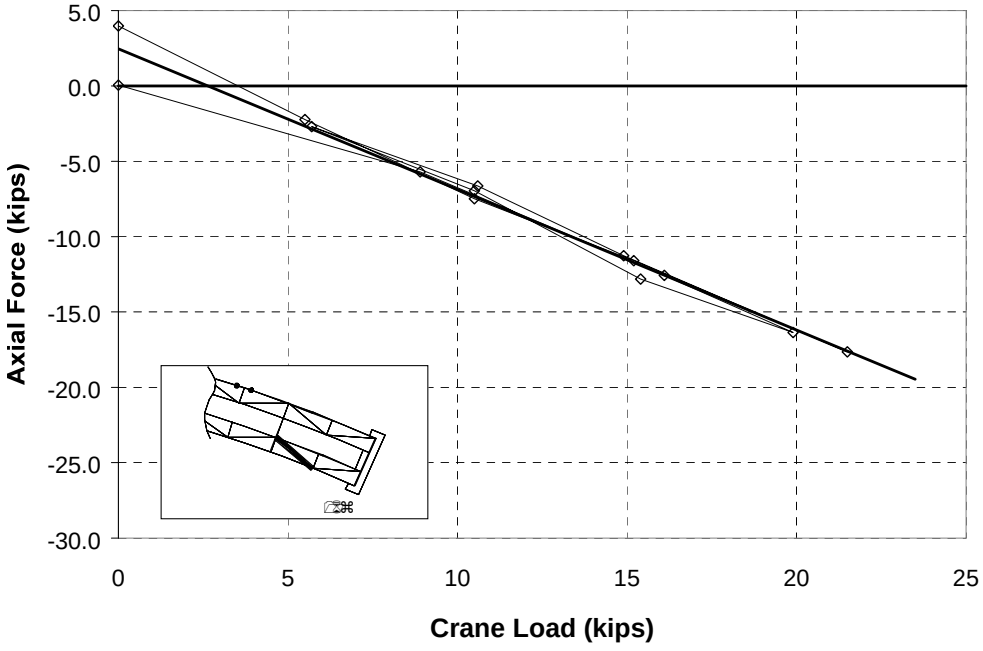

Figure 3.7 Inner 2nd Lateral Force VS Crane Load

Using the equation $F_{member} = \beta \times Load_{applied}$, where β is the slope of the trendline in Figure 3.4 through Figure 3.7, the measured force in each lateral was compared to the predicted force from the FEM. The results for the measured and predicted top lateral forces for an applied crane load of 10kips are shown in Figure 3.8. The axial forces predicted for the top laterals in the 1st panel are greater than in the 2nd panel. This is due to a higher torsion at the ends of the girder. Pulling upwards on the girder creates tension in the 1st laterals and compression in the 2nd panel laterals due to their orientation.

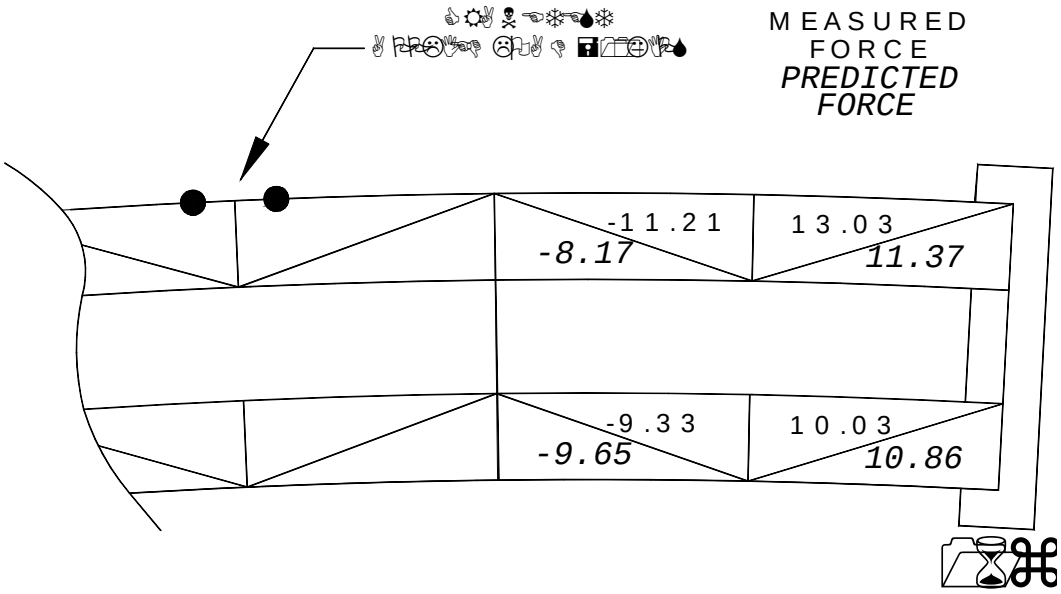

Figure 3.8 Top Lateral Crane Test Results

An interesting effect occurs within the top laterals under this loading. The 1st outer lateral is predicted to have a higher axial force than the inner lateral, but the 2nd outer lateral is predicted to have less force than the inner. This is probably because there are two components to the resultant axial force: a torsional component and a bending component. Bending creates tension in all of the top

laterals as the girders are lifted. Following the moment diagram, the 2nd panel laterals have a higher stress due to bending than the 1st panel. Also, the load is applied on the outer girder so the eccentricity of the load is much smaller than for the inner girder. Therefore, the axial force in the 2nd panel lateral for the inner girder is primarily due to torsion (compressive) while the 2nd panel lateral for the outer girder has a torsional (compressive) and bending (tensile) component.

The measured results show good correlation with the predicted results, although both outer girder laterals had a higher change in axial force than the inner girder laterals due to the crane load. This means that there was less torsional distribution from the outer girder to the inner than predicted. The discrepancy in the distribution may be due to the reduction in stiffness of the external diaphragms at the connection detail to the box girder. This effect will be examined further in Section 3.3.2.

3.3 EXTERNAL DIAPHRAGM ANALYTICAL MODEL

To understand the behavior of the external diaphragms used on Z-connect, a computer model using SAP was created. The crane load was applied eccentrically on the outer box girder. This load can be converted to an equivalent vertical force and torsion at the centroid of the outer girder (Figure 3.9). The two components were examined separately in the SAP model to determine the expected diaphragm forces from each one.

The diaphragm was modeled as frame elements with ends that have half of the rotational stiffness as the angle member. This approximation was used to account for the one welded leg of each angle at all connections. The ends of one side of the diaphragm were fixed while the other side of the diaphragm was attached to a cross section of a box girder that could translate and rotate (Figure 3.10). The components of the box girder were modeled as rigid elements. Figure

3.10 shows the applied loading condition and schematic of the SAP model of the external diaphragm.

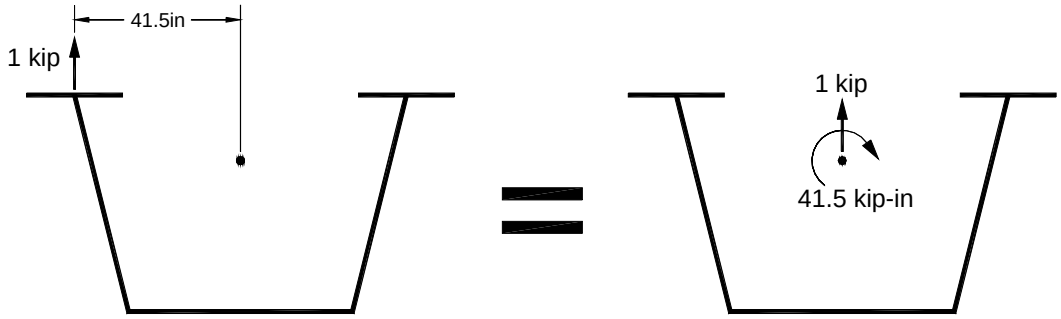

Figure 3.9 Applied Unit Load on External Diaphragm from Box Girder

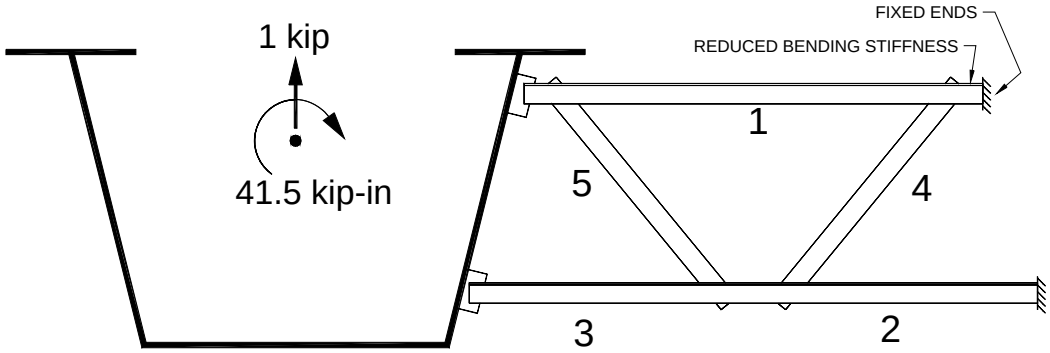

Figure 3.10 Schematic of SAP Model of External Diaphragm

The SAP model represents the forces in the external diaphragms as if all of the vertical load and torsion were distributed from the girder to the diaphragms. The true percentage of vertical load and torsion transmitted to the diaphragm is a function of (among other parameters) the diaphragm stiffness and the stiffness of the girders. If the girders were very stiff compared to the diaphragms, a majority of the load would stay in the outer girder. The measured results in the diaphragm will be compared to the FEM prediction by examining these percentages.

3.3.1 External Diaphragm SAP Model Results

The FEM described in Chapter 1 considered the entire curved girder, while the SAP model was only used to perform a more refined analysis of the external diaphragms. The results for the SAP model are shown in Table 3.1 for the forces due to an applied unit load on the outer flange of the outer girder.

Table 3.1 SAP Results on External Diaphragm

Load	Member 1	Member 2	Member 3	Member 4	Member 5
1 Kip Vertical Force at Tub Cent	-2.49	3.80	1.19	-1.69	1.68
41.5 Kip-in Torsion at Tub Cent	-1.11	1.11	1.12	0.00	0.00
Total	-3.60	4.91	2.31	-1.69	1.68

When only the vertical force is applied, member 5 goes into tension and member 4 goes into compression. To resist the horizontal thrusts from the diagonals, members 1, 2 and 3 also develop axial forces. For a torsional load on the girder, the diagonals have no change in axial force while the other members must react in equal and opposite direction to form a moment couple. The breakdown of the axial forces into the vertical component and torsional component will be used to compare the measured and predicted results for the external diaphragms.

3.3.2 Analytical Model of Diaphragm Connection Detail

As discussed earlier in Section 3.2, the external diaphragm connection detail to the girder may reduce the stiffness of the diaphragm. The ends of the

diaphragms are welded to WT stubs that are bolted to the webs of the girder as shown in Figure 3.11.

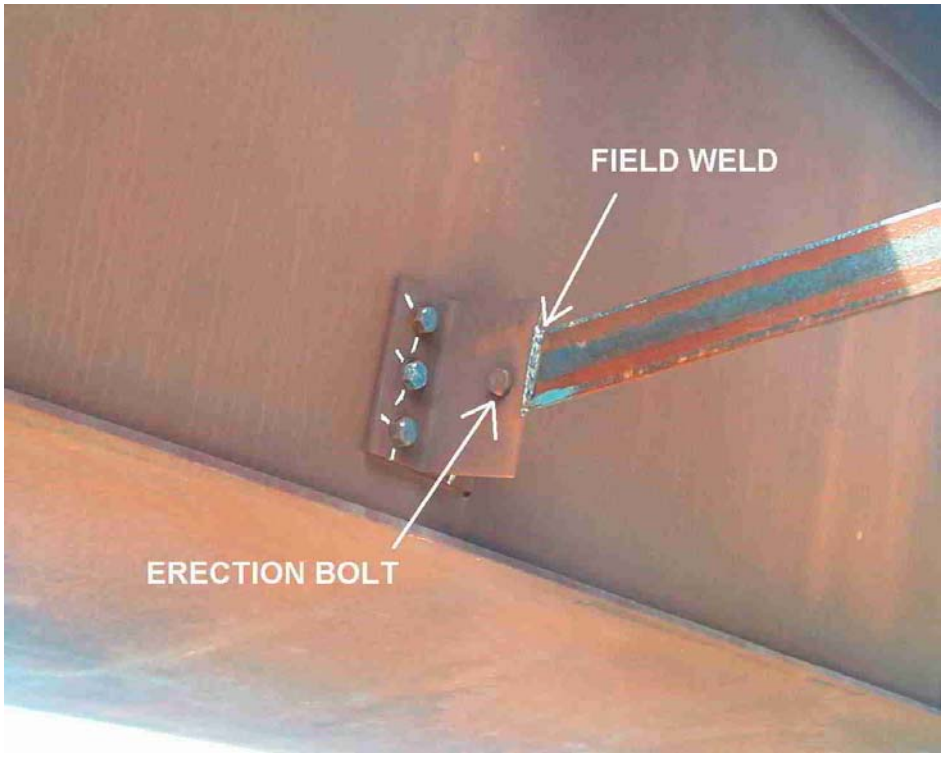

Figure 3.11 External Diaphragm Connection Detail

To investigate the role the connection detail stiffness played in reducing the stiffness of the diaphragm, a simple model was built using SAP. The model used the least conservative assumptions to determine the greatest possible stiffness of the connection, including the following details:

- Used the longest angle member on the diaphragm (110 in)
- Neglected axial deformation of bolts
- Assumed that the bolts completely fixed the WT stub at the edge of the bolt head
- Assumed that the entire WT stub acts as a single rigid beam element and that all distortions along its width were equal

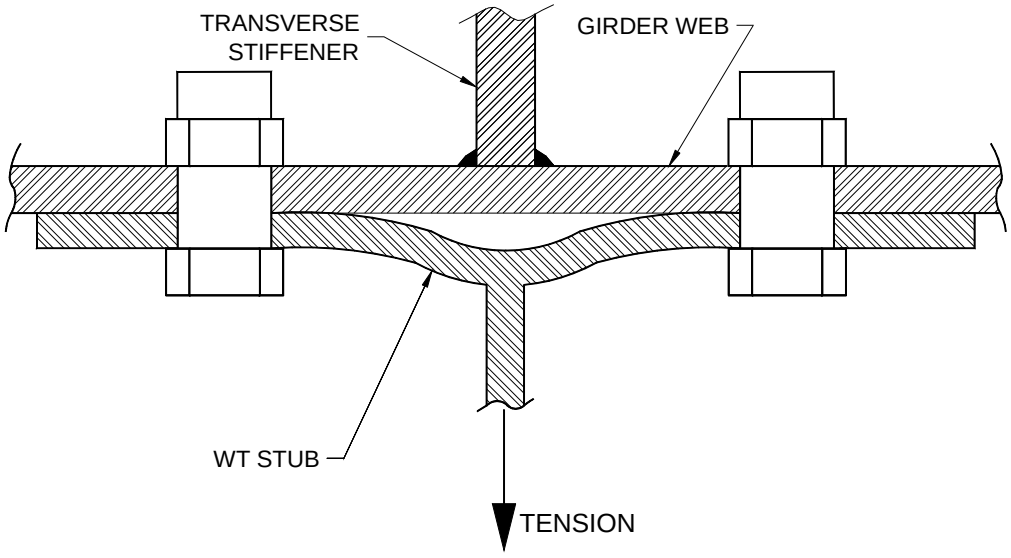

Figure 3.12 Distortion of WT Stub at Diaphragm Connection

The distortion of the WT would only occur when the angle is in tension, as it could pull away from the web. A schematic of this effect is shown in Figure 3.12. With the assumptions stated above in the SAP model, the axial deflection of the longest angle member increases by 50% due to the bending deformation of the WT connecting stub. This is a significant loss of stiffness in the diaphragm when the members connecting to the web are in tension. The stiffness of the connection detail has an even greater effect on the shorter members. This effect was not included in the analysis of the bridge; therefore the FEM may overestimate the predicted distribution from one girder to the other.

3.4 EXTERNAL DIAPHRAGM CRANE LOAD TEST RESULTS

All of the diaphragm data calculations in this section include the calibration factors discussed in Chapter 2. Diaphragm A (Figure 3.1) is on the opposite side of Pier 15z from the applied load and the forces in this diaphragm were very small during the test. Therefore, this section will only focus on the data

from the other two external diaphragms, which were very close to the applied load.

The force calculations for the diaphragms were not as reliable as the top lateral data since only one cross section was gaged per member, but there was some repeatability in the test results. Figure 3.13 through Figure 3.16 give an impression of the reliability of the diaphragm data. Two graphs are presented for each diaphragm; each graph represents a load and unload cycle.

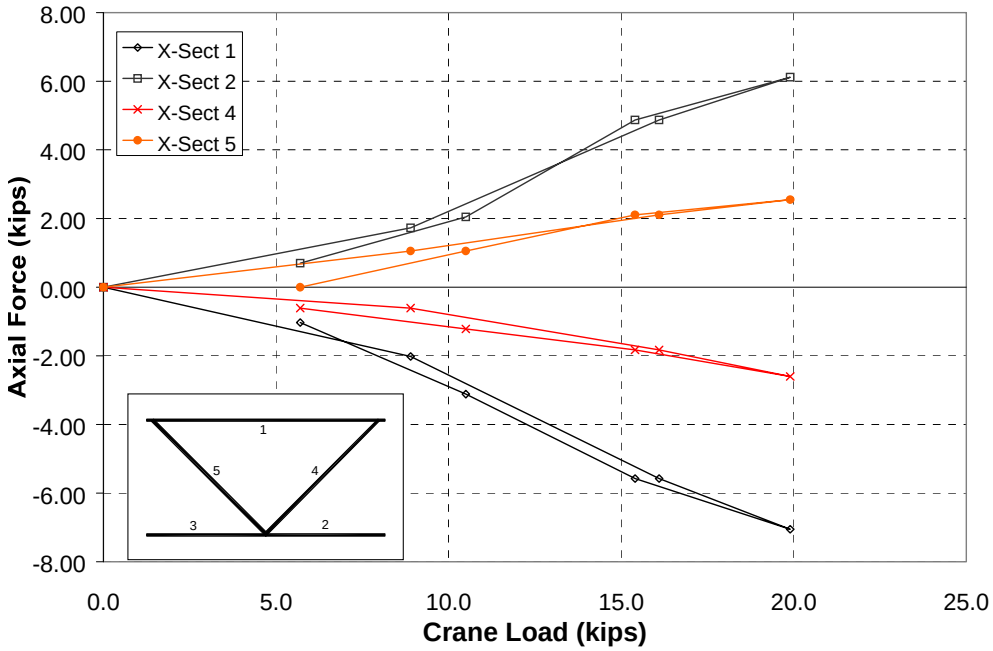

Figure 3.13 Diaphragm B Forces VS Crane Load 1

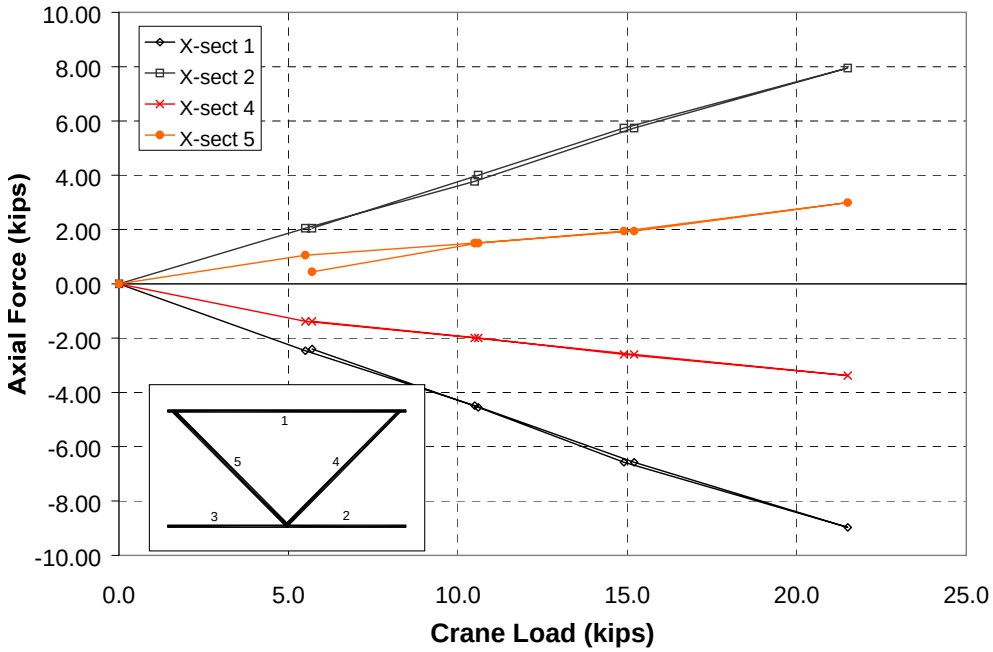

Figure 3.14 Diaphragm B Forces VS Crane Load 2

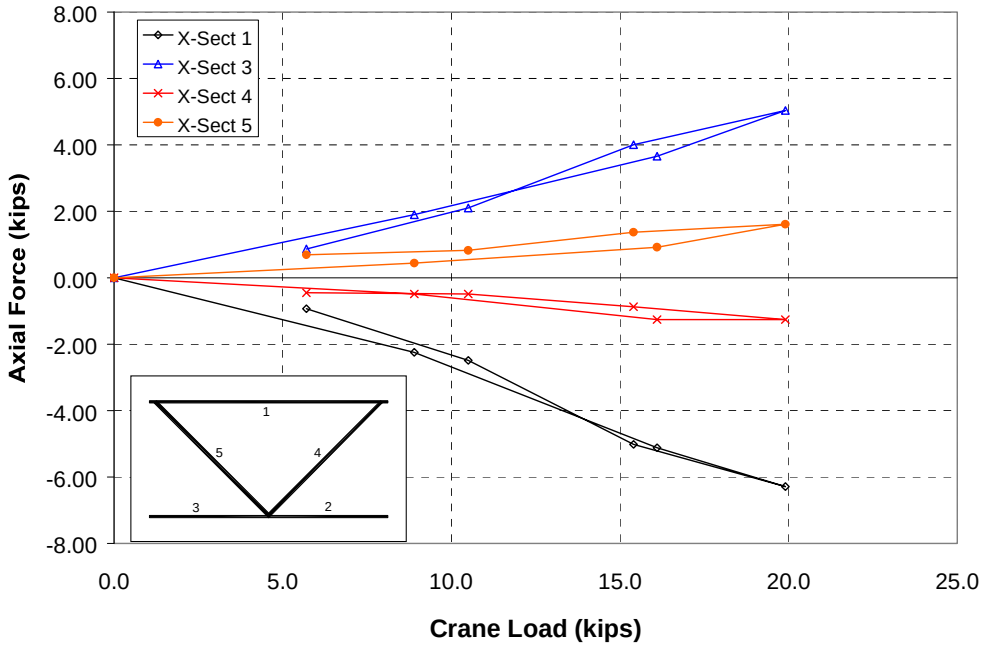

Figure 3.15 Diaphragm C Forces VS Crane Load 1

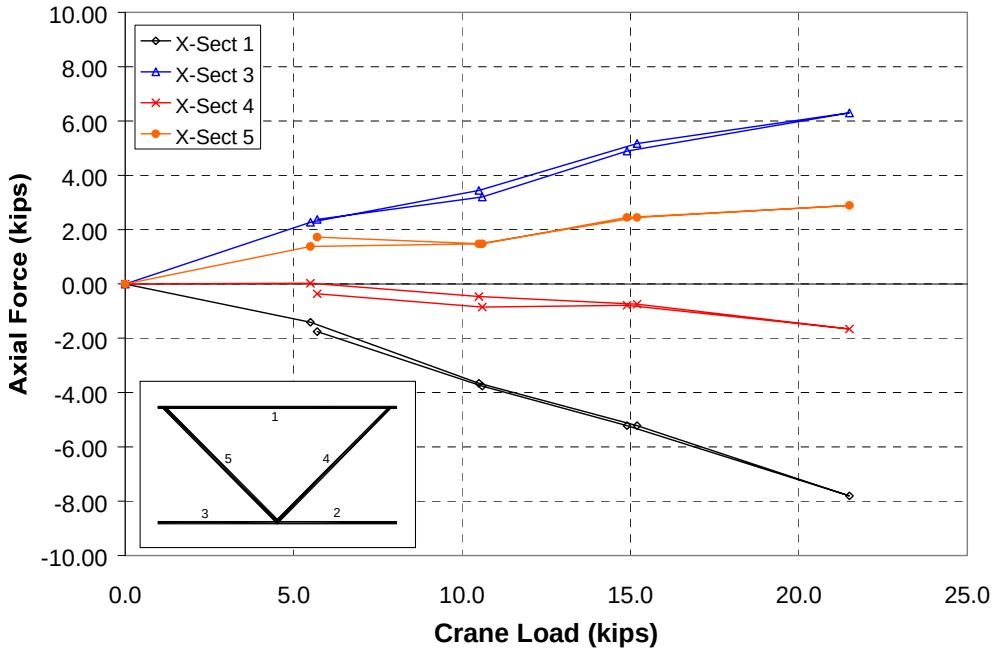

Figure 3.16 Diaphragm C Forces VS Crane Load 2

Figure 3.13 and Figure 3.14 do not show the results for member 3 on diaphragm B since this member had a bad gage. Similarly, Figure 3.15 and Figure 3.16 are missing the results for member 2 since it also has a bad gage. Since there are only 3 gages per member, if one gage does not function properly, the member's axial force cannot be calculated.

The graphs for each load and unload cycle were compared to determine the repeatability of the data. Similar to the analysis of the top lateral data, a best-fit linear trendline was created for each member and the slope of the trendline was used for the calculation of axial force due to a known crane load. The tabulated results of the slopes for the trendlines in Figure 3.13 through Figure 3.16 are shown in Table 3.2 and Table 3.3. The average slope of the trendline was used for all of the diaphragm force calculations. For example, the average slope for cross section 1 on Diaphragm B is –0.402. This means that the calculated compression in this member is 0.402 times the applied crane load.

Table 3.2 Diaphragm B Crane Test Results

	Slope of Best Fit Linear Trendline				
	Member 1	Member 2	Member 3	Member 4	Member 5
1st Load & Unload	-0.382	0.337	N/A	-0.130	0.146
2nd Load & Unload	-0.422	0.375	N/A	-0.149	0.136
Average Slope	-0.402	0.356	N/A	-0.139	0.141
% Difference in Slopes	10%	10%	N/A	13%	8%

	Member 1	Member 2	Member 3	Member 4	Member 5
Axial Force during 20 kip Crane Load = Average Slope x 20	-8.04	7.12	N/A	-2.78	2.82

Table 3.3 Diaphragm C Crane Test Results

	Slope of Best Fit Linear Trendline				
	Member 1	Member 2	Member 3	Member 4	Member 5
1st Load & Unload	-0.341	N/A	0.261	-0.065	0.074
2nd Load & Unload	-0.370	N/A	0.290	-0.074	0.122
Average Slope	-0.355	N/A	0.276	-0.070	0.098
% Difference in Slopes	8%	N/A	10%	12%	40%

	Member 1	Member 2	Member 3	Member 4	Member 5
Axial Force during 20 kip Crane Load = Average Slope x 20	-7.10	N/A	5.51	-1.39	1.96

The percent difference shown in the table is an indicator of the repeatability of the test data. Except for member 5 on Diaphragm C, every member has a repeatable slope of within 15%. Based on the lab tests discussed in Chapter 2, this is the reliability expected for these instrumented members. Some small error is also caused from the accuracy of the crane load cell. Typically, the members with higher stress changes had more repeatable data. Figure 3.17 shows the measured results for the diaphragms during the load test and compares them to the predicted results from the finite element model.

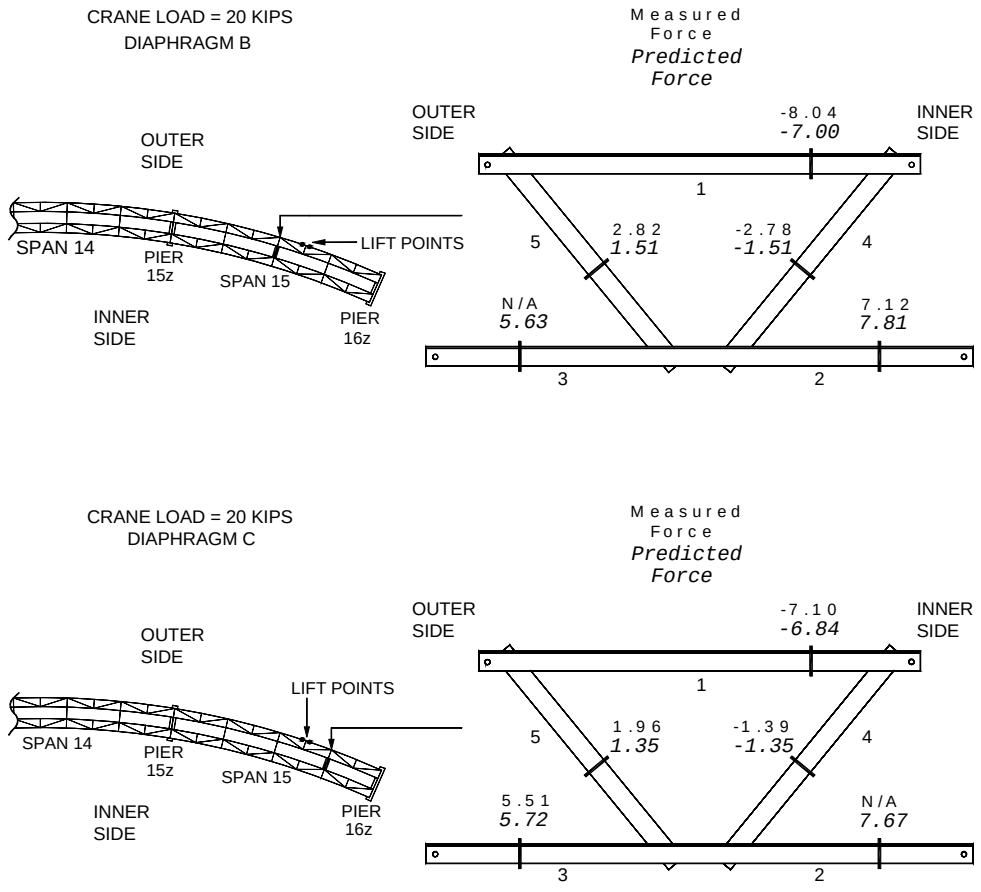

Figure 3.17 Diaphragm Crane Test Results

Considering the expected reliability of the external diaphragm data, the measured axial forces compare fairly well with the predicted forces. In diaphragm B, the measured diagonal forces are almost equal in magnitude, although almost twice than predicted. Since the diagonals do not see axial force from a pure twist of the girder, this diaphragm is probably transferring more vertical force than expected. One discrepancy in the measured results for diaphragm B is that member 1 is higher in magnitude than member 2. As seen in Table 3.1, a pure torsion on the girder would create forces of equal magnitude in these members and a vertical force on the diaphragm would create a higher axial

force in member 2. Therefore, the force in member 1 should never be greater than in member 2 for this type of loading. After taking a closer look at this data, it was found that one of the gages on member 1 behaved inconsistently during the load test and went out of range some time later. The force calculation for this member is not as reliable as the others.

Instead of only comparing the measured and FEM predicted forces of each member in a diaphragm, the % of girder torsion and vertical load transmitted through the diaphragm was investigated. Figure 3.18 shows a schematic of how the diaphragms were analyzed.

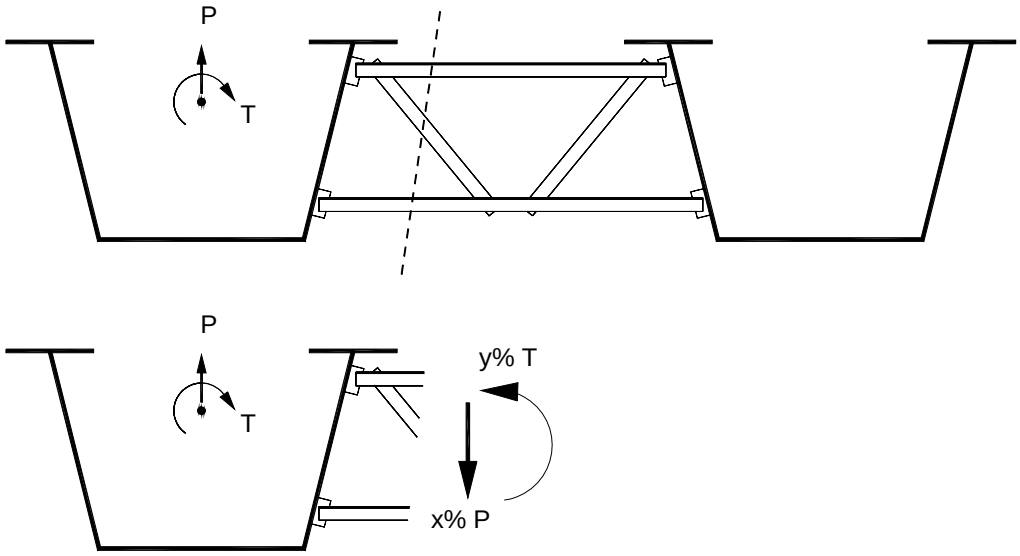

Figure 3.18 Force Breakdown on External Diaphragm

The FEM prediction for the external diaphragm was compared with the SAP model to determine what proportion of the load was distributed to the inner girder. The percentages of torsion and vertical load were adjusted on the SAP model results (Table 3.1) to match the FEM (Table 3.4). This was done by first adjusting the % of vertical load to match the diagonal forces since these members

are not affected by torsion. Then, the % of torsion was estimated to match the other member forces with as much correlation as possible.

Table 3.4 External Diaphragm FEM Results

Crane Test Results: Load = 20kips			Member				
			1	2	3	4	5
		FEM - B	-7.00	7.81	5.63	-1.51	1.51
Percentage of Torsion	Percentage of Vertical Load	SAP - B	-6.89	8.06	5.77	-1.51	1.50
21%	4.5%						
		% Difference	2%	3%	2%	0%	1%
		FEM - C	-6.84	7.67	5.72	-1.35	1.35
Percentage of Torsion	Percentage of Vertical Load	SAP - C	-6.77	7.82	5.77	-1.35	1.35
22%	4.0%						
		% Difference	1%	2%	1%	0%	0%

The best correlation between the models resulted in about 20% distribution of torsion from the crane load and 4% distribution of vertical force at both diaphragms. In other words, as compared to the SAP model in which 100% of the vertical force and torsion have to be transmitted through the diaphragms, the table shows the predicted percentages are forces that are distributed from the outer to inner girder. The SAP diaphragm and FEM diaphragm are modeled somewhat differently; hence there is some slight variance in the force predictions.

The measured results from the crane test were compared to the FEM results using the same technique. The percentages of torsion and force transmitted through the diaphragm in the SAP model were adjusted to correlate with the measured forces. The results are shown in Table 3.5.

Table 3.5 External Diaphragm Measured Results

Crane Test Results: Load = 20kips			Member				
			1	2	3	4	5
		Measured - B	-8.04	7.12	-	-2.78	2.82
Percentage of Torsion	Percentage of Vertical Load	SAP - B	-4.97	7.14	-	-2.79	2.77
4%	8.3%						
		% Difference	38%	0%	-	0%	2%
		Measured - C	-7.10	-	5.51	-1.39	1.96
Percentage of Torsion	Percentage of Vertical Load	SAP - C	-6.83	-	5.77	-1.44	1.43
21%	4.3%						
		% Difference	4%	-	5%	3%	27%

As expected, the measured results did not match the SAP model nearly as well as the FEM. For diaphragm B, the percentages adjusted for correlation between the SAP model and measured results were weighted much more heavily towards members 2, 4, and 5, rather than member 1 since this member's force calculation is questionable. Also, less consideration was given towards fitting the percentages with member 5 on diaphragm C, which did not show good repeatability during the crane test.

Comparing these percentages, diaphragm C compared extremely well with the predicted FEM. Both measured and predicted results show a distribution of torsion of about 20% and a distribution of vertical load of about 4% at this diaphragm. However, diaphragm B did not correlate well with the predicted values. Much higher forces were measured than predicted in the diagonal members; therefore more vertical load was transmitted through the diaphragm. The confidence in these readings is somewhat high since these members showed good repeatable during the test. Also, the compression in one diagonal is equal to the tension in the other. It is unclear whether this diaphragm's measured results are inaccurate or if this is a true phenomenon that is not predicted in the model.

CHAPTER 4
Concrete Deck Pour

4.1 DESCRIPTION

After the steel girders were erected, permanent metal deck forms (PMDF) that span between the top flanges of the girders were installed. Removable deck forms, which cantilevered from the outsides of the girders, provided additional space for the construction workers and the track for the screed (Figure 4.1). Longitudinal and transverse reinforcement were then placed on top of the PMDF and removable forms. Figure 4.2 and Figure 4.3 show before/after pictures of the deck, forms, and reinforcement installation. Figure 4.4 shows the screed used during a typical concrete pour.

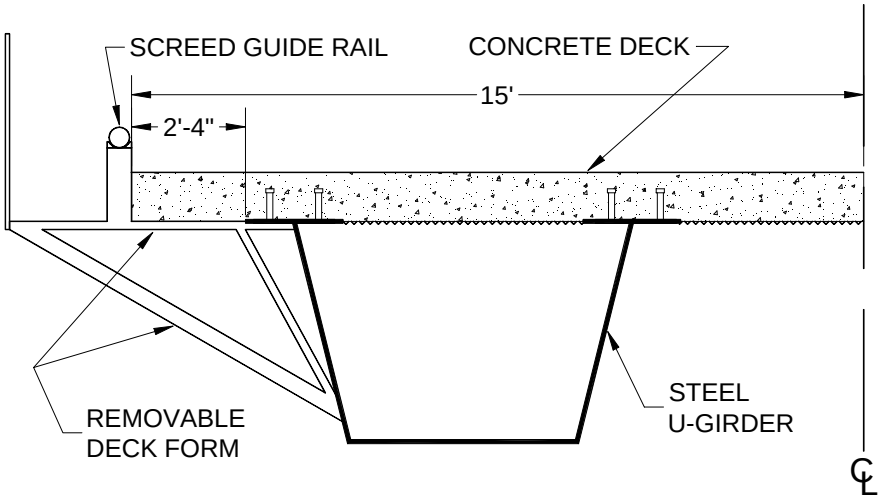

Figure 4.1 Cross Section View of Girder, Forms, and Deck

Figure 4.2 View of Z-Connect from Pier 16Z

Figure 4.3 Deck Forms and Reinforcement Installation

Figure 4.4 Concrete Screed

The designer specified five pours on the three-span bridge. As mentioned in Chapter 1, the original lengths of each pour segment were modified based on FEM results. The sequence is shown below in Figure 4.5. The arrows indicate the direction the screed moved during each pour segment.

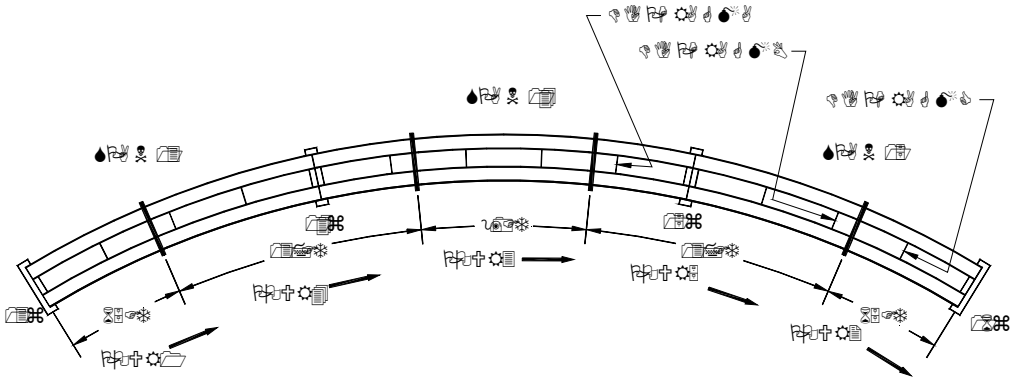

Figure 4.5 Concrete Pour Sequence

The sequence was selected to reduce the stresses in the girders and the top lateral bracing in the end spans. The negative moment regions (over piers 14z

and 15z) were poured last to prevent cracking of the concrete deck. Pours 1 through 3 took place on the early morning of September 1, 2000 while segments 4 and 5 were poured a week later on the early morning of September 8. The majority of the pours were performed before the sun came out; therefore stress changes in the bridge due to temperature effects were small for the majority of the concrete pours. The changes in stress due to thermal gradients were considered by comparing the concrete pour data with data from days prior to the pour during similar periods of time.

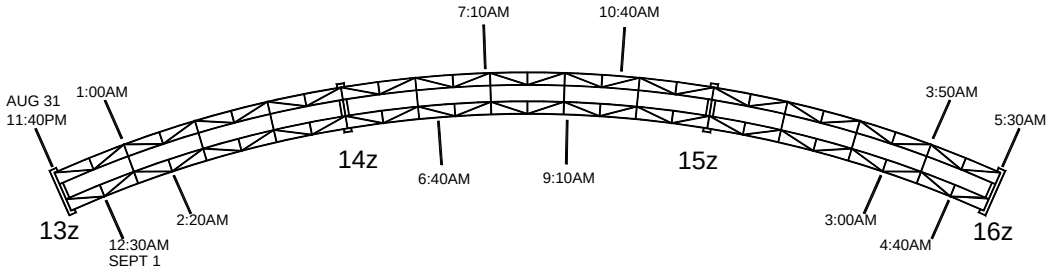

Figure 4.6 Progress of Pours 1, 2 and 3: Aug 31 - Sept 1

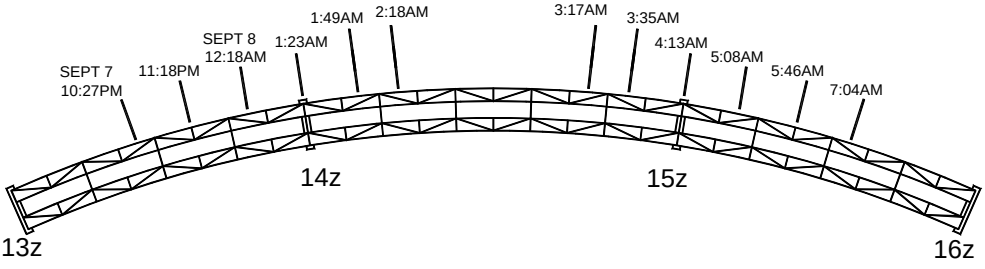

Figure 4.7 Progress of Pours 4 and 5: Sept 7 - Sept 8

Figure 4.6 and Figure 4.7 show the times that concrete was poured over certain sections of the bridge. The timing of the pour progress is important

because of its effect on early composite action between the new concrete deck and steel girders. This will be discussed further in section 4.2.1.

The stress changes from the concrete pour discussed in this chapter are due to the weight of the concrete, weight of the screed, and the weight of the construction crew during the pour. Compared to the screed and workers, the weight of the poured concrete is the dominant force acting on the bridge. For example, only 5ft of poured concrete along the width of the bridge weighs about 15kips. The weight of the screed is less than 2kips. The self-weight of the girders, the weight of the PMDF, removable forms, and deck reinforcement are all included in the zero reading for stress and force calculations.

4.2 TOP LATERAL RESULTS

Each top lateral WT had two cross sections gaged for redundancy. The majority of force measurements for the two sections of each member was nearly identical during the concrete pour as shown in Figure 4.8 through Figure 4.11. One cross section on the member is indicated by a "□" and the other by a "✕". Members that do not show both these symbols had a bad gage at one of the cross sections. Fortunately no member had a bad gage at both cross sections. The graphs shown are for pours 1 and 2, although similar results were found during every pour segment. When applicable, the two axial forces for each member were averaged for each time increment.

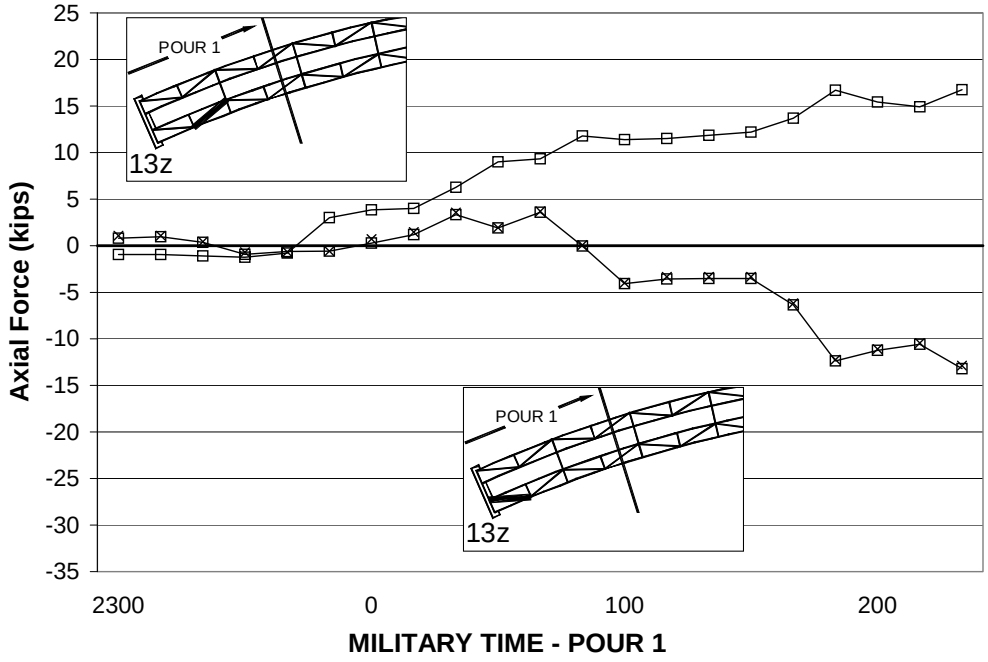

Figure 4.8 13Z Inner Top Lateral Forces during Pour 1

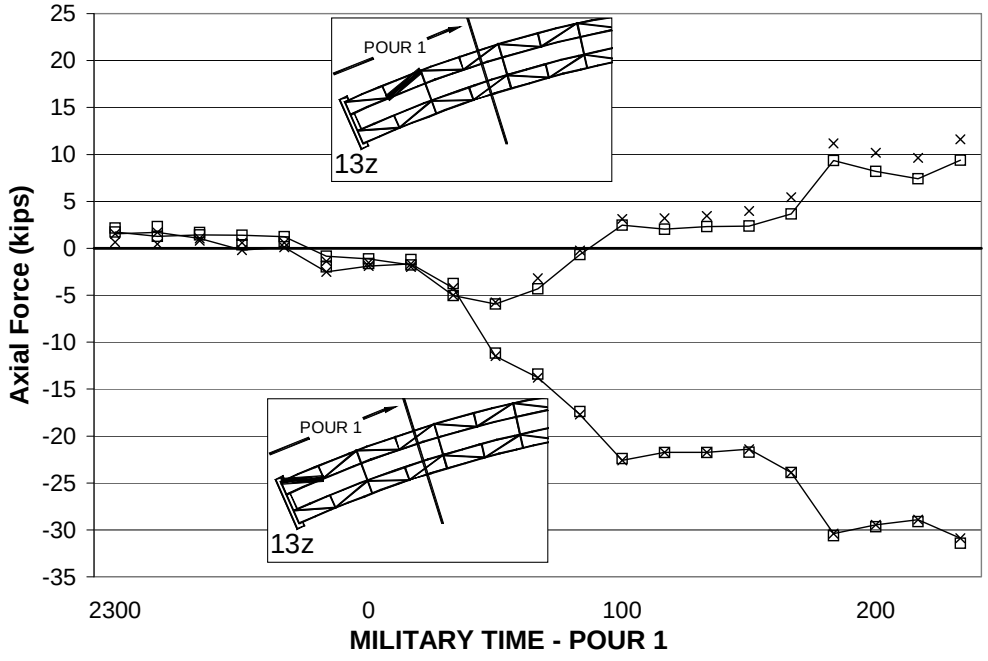

Figure 4.9 13Z Outer Top Lateral Forces during Pour 1

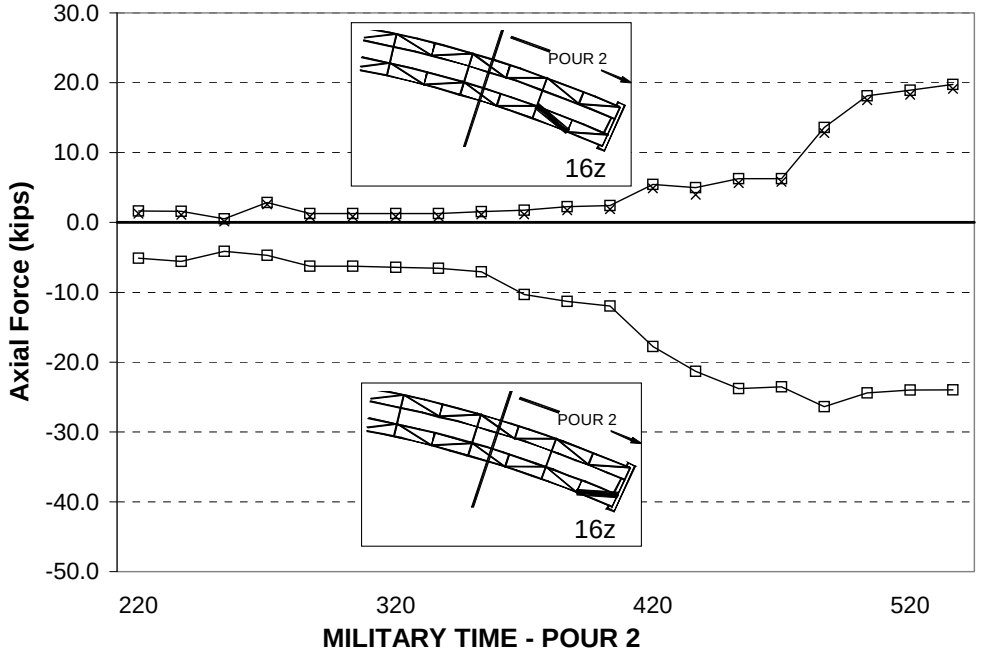

Figure 4.10 16Z Inner Top Lateral Forces during Pour 2

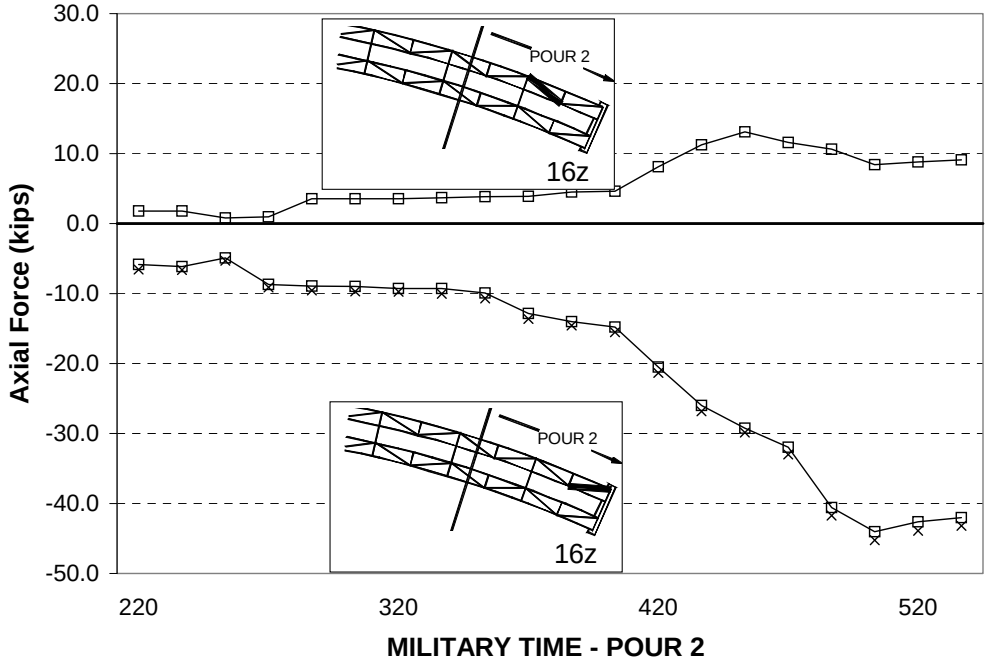

Figure 4.11 16Z Outer Top Lateral Forces during Pour 2

4.2.1 Early Composite Action

The measured top laterals were located under regions where the concrete was first poured; it was evident from the data that the concrete was beginning to harden before completion of the pouring sequence. The top laterals are located very close to the compression flange of the steel girder; hence they are far from the neutral axis of the non-composite section and very close to the neutral axis of the composite section (Figure 4.12). This means that the changes in stress due to bending in the members should be much higher before the section is composite. Also, the hardened concrete completes a closed box section that reduces the forces in the laterals due to torsion.

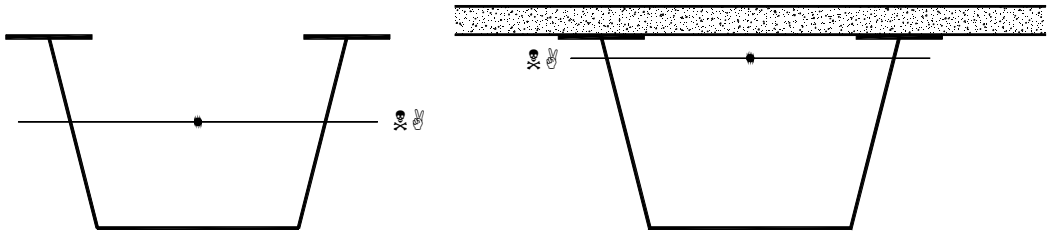

Figure 4.12 Approximate Neutral Axis Locations on Box Girders

The three-span bridge and the pour configuration are symmetrical. Therefore, when the middle span is poured (Pour 3 - Figure 4.5), the change in stress in the top laterals near pier 13z should be identical to the change in the top laterals near pier 16z. This is true assuming that all of the concrete from the first two pours has zero stiffness and does not contribute structurally. The concrete pour over the first two 13z laterals was at the earliest part of Pour 1 and the concrete pour over the first two 16z laterals was during the last part of Pour 2. Therefore, the concrete was setting for a much longer time over the 13z laterals than over the 16z laterals before the third pour. Table 4.1 shows the times for curing over these members during Pour 3.

Table 4.1 Curing Times During Pour 3

		Elapsed Time (hrs:min)			
Pier	**Lateral**	**Pour 3 (0 ft.)**	**Pour 3 (30 ft.)**	**Pour 3 (60 ft.)**	**Pour 3 (90 ft.)**
13z	1	6:10	6:40	8:40	10:10
	2	5:40	6:10	8:10	9:40
16Z	1	1:10	1:40	3:40	5:10
	2	2:00	2:30	4:30	6:00

The concrete that was poured over the first top lateral at pier 13z was in place and had more than 6 hours to cure before the start of Pour 3. The same section at pier 16z was only in place for about one hour before starting Pour 3.

The axial forces in the eight instrumented top laterals during Pours 1-3 are shown in Figure 4.13 through Figure 4.16. On each of the graphs, section "A" shows the change in axial force in the lateral due to the concrete pour over that lateral. Section "B" shows the change in axial force due to the concrete pour on the opposite side of the bridge. Section "C" shows the change in axial force due to Pour 3. The graphs are arranged in this orientation to show the effect of the curing on the top lateral forces. Ideally, both columns of each section in the graph should be identical if there was no effect from the curing.

Section "A" of each graph shows very similar behavior between the 13z and 16z laterals, as expected. These are nearly identical loading cases for the members. Less change in force occurs in the second section of the graph since the load is two spans away from the measured lateral. Section "C" of each graph shows convincingly that composite action from Pour 1 is occurring. The third pour induces a force change of 20-35kips in all of the 16z laterals. The 13z laterals, however, have barely any change in force during this pour. This is because the concrete is already hardening over this region carrying the load rather than the lateral. Although the concrete may not be near its full strength, it has increased significantly in stiffness during this time. If the concrete did not

contribute to carrying load, then the force change in the 13z laterals would be equal to the 16z laterals.

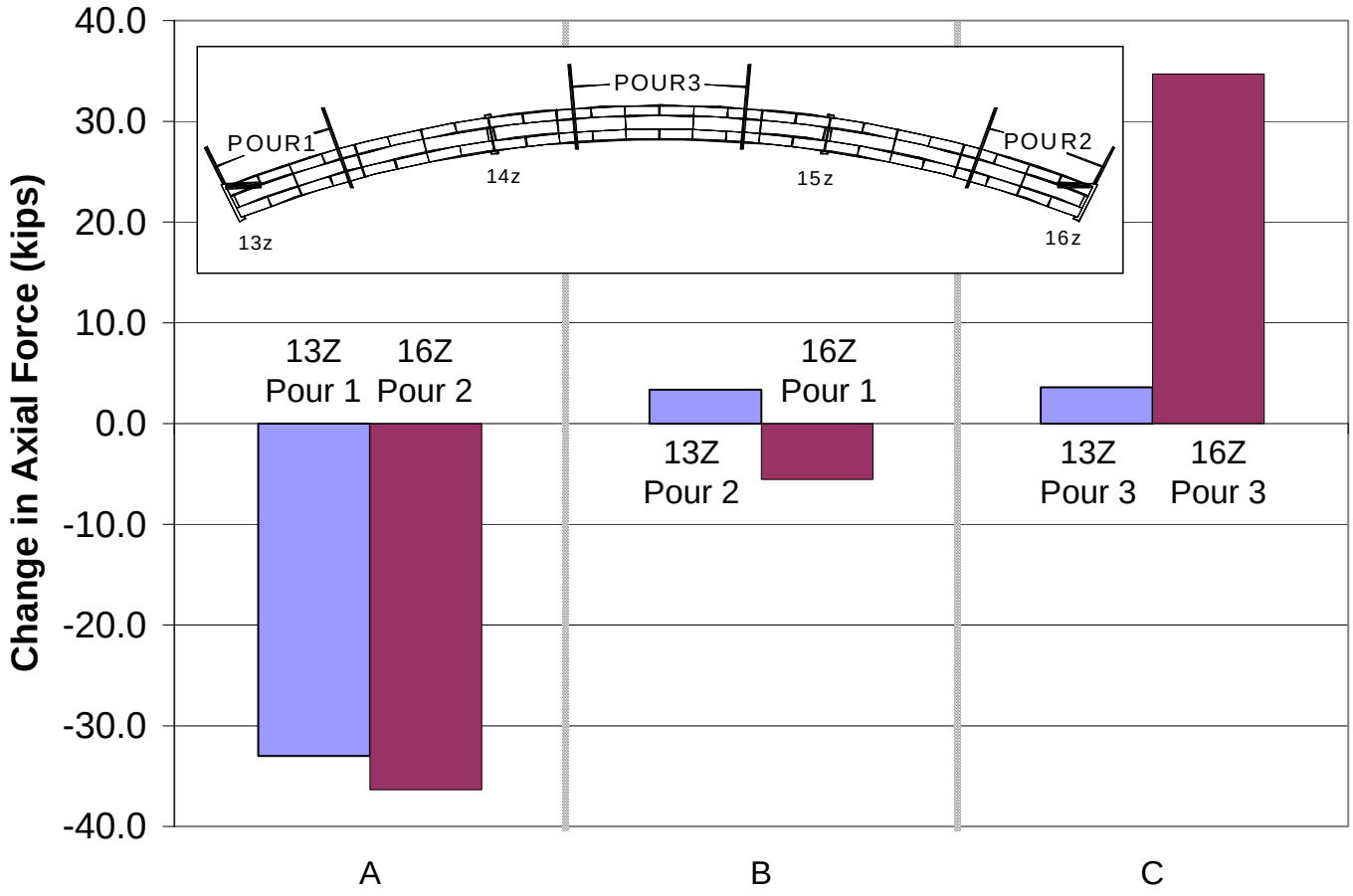

Figure 4.13 Outer 1st Top Laterals - Change in Axial Force due to Pours 1-3

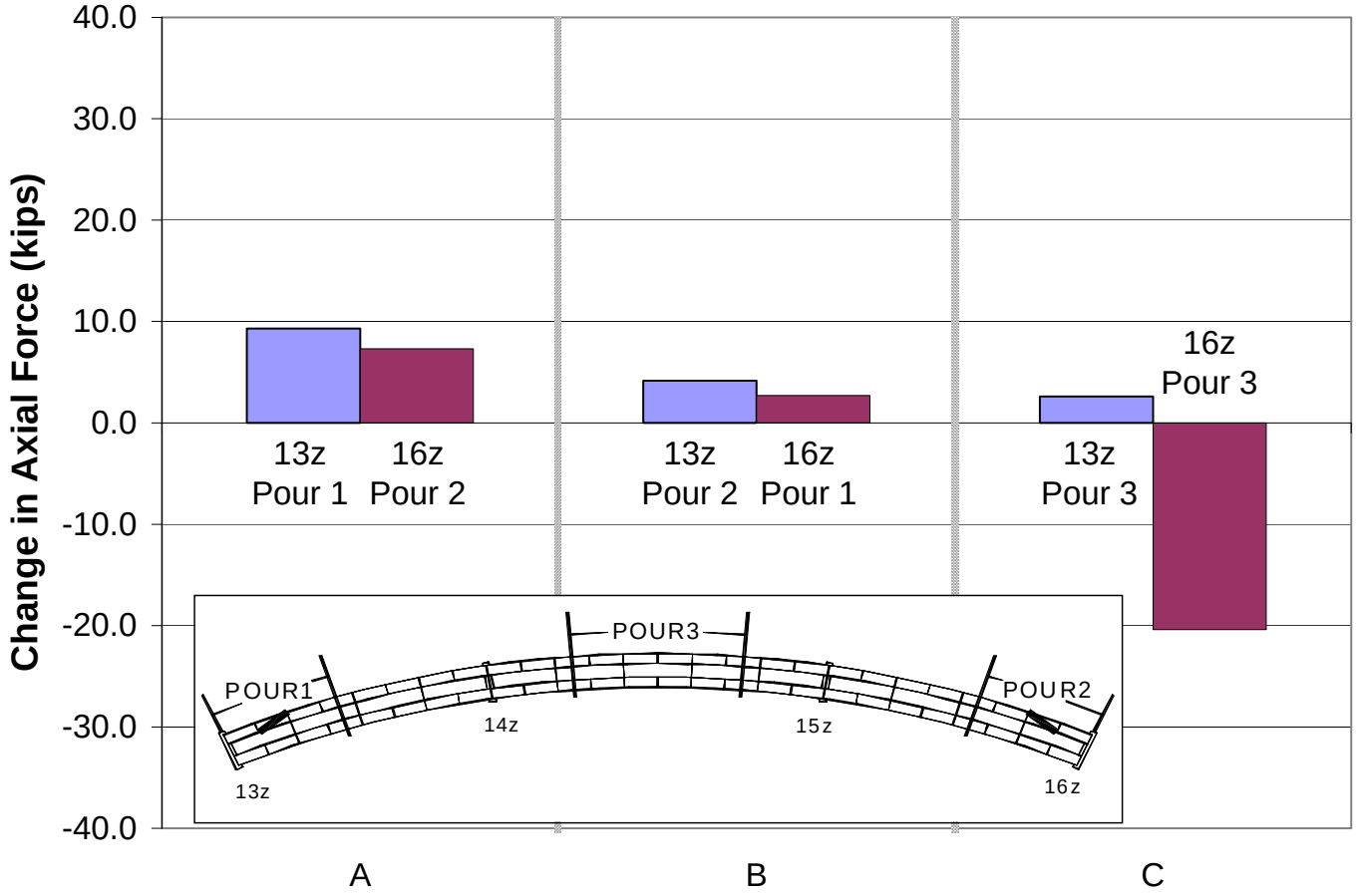

Figure 4.14 Outer 2nd Top Laterals – Change in Axial Force due to Pours 1-3

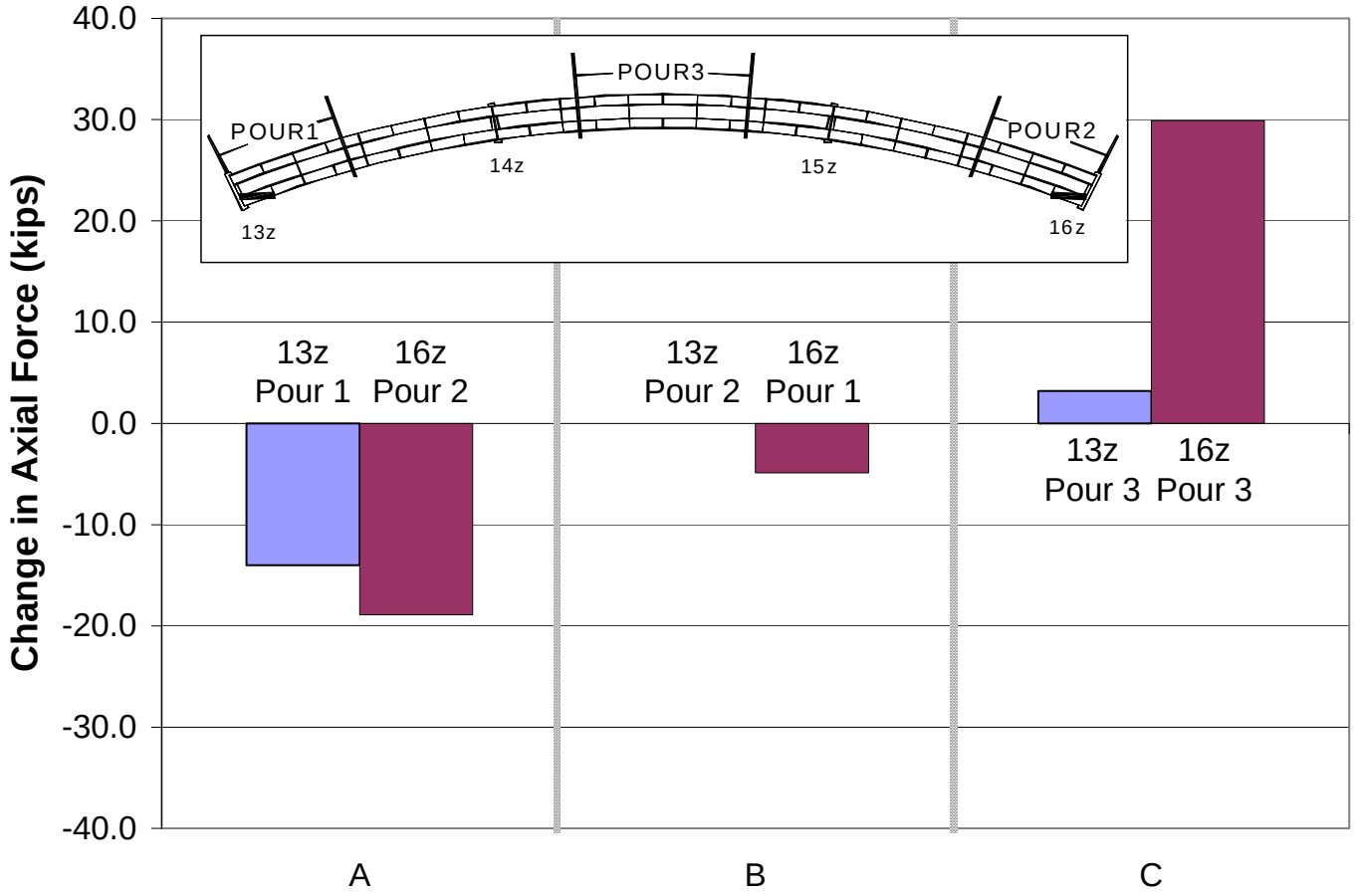

Figure 4.15 Inner 1st Top Laterals – Change in Axial Force due to Pours 1-3

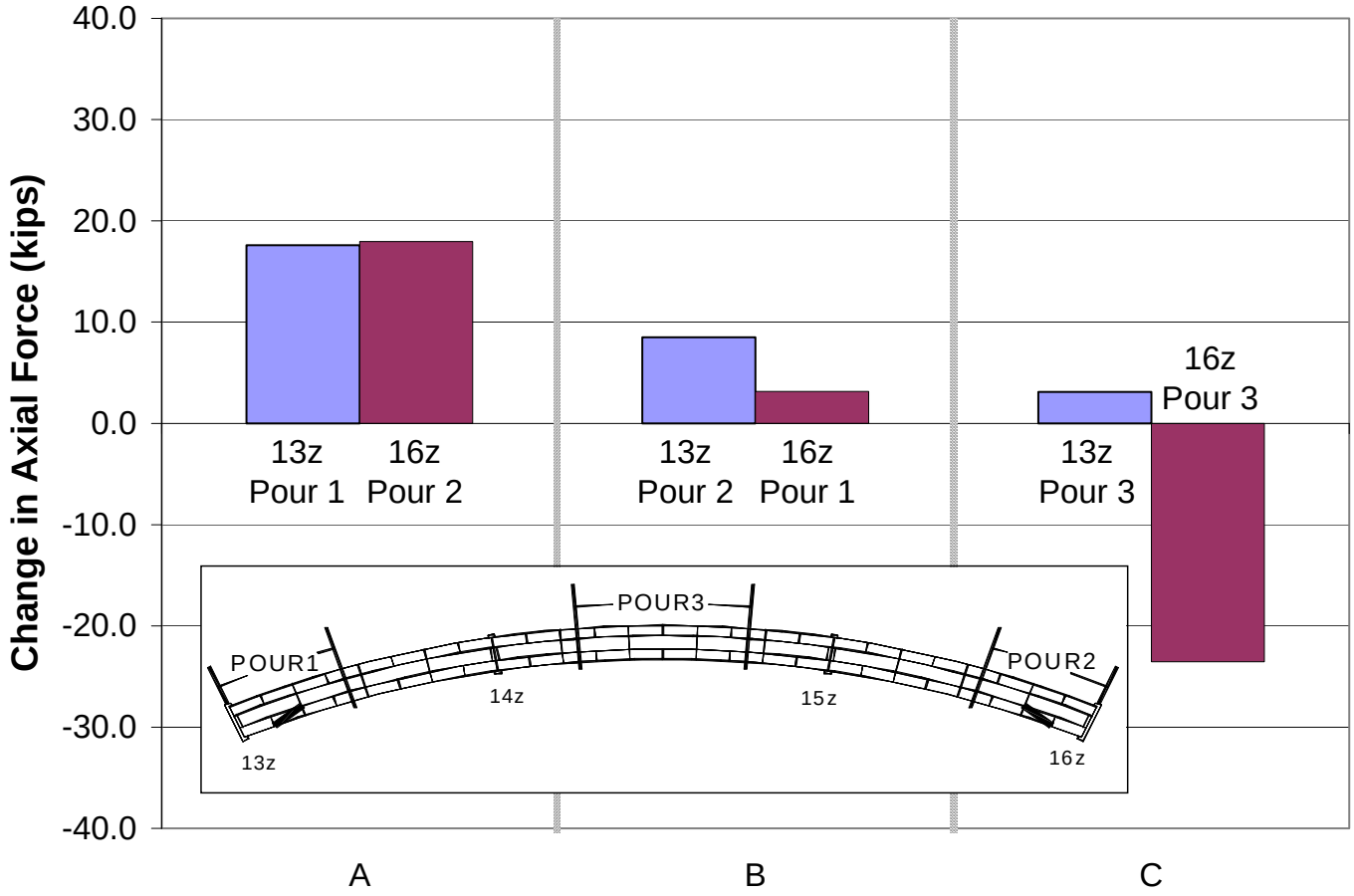

Figure 4.16 Inner 2nd Top Laterals – Change in Axial Force due to Pours 1-3

4.3 EXTERNAL DIAPHRAGM RESULTS

4.3.1 Temperature Effects on Diaphragms

The majority of the concrete pours took place while the sun was set. Lopez (1999) showed that thermal gradients during this period are small, hence force changes in the bridge should also be small. However, since the stresses developed in the external diaphragms from the concrete pour were not very large, the effect of temperature on the bridge was considered. This was done by examining force measurements of the same members throughout several days prior to the pour.

Figure 4.17 through Figure 4.20 show some typical measurements of force changes in the external diaphragm members during two nights before each pour. Although there is some slight variation in the change of axial force with time, the average force change during a certain time period for a member is nearly the same each day. The change in force due to temperature was examined separately for each pour period. For pours 1 through 3, data was used from days just prior to the pour so the effects of the formwork on thermal gradients would be included. For pours 4 through 5, different history data was used since the bridge was partially composite in some areas and had different thermal characteristics compared to the exposed girders. The temperature plotted in the figures was recorded by the data acquisition system's thermistor, which is located inside the box girder.

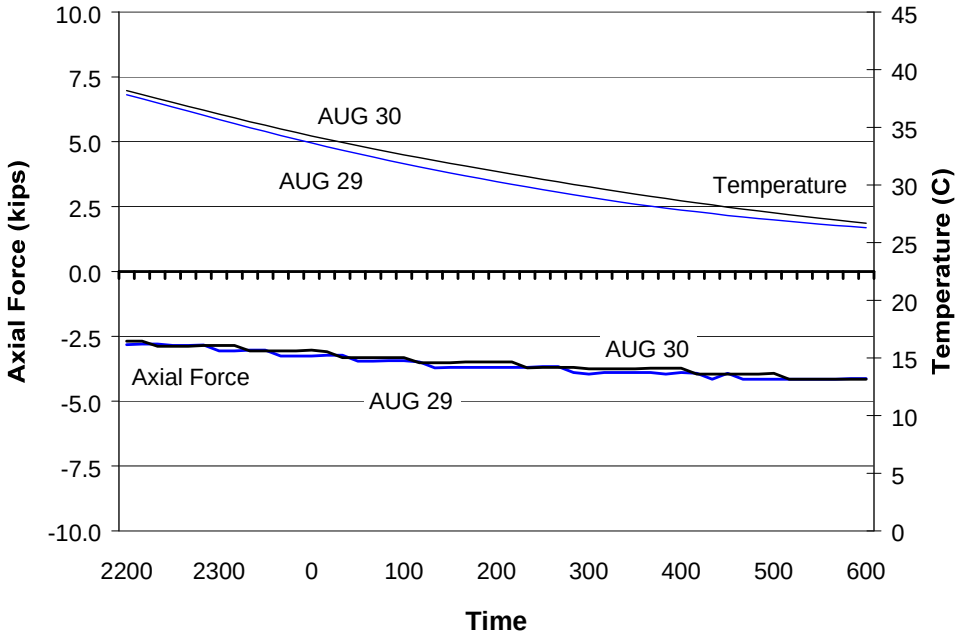

Figure 4.17 Diagonal Temperature Data Before Pours 1-3

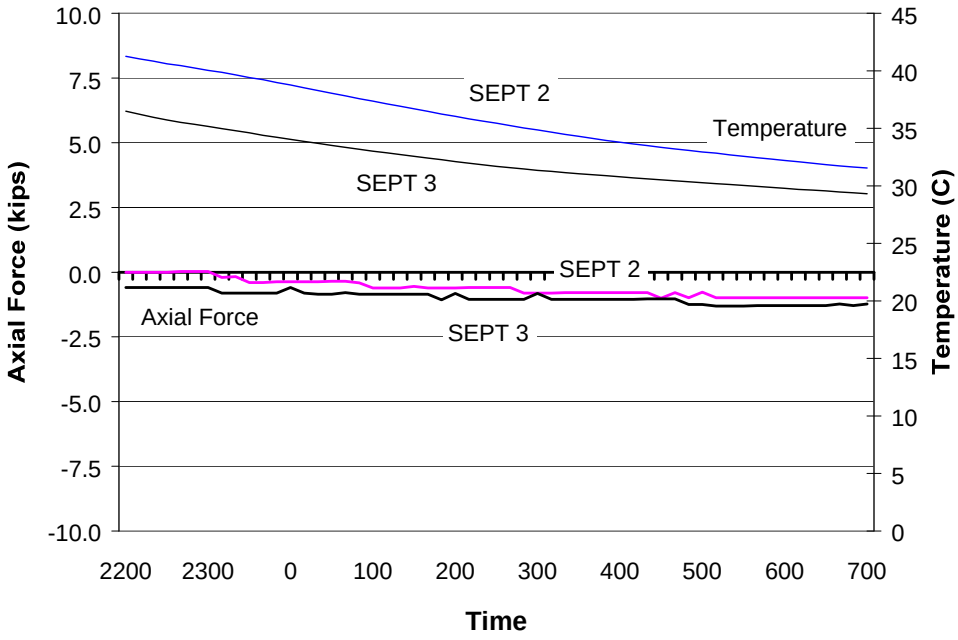

Figure 4.18 Diagonal Temperature Data Before Pours 4-5

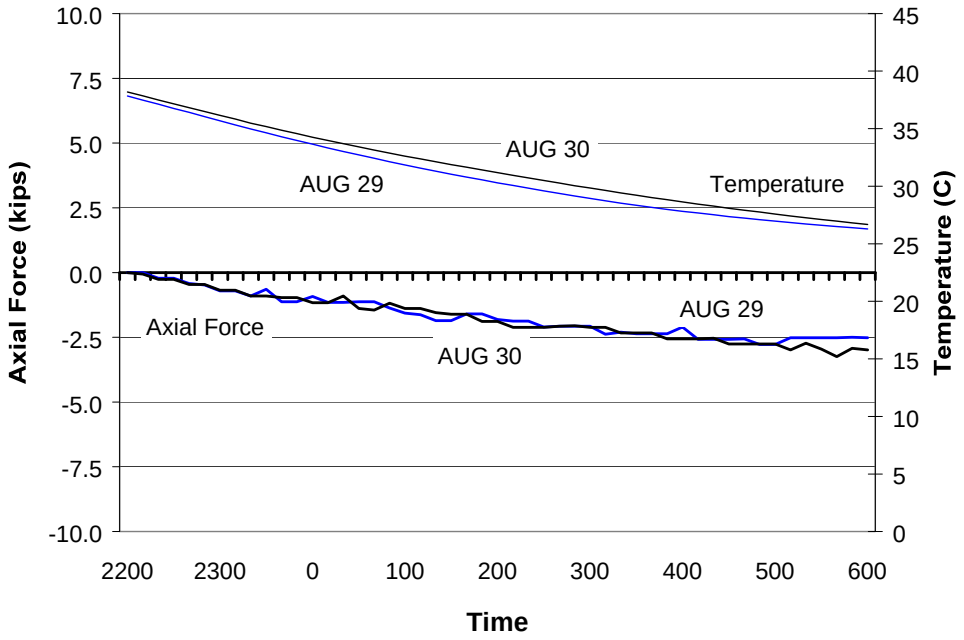

Figure 4.19 Bottom Chord Temperature Data Before Pours 1-3

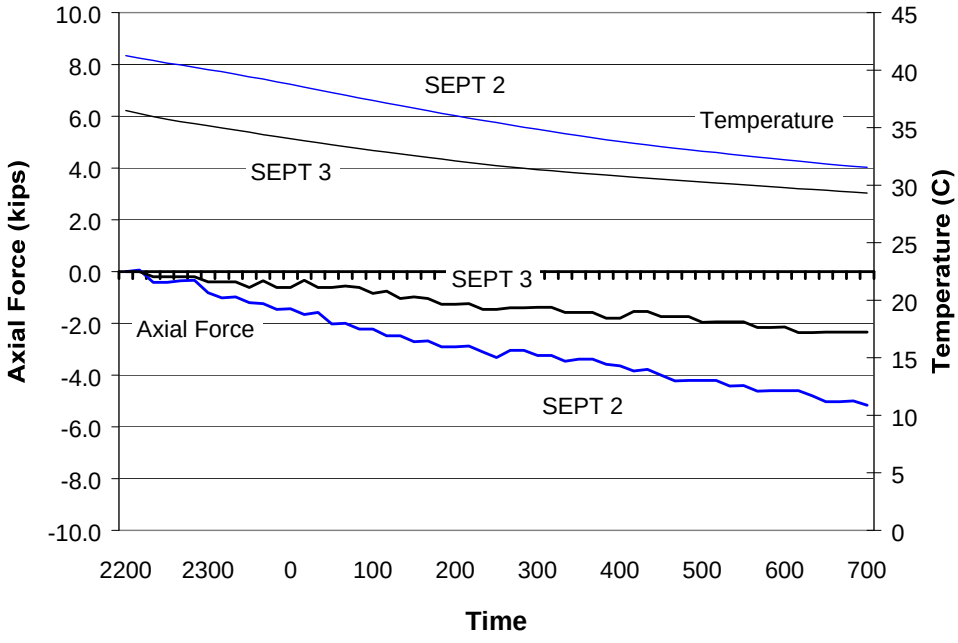

Figure 4.20 Bottom Chord Temperature Data Before Pours 4-5

Although the majority of temperature data was repeatable from one day to the next, there was some variation of force change as shown in Figure 4.20. This adds some uncertainty to the measurements when differentiating the stresses due to temperature and the stresses due to the concrete weight. However, the majority of the temperature data during the hours of the concrete pour showed good repeatability.

A linear trendline was used as an estimate for the temperature induced stresses in the diaphragms. This estimation is reasonable since the change in stress due to temperature gradients at this time of the day is very gradual. The predicted temperature stresses were subtracted from the original data to determine what stresses were only due to the weight of the concrete. All of the calculated forces in the diaphragms presented in this chapter already include the subtraction of predicted thermal effects.

4.3.2 External Diaphragm Analysis

The external torsional, horizontal and vertical loads on the diaphragms were calculated from the internal forces in the members. Since shear and moment are developed in each angle member, the external reactions from the box girders cannot be solved from axial forces alone. However, the instrumentation used on the diaphragms cannot measure the shears in each angle so a SAP model of the frame was used to predict the axial forces due to known torsional, vertical, and horizontal loads. This model includes the shear and moments in the angles; therefore the predicted axial forces can be used to predict the external reactions.

The SAP model used frame elements with reduced rotational stiffness at the ends due to the connection detail (Section 3.3). In the model (Figure 4.21), one side of the diaphragm was rigidly attached to the web of the box girder, which was restrained at its middle by a pin. The other side of the diaphragm was also

rigidly attached to a box girder web, except this member was attached to a roller to allow horizontal displacement of one end of the diaphragm. The girder web was modeled as a WT frame section with its stem dimensions equal to the longitudinal web stiffener and the thickness of the flange equal to the web thickness. The width of the flange was approximated as 20 inches. This estimation of web stiffness had very little effect on the axial forces in the diaphragms members.

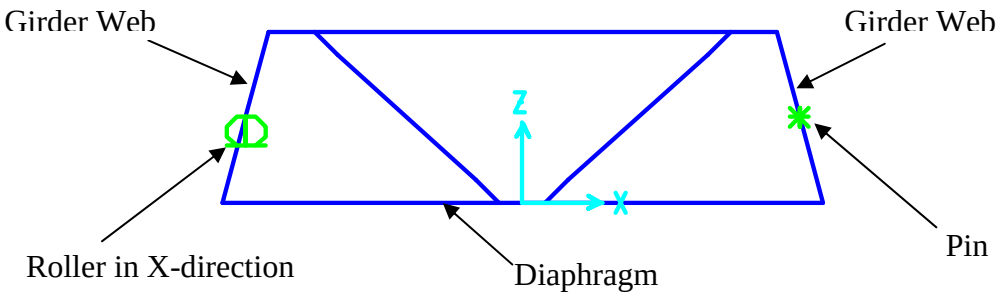

Figure 4.21 SAP Model of External Diaphragm

First, the forces in the diaphragm were determined from a unit torque applied to one side of the diaphragm. The same was done for a unit torque applied to the opposite side of the diaphragm. The forces were also determined for a unit horizontal load. The measured forces in the members for the three applied loading conditions are shown in Figure 4.22. The vertical shear transferred across the diaphragm can be calculated from the applied torsions. Figure 4.23 shows a deflected shape from an applied horizontal force and torsional loads.

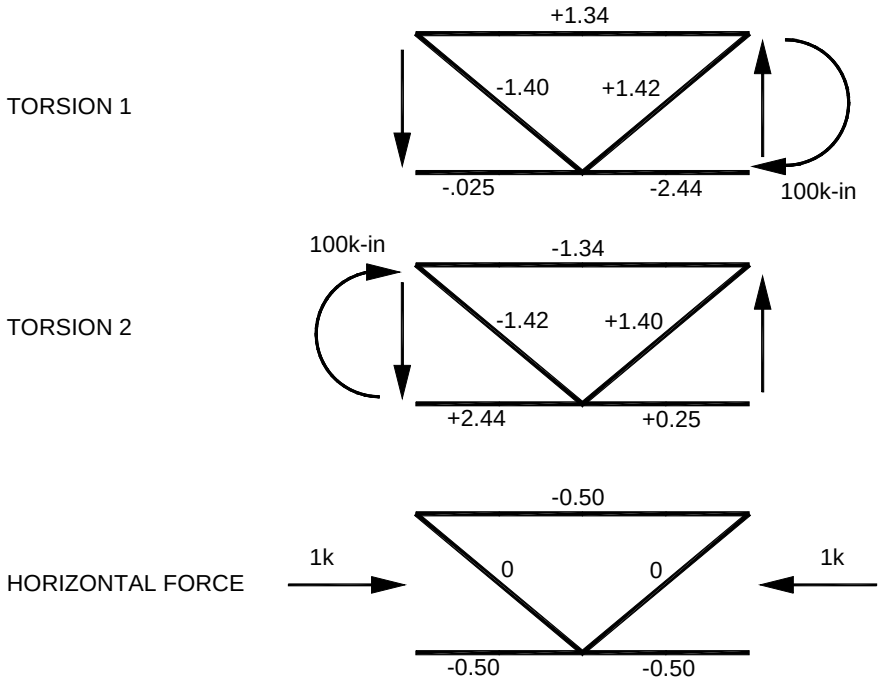

Figure 4.22 Diaphragm Forces from Applied Unit Loads

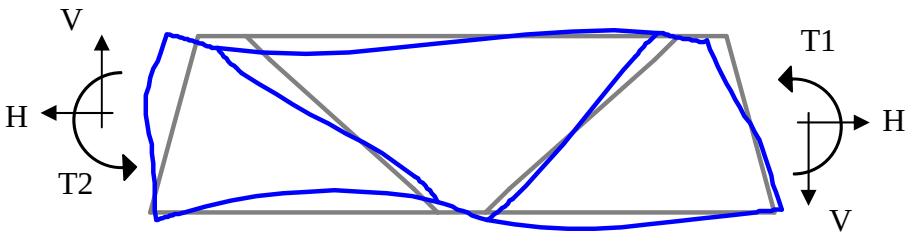

Figure 4.23 SAP Model - Deflected Shape

By taking the internal forces of three diaphragm members, the external reactions acting on the diaphragm can be solved. This is done by superimposing the unit loads in the SAP model until the internal forces for each member are equivalent to the measured or FEM internal forces. The external reactions on the diaphragm (T1, T2, and H) can be solved by using the equation

$T1 * M_{T1} + T2 * M_{T2} + H * M_H = F$, where M_i is the member force due to load i and F is the internal force of the angle. Using different member forces, three equations are solved for the three unknown external reactions. The solved torques and forces are applied to the SAP model and all of the member forces are compared with the measured or FEM forces.

There was some variation between the FEM force predictions in the diaphragm members and the SAP force predictions from the solved external reactions. This is due to small differences between the models. The members that were used to solve the external reactions acting on the diaphragm in SAP were equal to the axial forces in the FEM since the reactions were determined from these members. The other two members had some variation between the FEM and SAP model. To prevent the analysis from favoring the forces in some members from FEM more than others, two calculations were done on each diaphragm using different members. The calculated external forces from these procedures were then averaged in order to minimize the variation between the FEM and SAP model. An example of these calculations is shown in Table 4.2.

Table 4.2 External Reactions Calculated from Internal Forces in Diaphragms

				FEM Forces				
				1	2	3	4	5
				(kips)	(kips)	(kips)	(kips)	(kips)
				5.88	-3.82	-5.24	-1.01	0.95
	SAP Loads Calculated from FEM Forces			SAP Forces Caclulated from Loads				
	Torsion 1	Torsion 2	Horizontal	1	2	3	4	5
	(kip-in)	(kip-in)	(kips)	(kips)	(kips)	(kips)	(kips)	(kips)
From FEM 1,2,4	158.6	-233.0	-1.3	5.88	-3.82	-5.45	-1.01	1.09
From FEM 1,3,5	161.6	-226.2	-1.4	5.88	-3.82	-5.24	-0.87	0.95
AVERAGE	160.1	-229.6	-1.3	5.88	-3.82	-5.35	-0.94	1.02

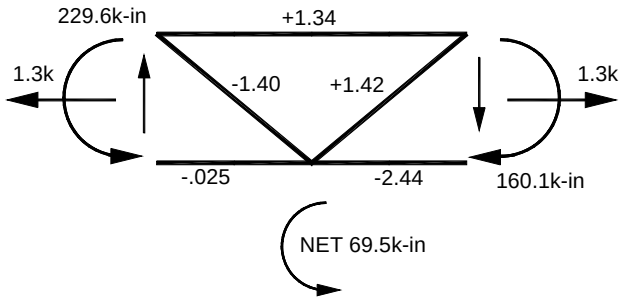

Figure 4.24 External Reactions Calculated in Table 4.2

4.3.3 External Diaphragm Results

Details of the FEM analysis are discussed in section 4.4. The FEM member force predictions in the external diaphragms were converted into an equivalent torsion, vertical force, and horizontal force applied to the box girder (Figure 4.25). These forces were determined from the SAP model and the analysis technique discussed above. The measured forces on the diaphragms were also analyzed using the same method. Unfortunately, the concrete deck was poured nine months after the instrumentation was installed and a considerable amount of degradation occurred over that time. Diaphragm A had only one out of

five members giving consistent axial force measurements. Diaphragm B had two out of five reliable force measurements and diaphragm C had four out of five. Therefore, the torques and forces acting on diaphragm C were calculated, but in diaphragms A and B, only the member forces were compared to the FEM. The results for the measured diaphragm forces during the concrete pour (Figure 4.5) are compared to the FEM predicted diaphragm forces in Figure 4.26 through Figure 4.28. These figures show the reactions by the diaphragm on the girders. The forces and torques shown are the changes due only to the individual pour sequence.

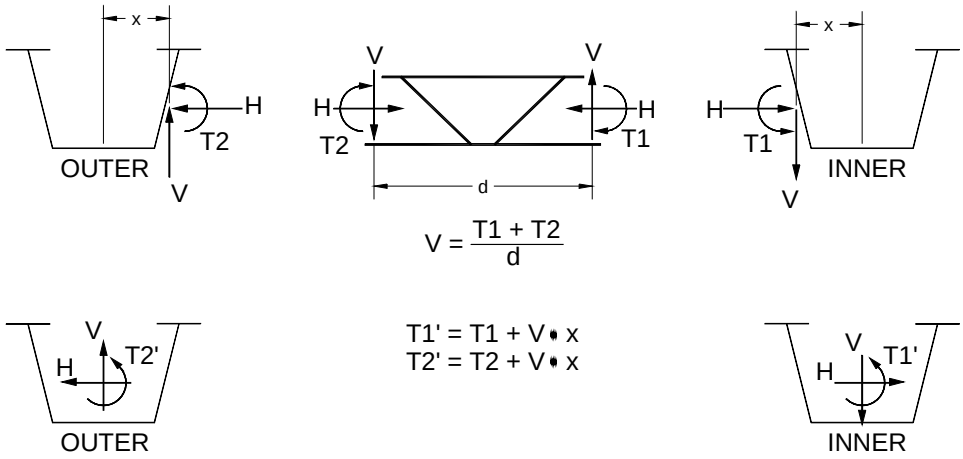

Figure 4.25 Reactions at Box Girder Centroid from External Diaphragms

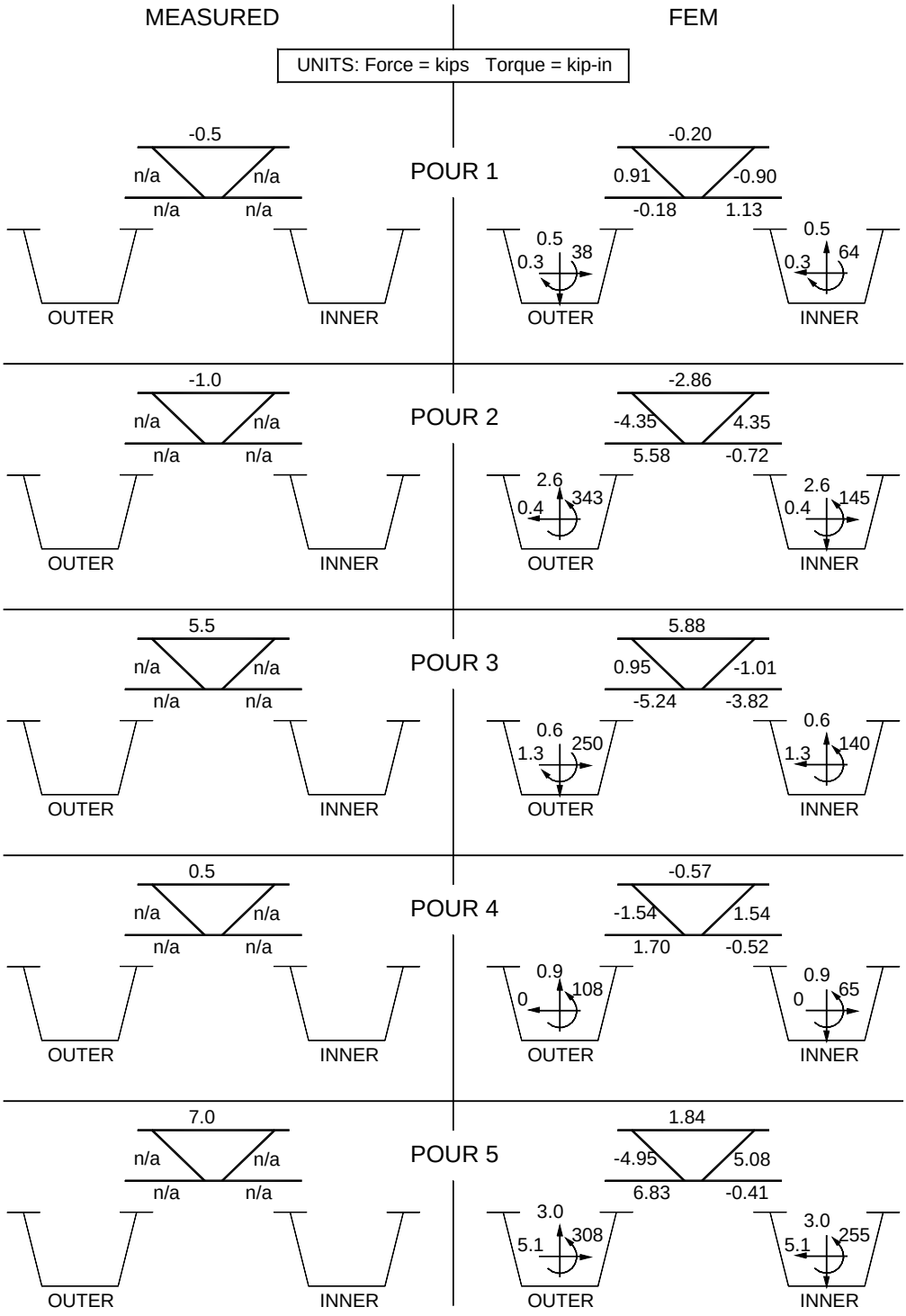

Figure 4.26 Diaphragm A Concrete Pour Results

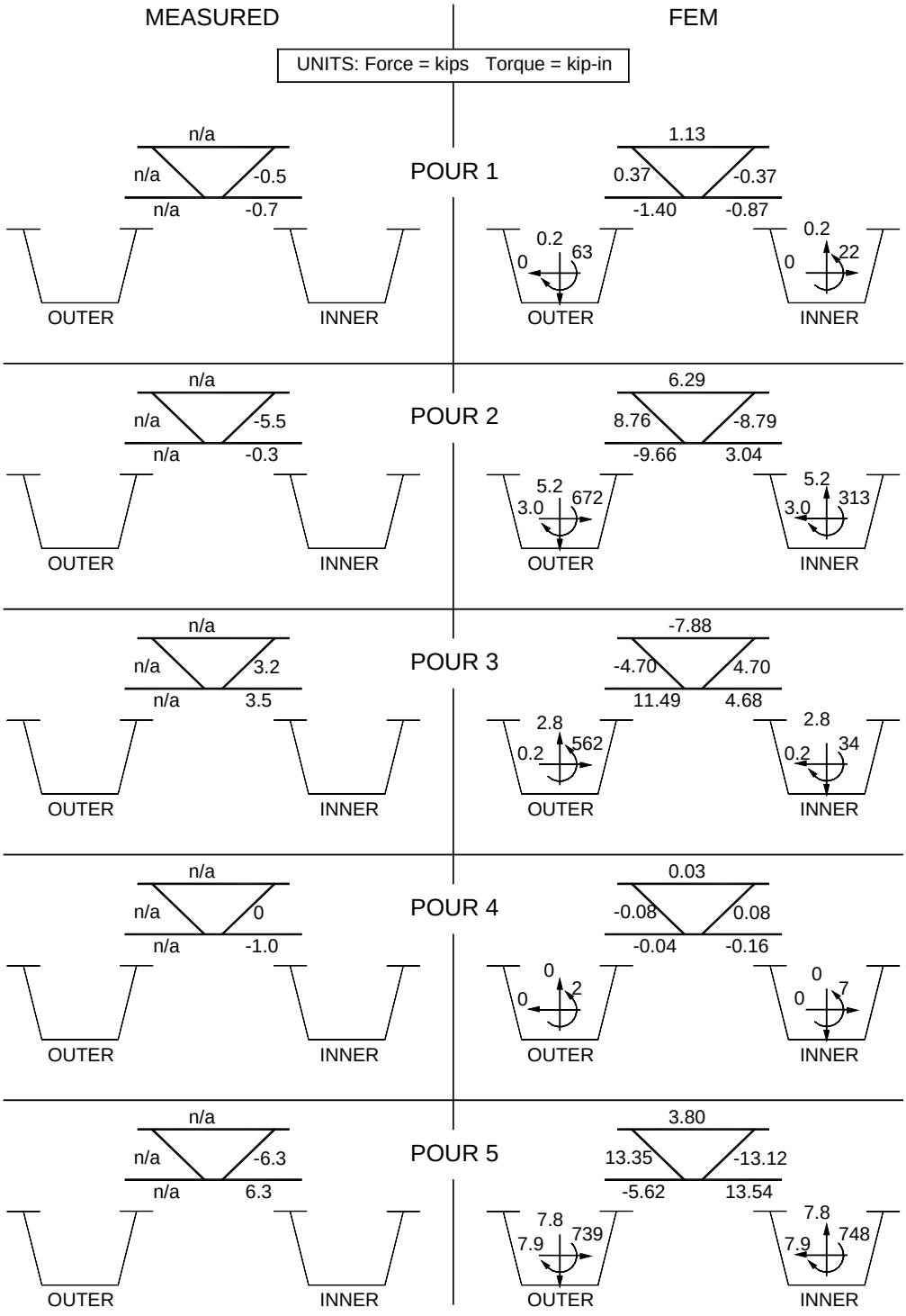

Figure 4.27 Diaphragm B Concrete Pour Results

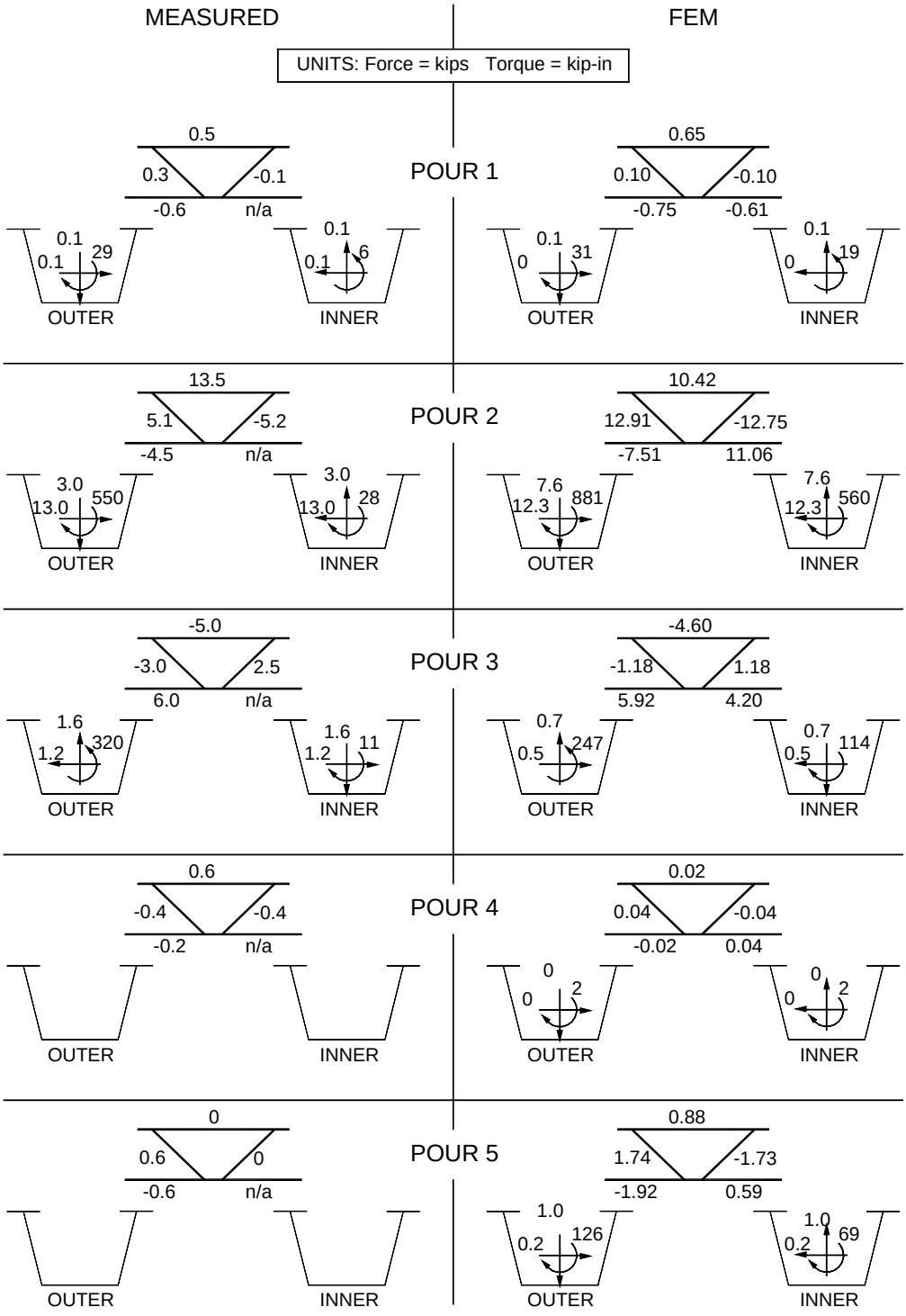

Figure 4.28 Diaphragm C Concrete Pour Results

4.4 DISCUSSION

It was apparent from the top lateral data that composite action was occurring between the poured concrete and steel girders within hours of placement of the concrete. This affected the force distribution throughout the girder as other pour segments continued. However, the amount of contribution from the hardening concrete is difficult to model in the FEM since the modulus of elasticity is uncertain and changes with time. Several different cases were modeled to predict the effect of a hardened deck on the external diaphragms, including the following:

	Pour 1	Pour 2	Pour 3	Pour 4	Pour 5
Case 1	Wet				
Case 2	Wet	Wet			
Case 2a	E=1000ksi	Wet			
Case 3	E=1000ksi	Wet	Wet		
Case 3a	E=1000ksi	E=1000ksi	Wet		
Case 4	E=5000ksi	E=5000ksi	E=5000ksi	Wet	
Case 5	E=5000ksi	E=5000ksi	E=5000ksi	Wet	Wet
Case 5a	E=5000ksi	E=5000ksi	E=5000ksi	E=1000ksi	Wet

In these cases, "wet" corresponds to zero stiffness. A modulus of elasticity of 1000ksi was estimated as partially hardened. A modulus of elasticity of 5000ksi was used to represent the fully hardened stiffness.

The thickness of the concrete deck in the model was determined from the measurements recorded in the TxDOT logbook during the pour. During pour 2, the FEM forces in diaphragms A, B, and C found to be independent of the stiffness of pour 1 (Case 2 VS Case 2a). Also, the forces in diaphragms B and C during pour 5 were independent of the stiffness of pour 4 (Case 5 VS Case 5a). However, there were differences in all of the diaphragm forces for Case 3 and 3a. This is because the concrete deck from pour 2 is very close to the external

diaphragms and significantly changes the force distribution in the girders when hardened. Also, the forces in diaphragm A during pour 5 were dependent on the stiffness of pour 4 (Case 5 VS Case 5a). Based on the measured results in top lateral forces, the FEM models used to predict the diaphragm forces (Figure 4.26 through Figure 4.28) were Cases 1, 2a, 3, 4 and 5. In other words, pour 1 was considered partially hardened during pours 2 and 3; pours 1, 2, and 3 were considered hardened during pours 4 and 5.

The measured reactions acting on the girders from external diaphragm A (Figure 4.26) are inconclusive since only one member was giving reliable axial force measurements. The top chord of diaphragm A has some correlation with the FEM during the first 3 pours. This is especially true during pour 3, in which the stresses are higher. There is very little correlation in diaphragm A during pour 4 and 5. This may be due to the estimation of the concrete stiffness in the previously poured segments. During pour 5, the top chord measured a much higher force than the FEM predicted. The measured force change occurred only during the very early portion of pour 5, while the concrete was poured near the diaphragm. Once the screed moved past the pier away from diaphragm A, there were minimal force changes. Strain readings in other members of the diaphragm show the same sudden increase in magnitude during this time interval.

In general, the measured forces in diaphragm B (Figure 4.27) are much lower than predicted with the FEM. During pours 3 and 5, the measured forces in the diagonal and bottom chord are almost equal in magnitude. The FEM predicts a similar behavior in the twisting of the girders as measured, although the magnitudes of the diaphragm reactions are overestimated. This may be due to the reduction in diaphragm stiffness from the connection detail discussed earlier in section 3.3.2. This detail is not modeled so the ratio of girder to diaphragm stiffness may be greater than predicted.

The external reactions on diaphragm C (Figure 4.28) were calculated from the measured internal forces. During pours 1 and 2, the measured restraining torque was higher in the outer girder than the inner. This is also predicted in the FEM. The measured and predicted results both show that the top of the outer girder twists away from the center of curvature as the diaphragm acts in the opposite direction to restrain it. However, the measured torsions are considerably less than predicted during pour 2. The predicted horizontal reaction from the diaphragm correlates well with the measured reaction during the first two pours.

During pour 3, the measured torsion in the outer girder is somewhat higher than predicted and the measured torsion acting on the inner girder is much smaller than predicted. The measured and predicted torsions on the inner girder are in the opposite direction from the torsions on the outer girder. The top flange of the inner girder is restrained from twisting away from the center of curvature while the top flange of the outer girder wants to twist towards the center of curvature.

The force calculations in the diaphragm members during pours 4 and 5 are smaller than the forces during the other pours since the concrete deck over diaphragm C had time to harden. Torsional and force measurements from the diaphragms were not calculated since the member forces were within expected errors in the measurements. Also, the expected temperature effects during these pours were not as easy to predict since the stiffness of the bridge was slowly increasing with time. This changes the response of the bridge to thermal effects so the background data are not as reliable.

The FEM predicts the same behavioral response in the diaphragms as measured, although it generally overestimates the contribution of the external diaphragms in restraining the girders. Some discrepancy between the predicted and measured results exists from the estimation of concrete deck stiffness. There were considerable changes in the predicted diaphragm forces in the analysis if the

concrete deck from previous pour segments was modeled as composite with the steel girders. The maximum axial stress measured in all of the external diaphragm members due to the weight of the concrete was about 3ksi. In comparison, the top lateral members that were measured had axial stresses up to 7ksi from the concrete pour.

CHAPTER 5
Truck Load Test

5.1 DESCRIPTION

On November 9, 2000, several weeks after the concrete deck was poured, a live load test was performed on the composite box girder bridge by using two trucks. The test was performed before the concrete guardrail was cast in place. To maximize the response out of the instrumented members, the trucks were placed in a back-to-back position (Figure 5.1). The trucks were placed in 20 different positions while about 10 readings on each diaphragm were taken for every position. The positions of the trucks on the bridge are shown in Figure 5.2.

Figure 5.1 Picture of Truck Configuration

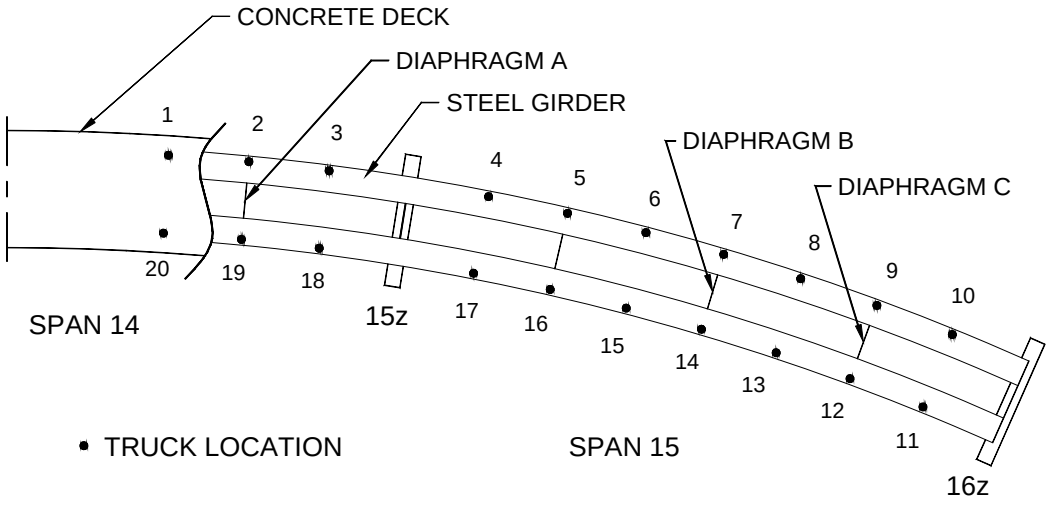

Figure 5.2 Positions of the Two Truck's Center of Gravity

Truck positions correspond to the location of the back of the trucks. The truck positions were marked before the load test so the outer wheel would only be 40 inches from the edge of the concrete deck. The trucks were positioned close to the edge of bridge (Figure 5.3) to create a high torque. This would maximize the response in the external diaphragms. Figure 5.4 shows the truck axles being individually weighed on the bridge using portable TxDOT scales. The truck weights are shown in Table 5.1.

Table 5.1 Wheel Loads (lbs) Measured on Bridge at Position 6

Truck 5474F - Rear Truck during position 1-10; Front Truck during position 11-20

	Front Wheel	Middle Wheel	Back Wheel
Driver's Side	6050	10150	9850
Passenger's Side	5000	8600	8150

Truck 3337H - Front Truck during position 1-10; Rear Truck during position 11-20

	Front Wheel	Middle Wheel	Back Wheel
Driver's Side	6050	7000	6850
Passenger's Side	6750	9000	8700

Figure 5.3 Front View of Truck in Position

Figure 5.4 Weighing of Back Axles

The data acquisition system read all of the gages on the bridge once every 30 seconds. The trucks were placed in the 20 positions for about 5 minutes each. The entire load test took about two hours. The temperature effects during the load

test were considered when determining the forces generated in the diaphragms due to the trucks.

5.2 TEMPERATURE EFFECTS ON DIAPHRAGMS

Unlike during the concrete pour, there was a considerable change in ambient temperature inside the girder throughout the truck load test. The temperature recorded inside the steel box girder by the datalogger increased about 4 or 5 degrees Celsius during the test. Also, there was a large variation in temperature from one day to the next prior to the load test. Examining the recorded data during the time interval during the test, there was no easily predicted trend in the change of axial force in the diaphragm members. All of these factors made it very difficult to predict the stresses in the diaphragms due to temperature gradients in the bridge. Figure 5.5 and Figure 5.6 show typical plots of the diaphragm data prior to the load test and the change in temperature with time during the load test (November 9).

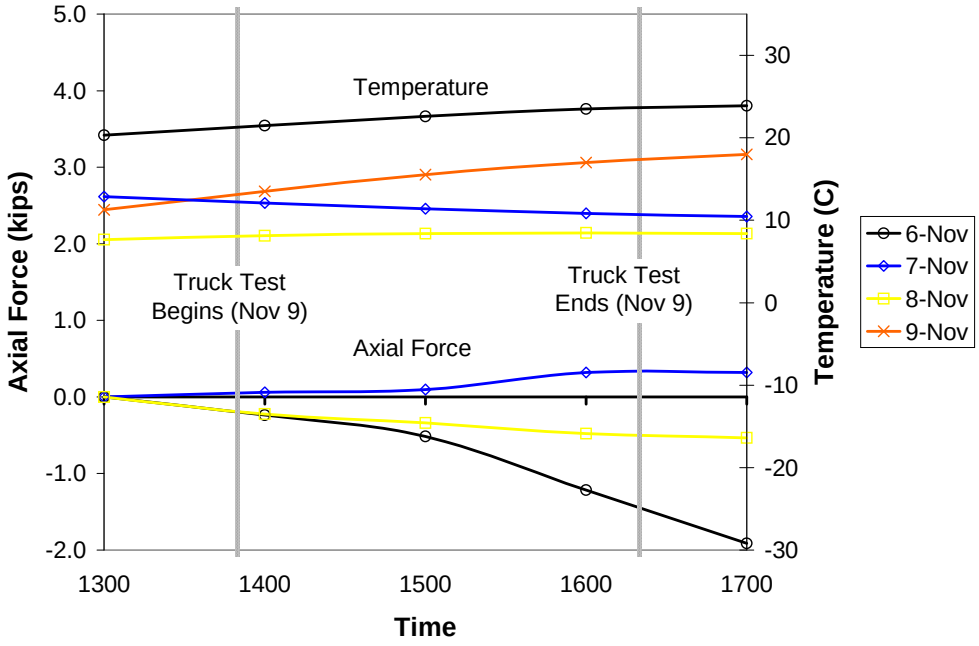

Figure 5.5 Top Chord – Axial Force and Temperature Data

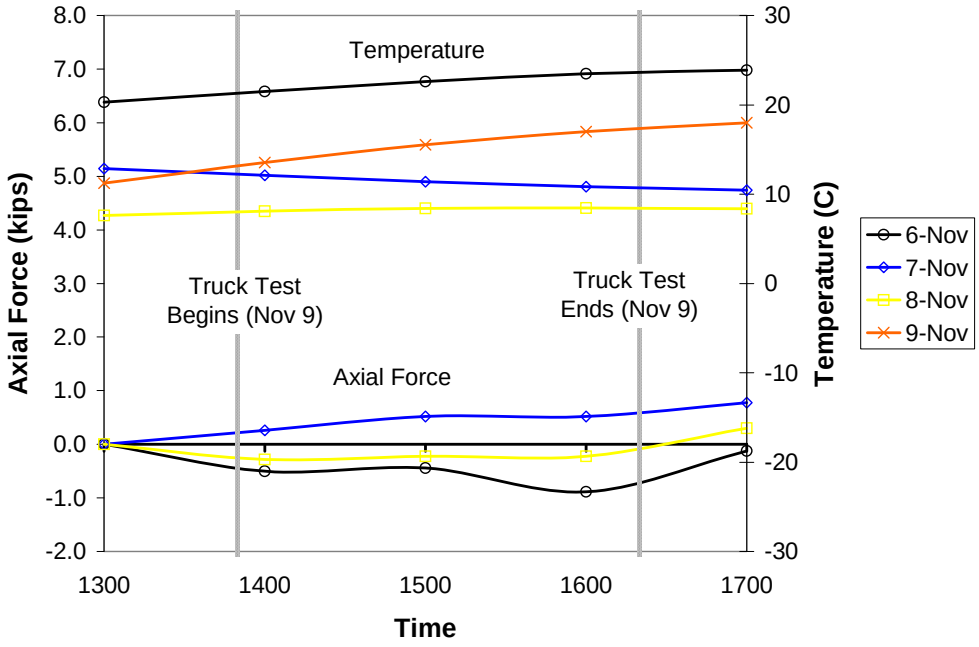

Figure 5.6 Bottom Chord – Axial Force and Temperature Data

The temperature data prior to the load test was too variable to predict the effects on the diaphragms. Instead, the temperature effects were estimated by examining only the diaphragm data during the load test. In a perfectly linear elastic system, the changes in force due to an applied external load are equal and opposite of the changes in force when the load is removed. Therefore the forces in the diaphragm members should be exactly the same before and after the truck load test, given there were no temperature effects. This also assumes that no yielding in any member of the bridge occurs and that the bearing pads supporting the bridge also act linear elastic. During the load test, the change in axial force due to temperature was estimated as being linear with time for each member. From reviewing the background data, this is probably the most reasonable estimate although not necessarily very accurate.

To avoid this problem in the future, the results could be interpreted much easier if the test were preformed between sunset and sunrise. The thermal gradients during this time are minimal since there is no solar radiation. However, a load test performed during these hours may not be feasible. Another solution to minimize effects would be to perform the test over a shorter duration. In this case, the change in forces due to temperature effects would not be as significant.

5.3 DIAPHRAGM RESULTS

5.3.1 Experimental Results

The external diaphragm member forces were determined by subtracting a linear estimation of the temperature effects from the measured force calculations. An example of this technique is shown in Figure 5.7 and Figure 5.8 on a member. The first graph is the original measured axial forces in one of the diagonals. A line representing the estimated temperature effect is superimposed over the plot from the origin to the last data point. The difference between the measured force

and the line is the estimated axial force due only to the weight of the trucks. The plateaus on the plots are caused from multiple data readings while the trucks are stationary.

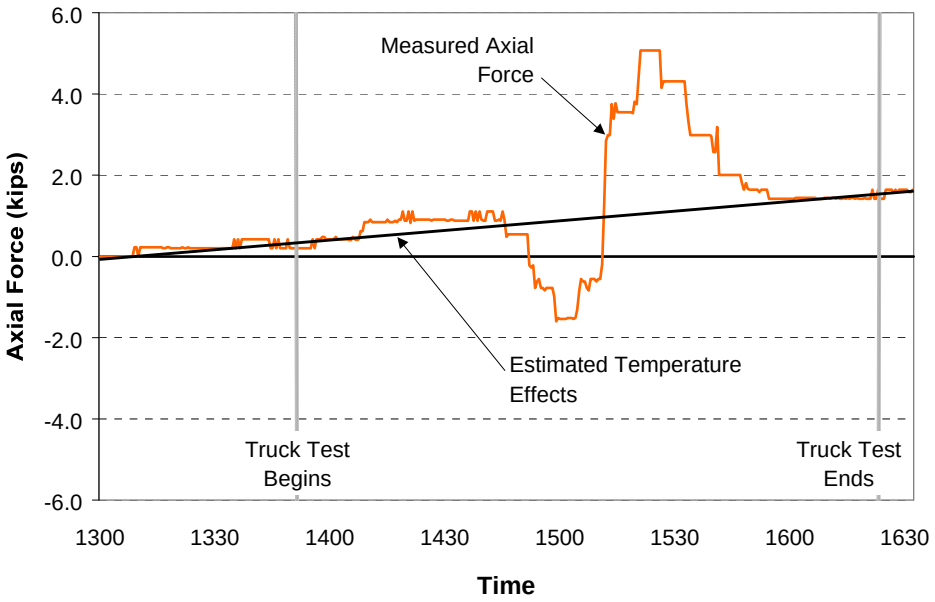

Figure 5.7 Measured Diaphragm Forces – Diagonal

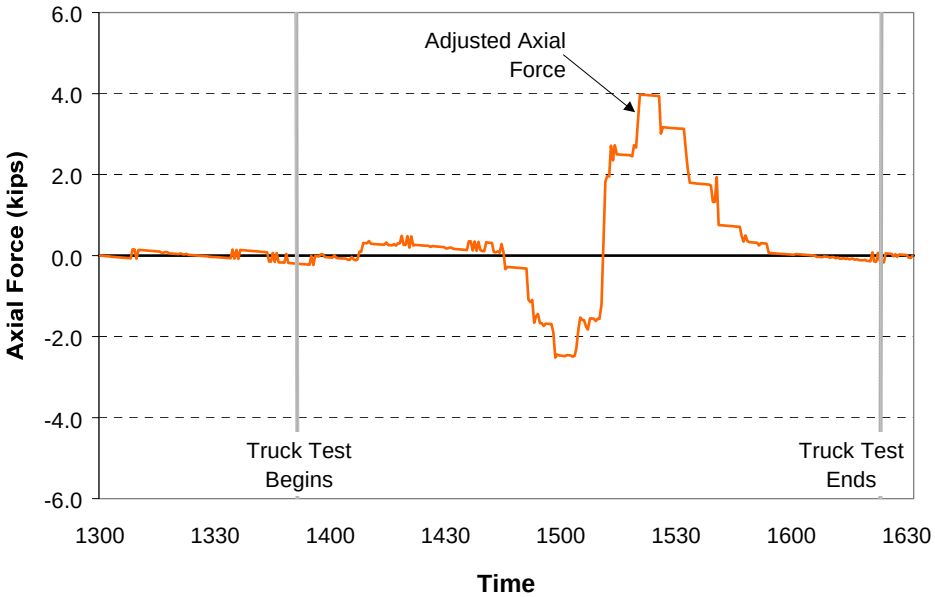

Figure 5.8 Adjusted Diaphragm Forces for Temperature Effects – Diagonal

This method of adjusting the measured forces by subtracting the temperature effects was used for the remainder of the diaphragm force calculations in this section. Figure 5.7 shows a substantial change in force from before and after the load test. In Figure 5.8, the axial force in the member remains fairly constant as the trucks are left in each position. There is a reversal in force at time 1510 (3:10pm) as the trucks are moved from the outer side of the curve (position 10 - Figure 5.2) to the inner side (position 11).

Figure 5.2 and Figure 5.9 shows the labeling system for the external diaphragms and their members. Diaphragm A had very little response during the load test. Member A1 had a change in axial force between 0-0.6kips. This is relatively close to the expected error in the readings. Therefore, only diaphragms B and C will be examined in this section. Half of the members on diaphragms B and C were reading reliable force measurements during the truck load test. Influence lines are shown for these members in Figure 5.10 through Figure 5.13. For each truck position, seven to eight data points are plotted. Ideally the data points at a certain truck position should identical. Therefore, the fewer points shown at a position yields more repeatability. Many of the symbols for the data points overlap on the graphs.

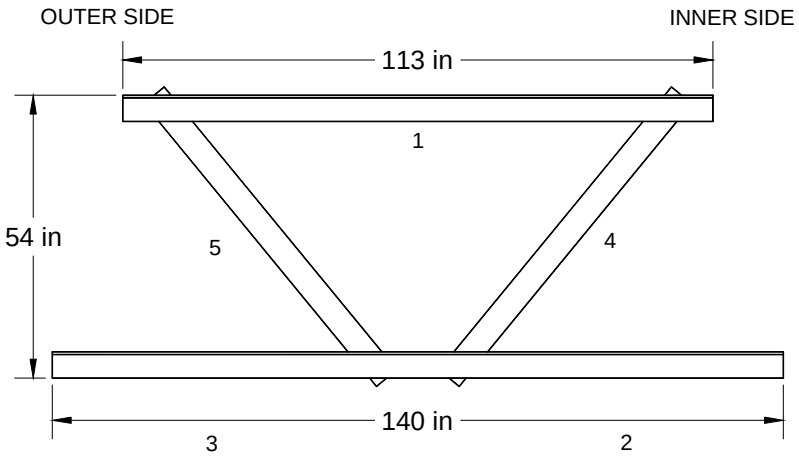

Figure 5.9 External Diaphragm

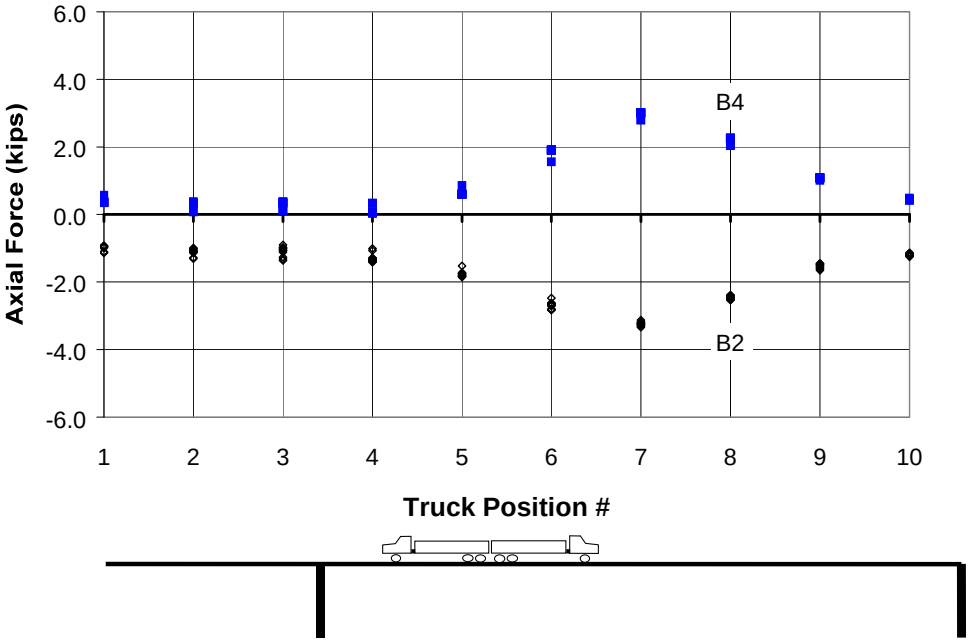

Figure 5.10 Outer Side Influence Line for Diaphragm B

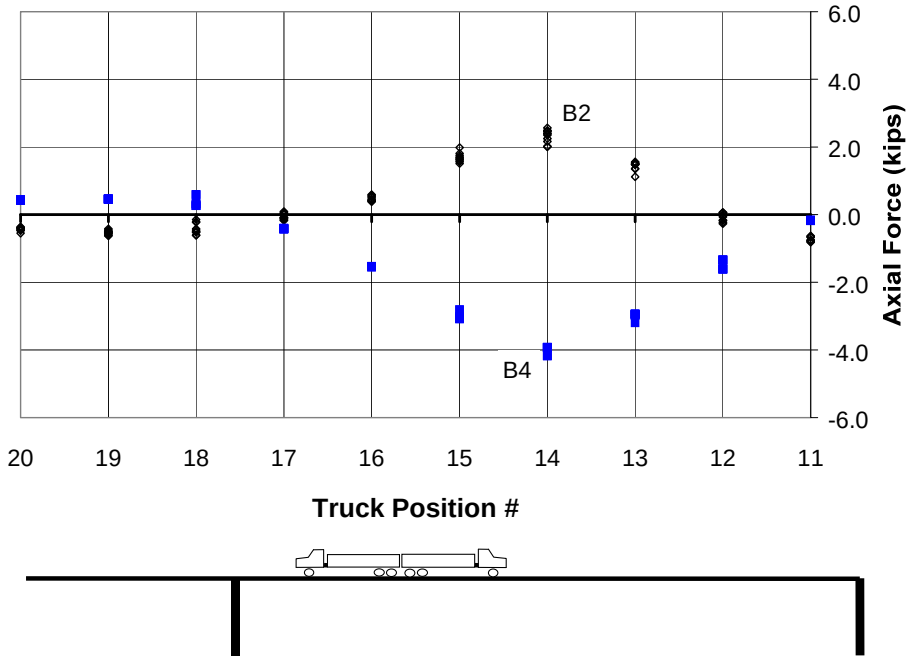

Figure 5.11 Inner Side Influence Line for Diaphragm B

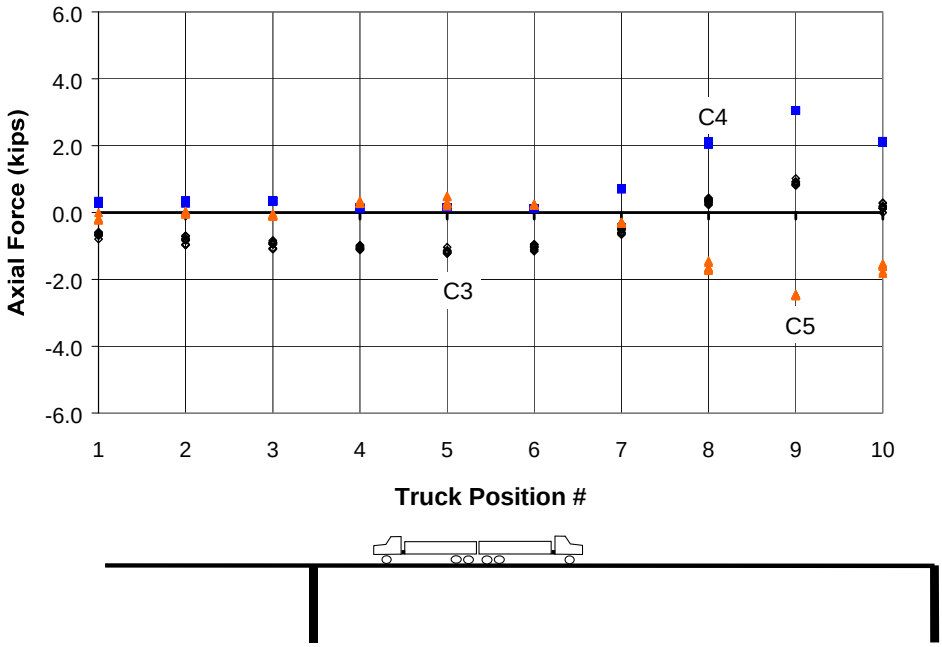

Figure 5.12 Outer Side Influence Line – Diaphragm C

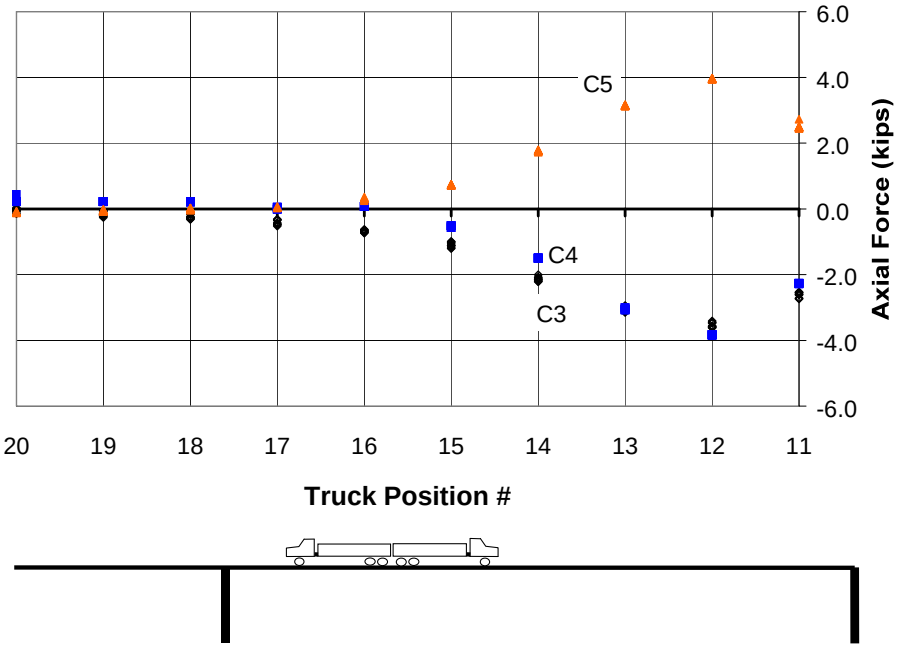

Figure 5.13 Inner Side Influence Line – Diaphragm C

As expected, the greatest magnitudes in diaphragm forces were measured while the trucks were positioned at the external diaphragm. Figure 5.10 and Figure 5.11 show that truck positions 7 and 14 produce the highest forces in diaphragm B. Similarly, Figure 5.12 and Figure 5.13 show the highest forces in diaphragm C occur when the trucks are in positions 9 and 12.

5.3.2 Predicted Results

The FEM of the composite girder modeled the concrete slab as having a modulus of elasticity of 4000ksi. The estimation of concrete stiffness was based on the equation from the current *AASHTO LRFD Bridge Design Specifications,* $E = 57000\sqrt{f'_c}$, where f'_c is the 28-day concrete strength equal to 5000psi. Analyses were performed using a higher modulus of elasticity of concrete than expected (E=5000ksi) and it was found that the FEM diaphragm forces were not very sensitive (approximately 3% difference).

The model generally predicted the same type of response out of the diaphragms as measured, although the forces that were predicted were higher. In general, the forces predicted by the model were 2-3 times higher than measured from the load test. Figure 5.14 through Figure 5.17 show the comparison between the predicted and measured axial forces in the diaphragm members. The measured force shown in each figure is the average of the force readings while the trucks remained in a certain position.

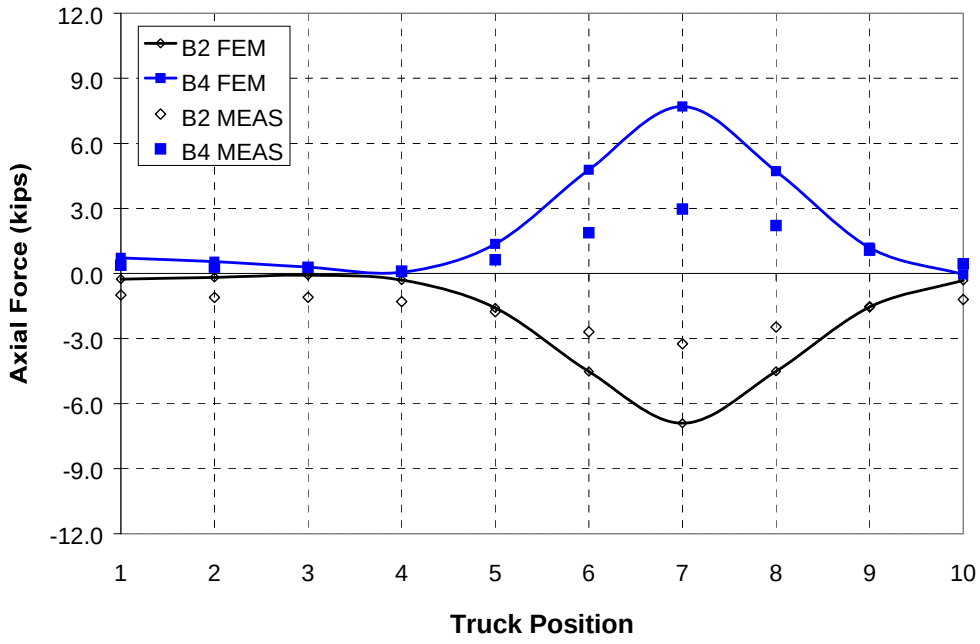

Figure 5.14 Outer Side – Measured and Predicted Forces in Diaphragm B

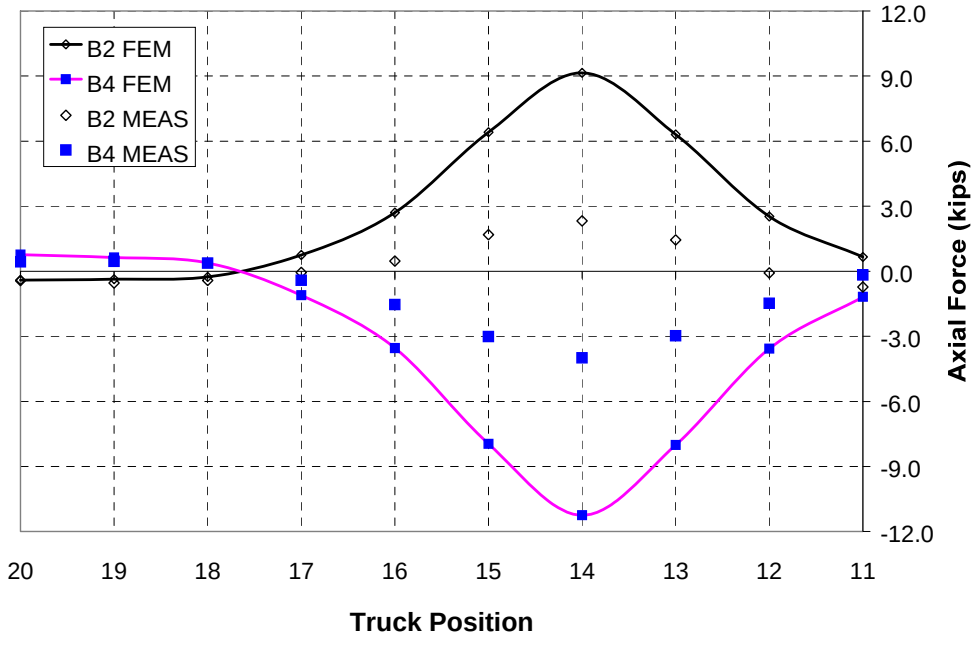

Figure 5.15 Inner Girder – Measured and Predicted Forces in Diaphragm B

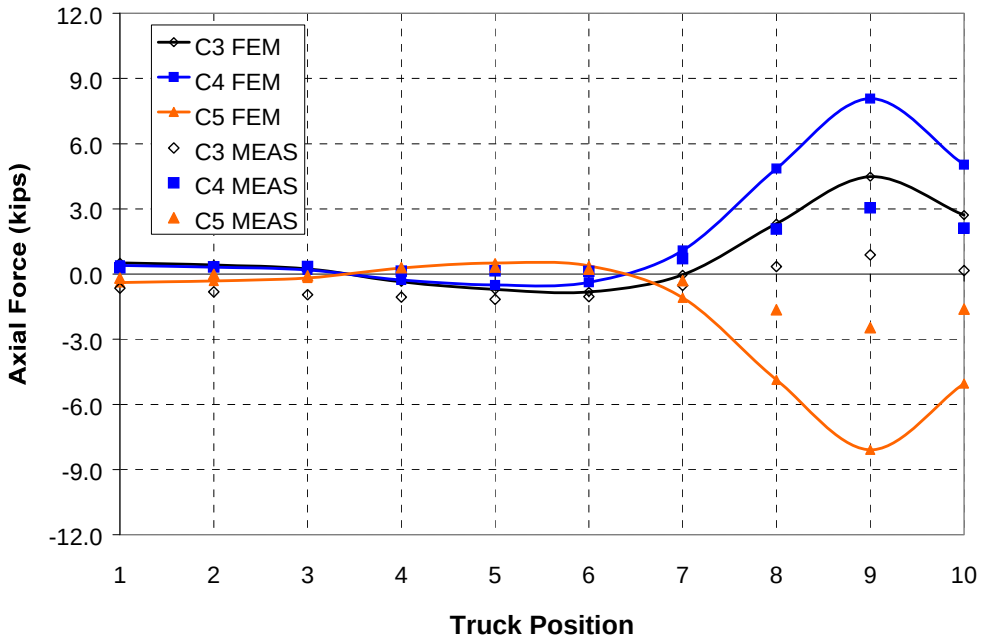

Figure 5.16 Outer Girder – Measured and Predicted Forces in Diaphragm C

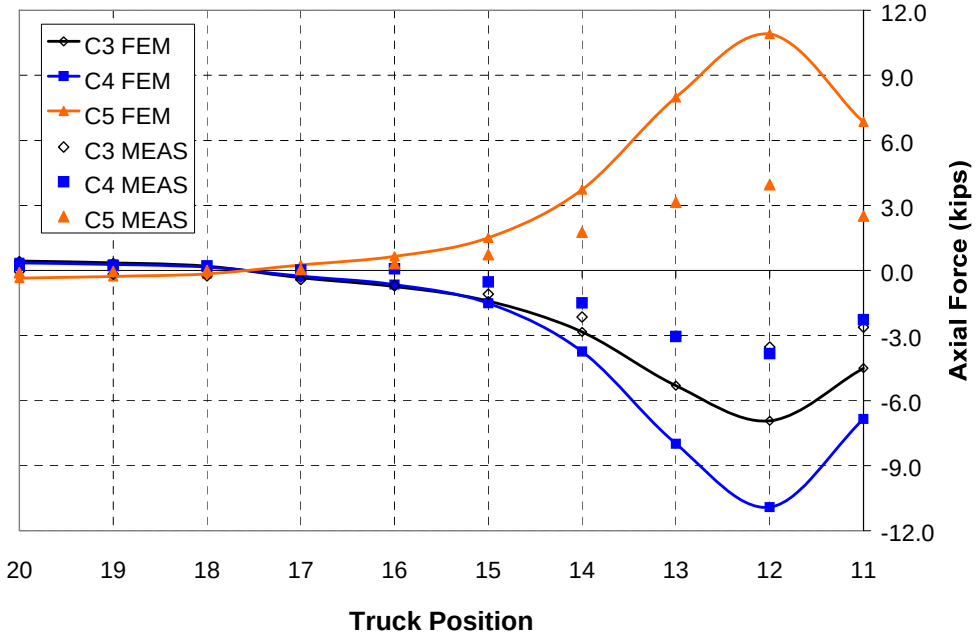

Figure 5.17 Inner Girder – Measured and Predicted Forces in Diaphragm C

In every member, the trends in the measured and predicted forces are the same although the measured forces were considerably less than predicted with the FEM. The highest measured forces from the load test were in the diagonal members while the trucks were positioned over the inner girder. Diaphragm member B4 recorded up to 4.0kips compression when the trucks were in position 14 and diaphragm member C5 recorded 4.0kips tension when the trucks were in position 12. In contrast, the FEM predicted 11.2kips compression in member B4 and 10.9kips tension in member C5 while the trucks were in these positions.

5.4 DISCUSSION

The measured forces in the external diaphragm members during the truck load test were comparable to the magnitude of induced forces from temperature gradients in the bridge. The changes in temperature-induced forces were estimated as linear with time and were subtracted from the original data to calculate the forces caused only from the trucks. This approximation adds some uncertainty to the accuracy of the measured results.

The measured forces in diaphragms B and C were much lower than predicted in the FEM. The predicted forces did not change significantly with a reasonable change in the estimation of deck stiffness. One reason for the overestimation of forces could be due to the reduction in diaphragm stiffness caused by the connection detail, as discussed in Chapter 3. The reduced diaphragm stiffness will have a larger effect on predicting diaphragm forces on the composite bridge than it did before the deck was cast. This is because the girders are much stiffer as a closed section and less force is distributed between girders since the diaphragms are relatively flexible. The reduction in diaphragm stiffness due to the connection detail was not accounted for in the FEM. However, there may be other reasons for the large discrepancy between the

predicted and measured results. Further investigation is required to achieve a more accurate prediction of the external diaphragm forces after the bridge is composite.

CHAPTER 6
Summary and Conclusions

6.1 SUMMARY

Forces in three external diaphragms and several top lateral-bracing members were measured during the construction of a three-span trapezoidal steel box girder bridge built in Austin, Texas. The stresses in the bridge were monitored during three main loadings. A full-scale load test was performed before the concrete placement using a crane equipped with a load cell. Measurements were also taken during the concrete deck pour, a stage in construction in which the expected stresses are high in the bracing and diaphragm members. The third loading used trucks that were placed in 20 different positions on the composite bridge. The measured forces in these members were compared to analysis using a Finite Element Model (FEM).

6.2 DIAPHRAGM FORCE MEASUREMENTS

The diaphragm used on the instrumented bridge consisted of singly symmetric angle members arranged as a K-frame. The angles were welded back-to-back which created an eccentric connection. Lab tests were performed on individual angle members and on a similar K-frame as used on the bridge to determine a reliable instrumentation configuration. It was found that the eccentric loading produced very high bending stresses in the members when loaded axially. This reduced the accuracy of the angle force measurements since small errors in strain measurement or gage locations could lead to large errors in force calculations. It was estimated from the lab tests results that 10-15% reliability could be expected in the diaphragm measurements.

6.3 CRANE LOAD TEST RESULTS

The crane used an attachment to lift on the outer girder a fraction of the dead weight of the bridge. The test was performed as a reliable comparison between the measured and predicted forces with a known load. The FEM predicted the axial forces in the top lateral bracing members in both the inner and outer girders very well during the crane load test. The load can only be transmitted from the outer girder to the inner girder through the use of external diaphragms. However, the measured outer girder lateral forces were higher than predicted and the measured inner girder lateral forces were lower than predicted. This means that the distribution of load through the diaphragms was lower than expected.

The shear and moments in the diaphragm can be determined by measuring the axial forces in the diaphragm members. On one diaphragm, it was found during the crane load test that the measured shear and torsion transferred from the outer girder to the inner correlated very well with predicted results. Another diaphragm measured higher shear, but much less torsion than predicted. The third diaphragm was far away from the crane lift points and had very small forces as predicted.

6.4 CONCRETE DECK POUR

Early composite action was evident from measurements in the top lateral forces. The concrete deck provided significant stiffness to the bridge within hours after being poured. Since the partially hardened deck stiffens the girders and contributes in load distribution between the two girders, the external diaphragm members had a reduction in force. This contribution is difficult to model since the concrete stiffness is uncertain and changes with time. This accounts for some of the discrepancy between the predicted and measured forces.

In general, the measured forces in the diaphragms were much lower than predicted with the FEM. The behavior of the diaphragms, namely the ratio of shear to moment transferred through the diaphragm, is relatively the same as predicted by the FEM. When the pour was over the same span as the diaphragm, the diaphragm restrained the top of the girders from twisting away from the center of bridge curvature. The magnitude of restraint, both vertical displacement and twisting of the girders, was generally much smaller than predicted. This means that the ratio of girder stiffness to diaphragm stiffness was higher than predicted.

Concrete decks are poured over continuous girders in several different segments. It was found that if a poured segment has sufficient stiffness during another segment pour, the external diaphragms below the harden section carried much less force than if the segment had no stiffness. This is because the hardened deck stiffens each box girder significantly and also provides another load path to transfer forces from one girder to the other.

Overall, the FEM predicted the same behavioral response in the diaphragms as measured, although it generally overestimated the amount of contribution the external diaphragms have in restraining the girders. The maximum axial stress measured in all of the external diaphragm members due to the weight of the concrete was about 3ksi. In comparison, the top lateral members that were measured had axial stresses up to 7ksi from the concrete pour.

6.5 TRUCK LOAD TEST

Two trucks were positioned over several different points on the composite girder bridge. They were placed in a back-to-back configuration very close to the edge of the concrete deck to maximize the response out of the external diaphragms. Unfortunately, the test occurred over several hours during the day and the changes in diaphragm forces due to temperature were comparable to the

forces due to the truck loads. This decreased the accuracy of the measured results since the temperature effects had to be estimated. However, it was clear that the diaphragm forces were still much less than predicted by the FEM. Again the behavior of the diaphragm action correlated well with the model, but the magnitude of forces were considerably less. The diaphragm forces measured during the load test were between 25-50% of the predicted forces.

6.6 FINITE ELEMENT MODEL

Generally, the finite element model overestimated the amount of force distributed from one box girder to the other. This means that the ratio of girder stiffness to diaphragm stiffness was higher than predicted. There are several possible reasons for the discrepancy in the measured and predicted results.

The connection detail from the diaphragm to each box girder caused a significant loss in diaphragm stiffness when the connection transferred tension. It was found that the WT stub that was bolted to the stiffened web of the girder could bend away from the girder when tensioned. This detail is difficult to model since the reduction in stiffness would only occur when the connection has net tension. If the diaphragms are prestressed (from temperature effects or stresses during erection), the connection will be in tension or compression during future loadings. If the connection has residual compression, a small tensile force on the angle would first relieve the compression and no loss in stiffness would occur at the connection. Conversely, if the connection has residual tension, even a compressive force would cause a reduction in stiffness in the diaphragm.

Another reason for the discrepancy is that the diaphragm in the model is connected to the girder at full depth. The real diaphragm is only about 70% of the depth of the girders. For the analysis to model the true depth of the diaphragm, a more detailed mesh would be required.

One other source of error is that the model does not consider any stiffness from the permanent metal deck forms that are placed between the top flanges of the girders. Although the forms are very thin, they can act as a shear diaphragm and provide additional bracing to the flanges. They also add torsional stiffness to the U-girders by closing the cross section.

6.7 FUTURE RESEARCH

The measured forces in the external diaphragms on this bridge showed that the diaphragms have very low stresses throughout construction. However, many gages did not consistently function well since they were exposed for many months and access to fix them was not feasible. Further field studies are required to determine the necessity of external diaphragms on curved box girder bridges.

Improvements that could have been made towards the field monitoring of forces in these members are the following:

- More redundancy per cross section or member
- Quicker load tests or load tests during the night to minimize temperature effects
- Thermocouples arranged in strategic positions along the bridge to measure temperature gradients
- Fabrication of K-frames consisting of concentrically-loaded pipes (Zureick et al, 2000) in place of external diaphragms for better reliability in measurement than eccentrically-loaded angle members

Some of these techniques were proposed for the instrumentation during this research, although it was not feasible due to time constraints and changes in construction.

APPENDIX A

Supplementary Bridge Dimensions

Table A.1 Bridge Span Lengths: Z-Connect

Span #13	Span #14	Span #15
151.5ft	190.0ft	151.5ft

Table A.2 Bridge Radius (Centerline): Z-Connect

Inner Girder	Bridge	Outer Girder
441.833ft	450.000ft	458.167ft

TOP FLANGE THICKNESS

Lengths measured horizontally at bottom of web along centerline of Girder.

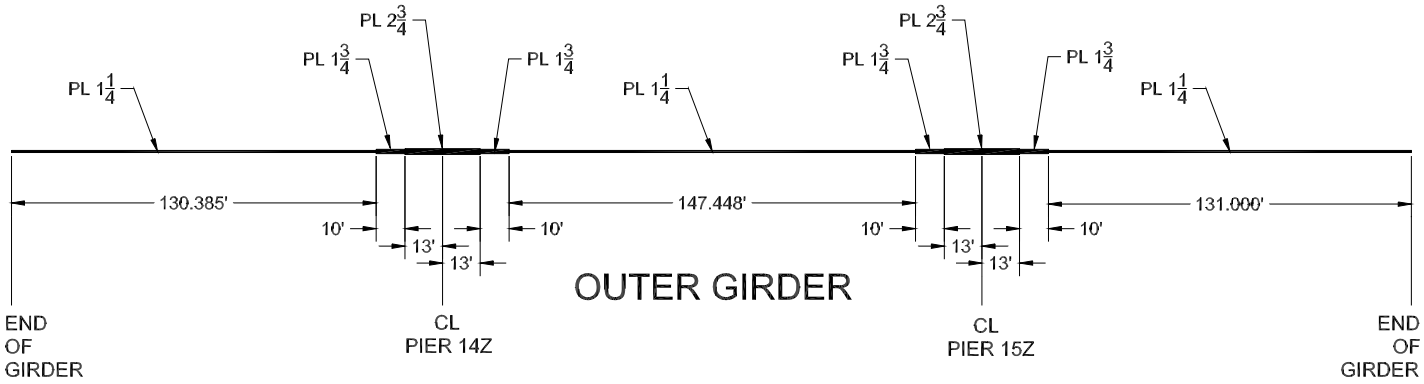

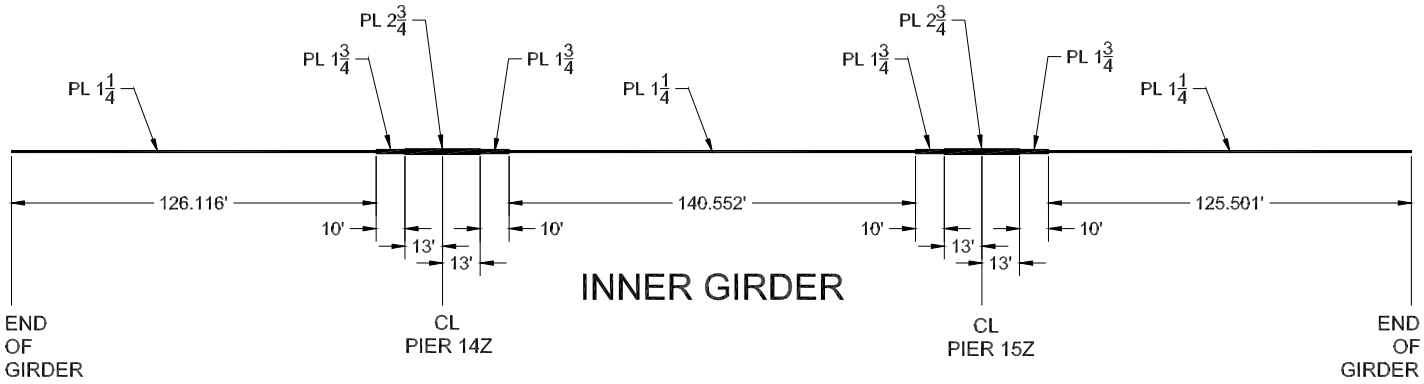

BOTTOM FLANGE THICKNESS

Lenghts measured horizontally at bottom of web along centerline of Girder

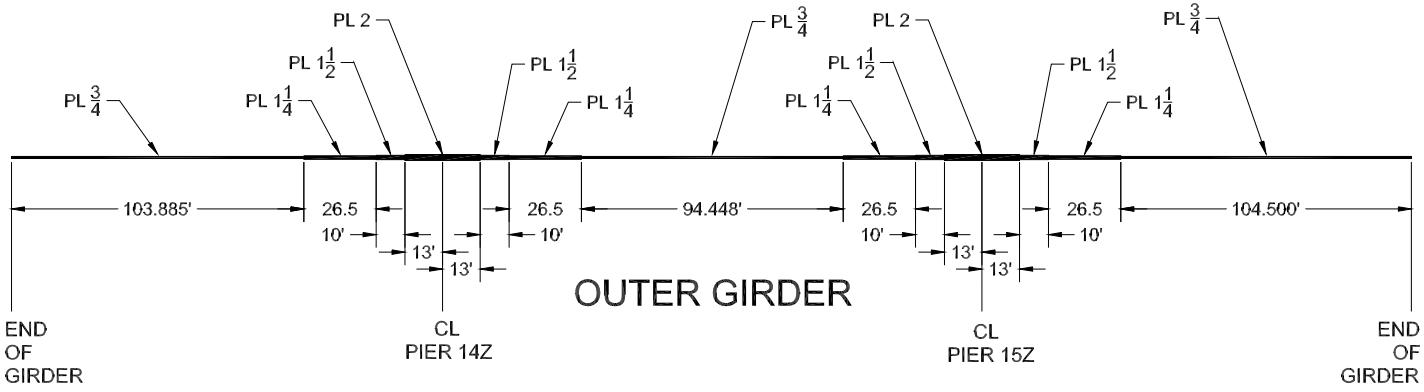

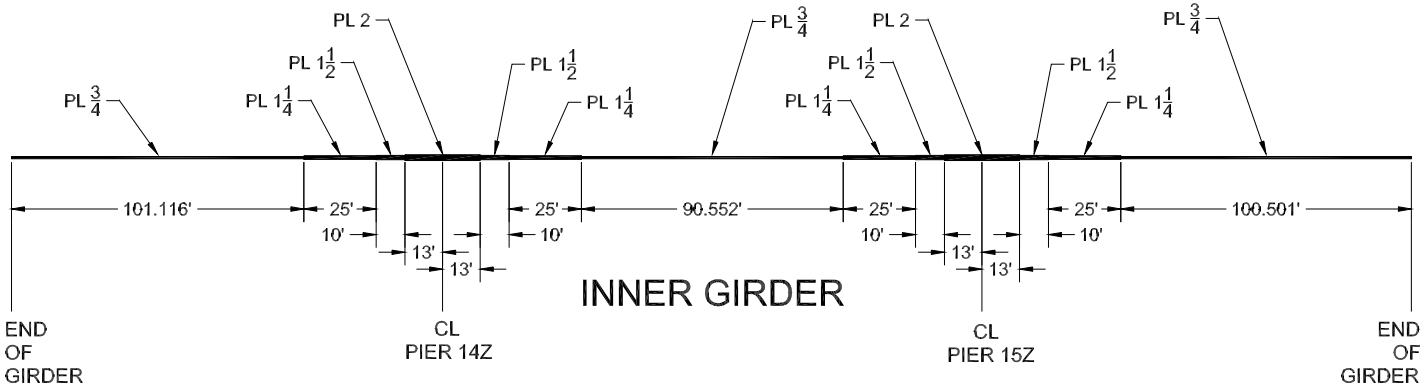

APPENDIX B

Angle Force Calculation Example

Axial Force Calculations for External Diaphragms Members

Composed of Angles: L5x5x1/2

$ksi := 1000\,psi$ $kip := 1000\,lbf$

Cross-Sectional Properties

Cross-Sectional Area $A := 4.75\,in^2$

Centroid Location: $x := 1.43\,in$ $y := 1.43\,in$

Strain at Centroid

$\varepsilon_{centroid} = c_1 x_{centroid} + c_2 y_{centroid} + c_3$

c_1, c_2, and c_3 are constants for a specific load. They are stored as matrix "C"

where

$$\varepsilon_1 = c_1 x_1 + c_2 y_1 + c_3$$

$$\varepsilon_2 = c_1 x_2 + c_2 y_2 + c_3$$

$$\varepsilon_3 = c_1 x_3 + c_2 y_3 + c_3$$

$$\begin{pmatrix} \varepsilon_1 \\ \varepsilon_2 \\ \varepsilon_3 \end{pmatrix} := \begin{pmatrix} x_1 & y_1 & 1 \\ x_2 & y_2 & 1 \\ x_3 & y_3 & 1 \end{pmatrix} \cdot \begin{pmatrix} c_1 \\ c_2 \\ c_3 \end{pmatrix}$$

Measured Strain at 3 Gages $\varepsilon := \begin{pmatrix} 55 \\ 10 \\ 21 \end{pmatrix}$ All ε data are in microstrain

Matrix "Coord" represents gage location.
Each row is a different gage.
Columns 1 and 2 are x and y respectively.

$$Coord := \begin{pmatrix} 1.75 & 0.5 & 1 \\ 4.5 & 0.5 & 1 \\ 0.5 & 4.5 & 1 \end{pmatrix}$$

Solve for c_1, c_2 & c_3 $C := Coord^{-1} \cdot \varepsilon$ $C = \begin{pmatrix} -16.36 \\ -13.61 \\ 90.44 \end{pmatrix}$

Stress at Centroid

$\sigma = \varepsilon_{centroid}$ * 29,000,000 psi / 1,000,000

Axial Stress $\sigma := 29psi \cdot \left(C_1 \cdot \frac{x}{in} + C_2 \cdot \frac{y}{in} + C_3 \right)$ $\sigma = 1.38ksi$

Axial Force $F := \sigma \cdot A$ $F = 6.55kip$

REFERNCES

AASHTO LRFD Bridge Design Specifications, (1996), American Association of State Highway and Transportation Officials.

Basler, K., and Kollbrunner, C. F. (1969). *Torsion in Structures.* Springer-Verlag, Berlin, Germany, pp. 14-15.

Bridge Design Manual, (1991), Colorado Department of Transportation. Accessed through http://www.dot.state.co.us.

Chen, Brian S. (1999). "Buckling of U-Shaped Girders with Top-Flange Lateral Bracing," thesis presented to The University of Houston, in partial fulfillment of the requirements for the degree of Master of Science.

Davidson, J. S., Keller, M. A., Yoo, C. H. (1996). "Cross-Frame Spacing and Parametric Effects in Horizontally Curved I-Girder Bridges." *Journal of Structural Engineering,* Vol. 122, No. 9, September, pp1089-1096

Fan, Zhanfei. (1999). "Field and Computational Studies of Steel Trapezoidal Box Girder Bridges," thesis presented to The University of Houston, in partial fulfillment of the requirements for the degree of Doctor of Philosophy.

Fan, Zhanfei and Helwig, Todd A. (1999). "Behavior of Steel Box Girders with Top Flange Bracing." *Journal of Structural Engineering*, Vol. 125, No.8, August, pp829-837

Guide Specifications for Horizontally Curved Highway Bridges. (1993) American Association of State Highway and Transportation Officials.

Lopez, Michael G. (1999). "Thermally-Induced Deformations and Stresses in a Steel Trapezoidal Twin-Box Girder Bridge," thesis presented to The University of Texas at Austin, in partial fulfillment of the requirements for the degree of Master of Science in Engineering.

Recommended Specifications for Steel Curved-Girder Bridges, (1998), National Cooperative Highway Research Program, Transportation Research Board, National Research Council.

Topkaya, Cem. (2001). Thesis in progress: to be presented to The University of Texas at Austin, in partial fulfillment of the requirements for the degree of Doctor of Philosophy.

Zureick, A., Linzell, D., Leon, R. T., Burell, J. (2000). “Curved Steel I-Girder Bridges: Experimental and Analytical Studies.” *Engineering Structures,* Vol. 22, No.2, pp180-190. Accessed through Elsevier Science Ltd.